석 사 학 위 논 문
Master's Thesis

전단파를 이용한 연약 점토 지반의 압밀 상태 및 강도 평가

Evaluation of the Consolidation State and Strength of Soft Clay using Shear Waves

장 일 한 (張 一 韓 **Chang, Il Han**)

건 설 및 환 경 공 학 과
Department of Civil and Environmental Engineering

한 국 과 학 기 술 원
Korea Advanced Institute of Science and Technology

2 0 0 6

전단파를 이용한 연약 점토 지반의
압밀 상태 및 강도 평가

Evaluation of the Consolidation State and Strength of Soft Clay using Shear Waves

Evaluation of the Consolidation State and Strength of Soft Clay using Shear Waves

Advisor : Professor **Gye-Chun Cho**

by

Il Han Chang

Department of Civil and Environmental Engineering

Korea Advanced Institute of Science and Technology

A thesis submitted to the faculty of the Korea Advanced Institute of Science and Technology in partial fulfillment of the requirements for the degree of Master of Engineering in the Department of Civil and Environmental Engineering

Daejeon, Korea
2005. 12. 30.
Approved by

Professor Gye-Chun Cho

전단파를 이용한 연약 점토 지반의 압밀 상태 및 강도 평가

장 일 한

위 논문은 한국과학기술원 석사학위논문으로 학위논문 심사위원회에서 심사 통과하였음.

2005년 12월 30일

심사위원장 조 계 춘 (인)

심사위원 이 승 래 (인)

심사위원 김 동 수 (인)

To my Parents

MCE 20043509	장 일 한. **Il Han Chang. Evaluation of the Consolidation State and Strength of Soft Clay using Shear Waves.** 전단파를 이용한 연약 점토 지반의 압밀 상태 및 강도 평가. **Department of Civil and Environmental Engineering. 2006. 188p.** **Advisor Prof. Gye-Chun Cho. Text in English.**

Abstract

Reliable estimation of the consolidation state and strength of soft soils is important for the prediction of permanent settlement and strength, particularly when an additional load induced by civil structure construction is added in situ. The effective stress state and void ratio value are particularly critical as they are the most important parameters for consolidation state evaluation and strength estimation. To date, the consolidation behavior of clay has been studied in various civil engineering practices. However, the existing in-situ consolidation characterization approach entails several difficulties in monitoring the effective stress and density variation during the consolidation process.

This thesis focuses on the evaluation of the consolidation state and strength of soft soil using shear waves. The shear wave velocity is a function of the particle composition and inter-particle force, because the shear wave propagates through particle contact in saturated clay. Therefore, the effective stress of a clay media can be evaluated using the shear wave velocity. Several shear wave-based laboratory tests are performed so as to monitor the shear wave velocity variation during consolidation. Piezoelectric bender element sensors are used to generate and receive shear waves inside laboratory specimens, without soil disturbance.

First, the consolidation state and properties of natural clay deposits are characterized by laboratory consolidation tests using bender element sensors installed in non-disturbed Shelby tube specimens. The vertical effective stress – shear wave

velocity relationship for the normally consolidated state is evaluated from laboratory tests. The in-situ consolidation state is evaluated by comparing the in-situ shear wave velocity with the estimated effective stress – shear wave velocity trend. However, the accuracy of the in-situ consolidation state evaluation depends on the in-situ shear wave velocity data. As such, reliable in-situ shear wave velocity testing is one of the most important prerequisites for a reliable in-situ consolidation state evaluation.

The site of interest in this study is evaluated as over-consolidated when the in-situ shear wave velocity is higher than the value estimated in the laboratory, and is conversely determined as under-consolidated when the velocity is lower than the laboratory determined value. The site is classified as normally-consolidated when the in-situ shear wave velocity is close to the laboratory result.

The compressibility parameters of each test are evaluated from the effective stress – void ratio curve from the laboratory data. The in-situ settlement according to additional loading is predictable using the compressibility parameters. The inflection point agrees well with the estimated pre-consolidation stress value.

Laboratory sedimentation tests and consolidation tests are performed to reconstitute the in-situ soil structure and fabric, and to simulate the in-situ sedimentation and self weight consolidation process of normally consolidated dredged and reclaimed deposits. Bender element sensors are used to measure the shear wave velocity during laboratory consolidation tests. In the laboratory consolidation test, the total amount of expected effective stress is applied on the specimen at once. From the measured shear wave velocity and displacement data, the effective stress, void ratio, degree of consolidation, coefficient of consolidation, coefficient of earth pressure at rest, and permeability variation during consolidation are evaluated. Generally, the effective stress, degree of consolidation, and coefficient of earth pressure increase as the vertical shear wave velocity increases, while the void ratio, coefficient of consolidation, and permeability decrease as the shear wave velocity decreases.

As the undrained shear strength of clay is strongly affected by its void ratio, the undrained shear strength can be correlated with the shear wave velocity by comparing the void ratio – shear wave velocity relation and the void ratio – undrained shear strength relationship. Laboratory loading and unloading tests are performed to reconstitute different void ratio conditions under a single effective stress state. The undrained shear strength values are measured via laboratory vane shear tests after unloading. The undrained shear strength shows a linear relationship with the void ratio. Approximation of the undrained shear strength – shear wave velocity relationship appears to be an accurate method to predict the in-situ undrained shear strength of reclaimed deposits.

The purpose of this study is to verify the accuracy of employing shear waves for soft soil parameter evaluation and to develop an evaluation method for the consolidation state and strength. From the results, it is shown that the shear wave velocity accurately correlates with the effective stress, void ratio, degree of consolidation, coefficient of consolidation, coefficient of earth pressure, permeability, and undrained shear strength. It is expected that the techniques outlined in this thesis will be widely applicable to in-situ monitoring of dredged and reclaimed sites and other soft soil deposits.

CONTENTS

LIST OF TABLES

Table

LIST OF FIGURES

CHAPTER I
INTRODUCTION

1.1 Background

The consolidation behavior of clay has been studied in various civil engineering practices. Since Terzaghi (1923) introduced the one-dimensional consolidation theory, notable improvements overcoming the assumptions and limitations of his theory have been presented by Mikasa (1963), Gibson, et al. (1967; 1981), and Pane and Schiffman (1997), among others. In particular, the large strain consolidation model shows more reliable applicability for soft soil behavior in field. While it still assumes the constancy of the coefficient of consolidation (C_v), the large strain theory is also applicable for the self-weight consolidation process of sedimentation.

However, in-situ consolidation characterization has several weaknesses in relation to monitoring the effective stress and density variation during the consolidation process. Notably, it is more difficult to simulate the in-situ sedimentation process of dredged and reclaimed sites in the laboratory. The consolidation state and compressibility evaluations are required in order to predict the in-situ stress – strain behavior after additional loading is applied on the present field.

The shear wave velocity is a function of the particle composition and inter-particle force, because the shear wave propagates only through particle contact in saturated soil conditions. Therefore, the effective stress of a soil element can be evaluated using the shear wave velocity inside (Santamarina, et al. 2001).

In this thesis, shear wave-based laboratory tests are performed so as to monitor the shear wave velocity variation during consolidation. Piezoelectric bender element sensors are used to generate and receive shear waves inside laboratory specimens, without disturbing the soil. A series of experimental procedures are proposed for minimizing the disturbance of Shelby tube samples and simulating the in-situ self-weight consolidation process of dredged and reclaimed sites.

Several important design parameters, including effective stress, consolidation state, void ratio, compression index, permeability, and strength, are evaluated using the shear wave velocity data from laboratory measurements. The evaluated parameters are also correlated with the shear wave velocity of the soil of interest. The in-situ consolidation parameters can be estimated from in-situ shear wave velocities with the aid of those correlations obtained in laboratory testing results. Thus, reliable in-situ shear wave velocity data should be obtained for accurate in-situ application. However, in-situ testing methods are beyond the scope of this thesis.

1.2 Scope of Thesis

The goals of this study are to review previous studies on the one-dimensional consolidation theory of clay; to develop a consolidation state evaluation method for natural soil deposits using shear waves; to develop a laboratory testing procedure to simulate the in-situ self-weight consolidation process of dredged and reclaimed sites; to characterize the in-situ self-weight consolidation using shear waves; and to identify a shear wave – void ratio – strength relationship for a normally-consolidated clay.

Chapter II presents a literature review related to the one-dimensional consolidation theory. The nonlinearity of large strain consolidation is discussed, and the necessity of shear wave-based consolidation characterization is highlighted.

Chapter III studies the consolidation state evaluation of natural clay deposits using a shear wave based laboratory consolidation test. A specimen preparation method is introduced using the Shelby tube itself for the oedometric cell so as to minimize sample disturbance. In-situ consolidation characteristics are evaluated for field application.

Chapter IV is related to the development of a laboratory test method to simulate the in-situ sedimentation and self-weight consolidation process in laboratory. Shear wave velocity data obtained during the consolidation test are used to evaluate various kinds of soil properties during the self-weight consolidation process. Case studies are discussed for field application.

Chapter V develops the relationships among shear wave velocity, void ratio, and undrained shear strength during consolidation. In addition, the shear wave velocity –

void ratio relationship under the same confining pressure is evaluated via an unloading test.

Finally, Chapter VI summarizes the main conclusions drawn from this study and suggests areas for further research.

CHAPTER II
LITERATURE REVIEW

2.1 Introduction

The characterization of a soft clay deposit in nature is important for the prediction of its permanent settlement and strength, particularly when an additional load induced by civil structure construction is added in situ. The most common process for clay deposit formation in nature is a combination of sedimentation and consolidation. Eroded particles carried by streams or wind settle down when the effect of gravity is relatively larger than the speed the transporting medium. Settling particles flocculate by electrical attraction and repulsion acting among them and thereby form larger clumps. Electrical attraction and repulsion are caused by electrical charges on the clay particle surfaces. Settled particles form a sediment on the base. Volumetric decrement then occurs from the weight of the sediment. Specifically, the weight of the overburden soil acts as an applied load to the underlying soil. As a result, the volume of soil decreases and the density increases, aided by the soil's own weight. Additional volume decrease and density increase occur as a result of supplement loads, particle bonding, cementation, etc.

Most clay deposits in nature are formed by the slow repetition of slight additional accumulation and a hardening process over a long period of time. Time discontinuities exist along different depths and layers. Accordingly, soil type, particle composition, strength, and density could vary extensively even in the same vertical profile.

Reclamation provides a good example of a rapid artificial soil deposit formation in field. Generally, a huge amount of dredged slurry is dumped at once into the target site, and then each particle undergoes sedimentation and self-weight consolidation processes independently. Finally, a soft soil deposit with similar soil type and particle arrangement is formed during in a relatively short time.

Briefly, even though the origin and formation history differ, the main formation procedures of all clay deposits are sedimentation and consolidation.

In this chapter, previous studies on sedimentation and one-dimensional consolidation processes of clay are reviewed. The advantages for applying the improved large strain consolidation model to self-weight consolidation characterization are discussed. Furthermore, the availability of shear waves for an effective stress evaluation and an accurate sensor device for shear wave measurement in particulate media are considered.

2.2 Sedimentation Theory

2.2.1 Free Settling of Isolated Particles

The settling behavior of a particle in a very low concentration suspension is affected by the gravity and buoyancy of the particle as well as the viscous friction between the particle and fluid. Thus, the settling speed of a spherical shaped particle can be defined according to Stoke's law:

$$v_o = \frac{(\rho_p - \rho_l)g}{18\mu_l} d^2 \tag{2.1}$$

where v_o is the speed of particle fall, ρ_p is the particle density, ρ_l is the fluid density, g is the acceleration of gravity (=9.81m/s^2), μ_l is the viscosity coefficient of the fluid, and d is the particle diameter.

In free isolated settling, every particle falls independently without any interaction with other particles. Generally, heavy particles settle faster, and the particles and fluid are isolated. Several modified equations of the settling speed, with consideration of the fluid concentration, are shown in Table 2.1 (Imai et al. 1979).

Table 2.1 Settling velocity – mixture concentration equations.

Equation	Reference
$v = v_o(1-KC)^{4.65}$	Richardson and Zaki (1954)
$v = v_o(1-KC)^2 \cdot 10^{-1.83KC}$	Steinour (1944)
$v = v_o 10^{-aKC}$	Tomas (1964)
$v = ac^{-b}$	Cole (1968)
$v = v_o\left[1-2.78(KC)^{2/3}\right]$	Bond (1960)
$v = v_o c^{-ab}$	Vesilind (1969)
$v = v_o\left[1+\frac{3}{4}KC\left(1-\frac{8}{KC-3}\right)\right]$	Brinkman (1948)
$v = v_o(1-KC)^a$	Maude and Whitmore (1958)
$v = v_o(1-aKC)\left[1-b(KC)^{1/3}\right]$	Oliver (1961)
$v = \dfrac{v_o\left[3-\frac{9}{2}(KC)^{1/3}+\frac{9}{2}(KC)^{5/3}-3(KC)^2\right]}{3+2(KC)^{5/3}}$	Happel (1958)

Note that v is the settling velocity, v_o is the Stoke's law velocity, KC is the volume ratio of particles to the mixture, and a, b are constants.

2.2.2 Hindered Zone Settling

When the solid concentration of slurry mixture increases, the settling of large size particles is interrupted by collisions with smaller particles falling with lower rates. Therefore, flocks of soil particles are consequently formed (Imai 1980). The formed flocks may then fall freely in the case of a relatively low solid concentration. This type of settling behavior is called hindered settling.

Conversely, when the solid concentration is relatively high, interactions between flocks restrict their free fall tendency, and the flocks settle in the aggregate at a unified rate. forming a clear interface between the dispersion and clear water (Imai 1980). This type of settling process is called zone settling.

Zone settling was first theorized by Kynch (1952). Kynch considered the partial derivative of the solid concentration with time and location during the sedimentation process. Kynch's equation has been modified as follows (Pane and Schiffman 1985):

$$V(c)\frac{\partial c}{\partial \xi} + \frac{\partial c}{\partial t} = 0 \tag{2.2}$$

where c is the solid concentration, ξ is the Eulerian coordinate, and

$$V(c) = v_s + c\frac{dv_s}{dc} \tag{2.3}$$

where v_s is the velocity of settling, which is a function of the local concentration:

$$v_s = v_s(c) \tag{2.4}$$

Eqs. 2.3 and 2.4 show that several different types of settling may occur depending on the v_s - c relationship and the initial conditions of the sedimentation process. A settling theory considering time and spatial distribution was advanced by Mikasa (1963), and McRoberts and Nixon (1975). Mikasa (1963) defined compression settling, which occurs when the solid concentration is much higher than in the case of zone settling. The mechanisms of compression settling were successfully interpreted with the consolidation theory for very soft clays.

2.2.3 Settling Behavior of Soils in Nature

The settling behavior of soils, especially clay particles, is affected by the following factors:

1. Type of clay minerals
2. Type of dissolved electrolytes
3. Concentration of solid materials (water content)
4. Concentration of the ionic contents in water

Imai (1980) prepared an experimental test to observe different settling types, and how they are affected by clay type, initial water content, and ionic concentration (Fig. 2.1). Four different types of settling were confirmed from the results as follows:

- Type I Dispersed free settling

  Dispersed soil particles do not flocculate, and settle down without any particle interactions.

- Type II Flocculated free settling

  Soil particles flocculate and form different-sized flocks. However, the flocks settle freely depending on their sizes.

- Type III Zone Settling

  Flock settling behavior is hindered by strong interaction between the flocks. However, even though the settling rate of individual flocks is uncertain, the settling rate of the whole aggregate of flocks is constant.

- Type IV Consolidation Settling

  The settling period is relatively short, and therefore the mixture settles as a whole mainly due to the consolidation effect.

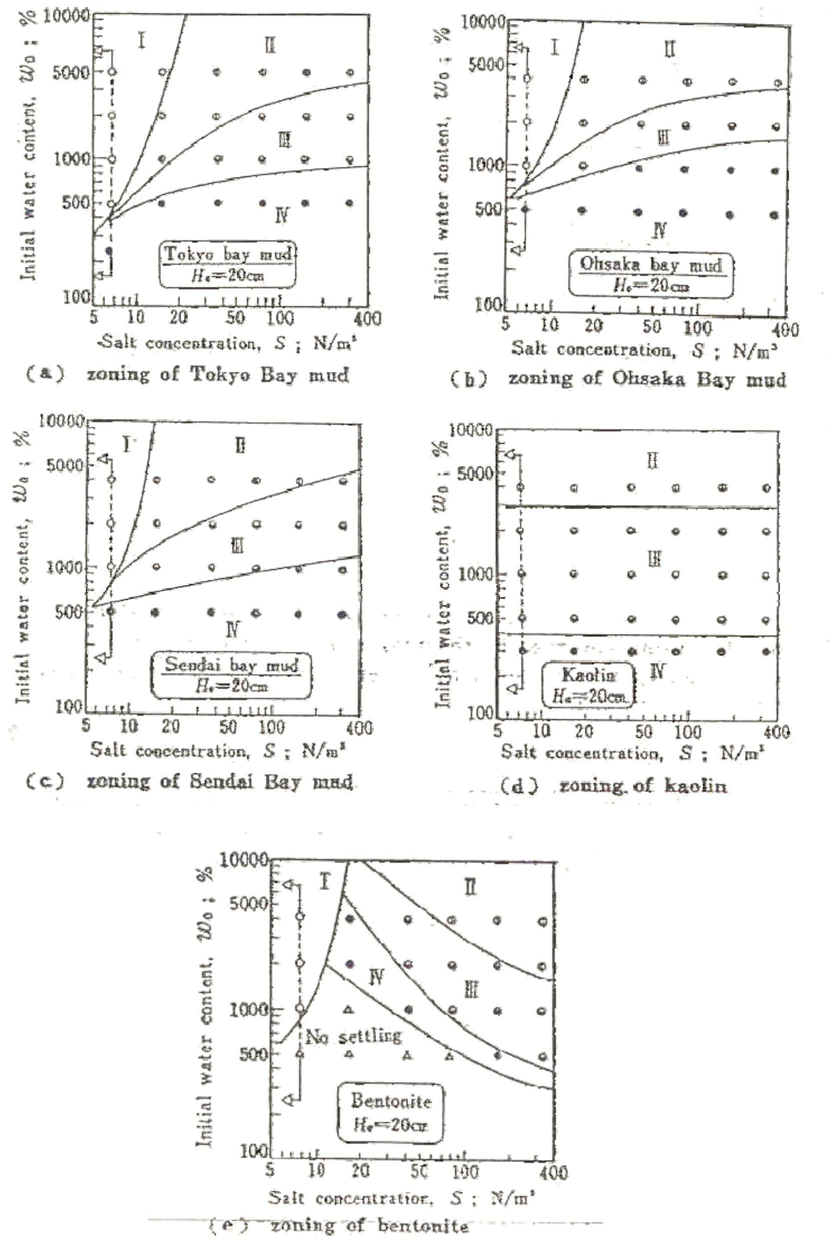

Figure 2.1 Different settling types for different soils (Imai 1980).

From Fig. 2.1 illustrates that, for the case of kaolinite clay soils, the settling behavior of soil particles follows the consolidation settling process, when the initial water content is below 400 ~ 500%. The settling type does not differ because the electrical attractions between kaolinite particles are relatively smaller than the effect of its own gravitation under a relatively low initial water content. However, the ionic concentration affects the double layer thickness and particle contact characteristics, resulting in the formation of a soil structure. Therefore, the in-situ ionic concentration must be confirmed in a laboratory simulation.

The general characteristics of sedimentation of a clay-water mixture are shown in Fig. 2.2.

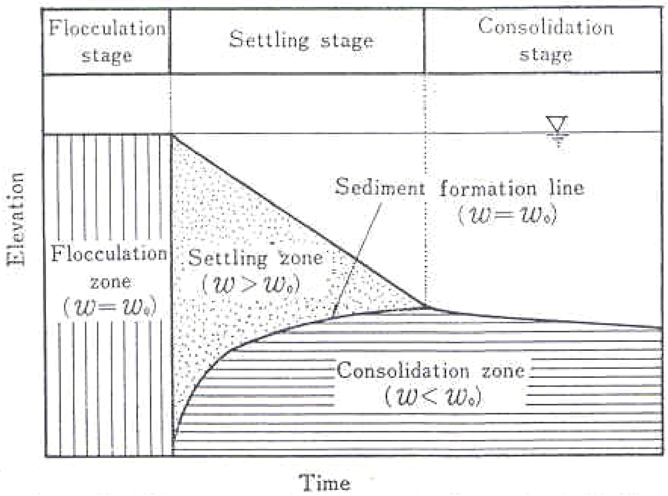

Figure 2.2 General characteristics of sedimentation of a clay-water mixture (Imai 1981).

Fig. 2.2 shows that the self-weight consolidation process starts at the bottom of the soil layer from the beginning of sedimentation. Therefore, the settling and the self weight consolidating coexist during the settling stage. The shock boundary, where the particle settling velocity shows an abrupt decrease, between the settling zone and the consolidation zone is well predicted by FEM programming (Lee et al. 2000). However, when the settling stage is short enough to be ignored, the self-weight consolidation process is dominant in terms of characterizing the sedimentation behavior.

In the case of kaolinite clay, one of the most commonly used dredge materials for reclamation in Korea, the characterization of reclaimed sites must focus on the self-weight consolidation.

2.3 One Dimensional Consolidation Theory

2.3.1 Terzaghi Soil Mechanics for Consolidation

Consolidation can be defined as “every time-dependent process involving a decrease of the water content of a saturated soil without replacement of the water by air” (Terzaghi 1943). The consolidation process can be described as time-dependent volumetric compression induced by an applied load. The opposite process – volume extension according to the increase of water content – is called a swelling process.

Terzaghi’s theory is based on several assumptions:

(1) The soil layer is completely saturated.

(2) Both water and soil particles of the soil are incompressible.

(3) Darcy’s law is valid

(4) The permeability (k) / coefficient of consolidation (C_v) is constant during consolidation.

(5) Time lag of consolidation is due entirely to the low permeability of the soil.

The ratio of void volume contraction due to effective stress increment is referred to as the compression index, C_c.

$$C_c = \frac{e_i - e_f}{\log \sigma'_f - \log \sigma'_i} = \frac{\Delta e}{\log(\sigma'_f / \sigma'_i)} \tag{2.5}$$

where e is the void ratio, σ′ is the effective stress, the sub index i = the initial state, and the sub index f = the final state.

The swelling index (C_s) is clearly smaller than the compression index. The swell index is almost the same as the recompression index (C_r) of unloaded / over-consolidated soils. The swelling index is defined as the slope of the effective stress – void ratio curve during an unloading process.

$$C_s = \frac{e_r - e_c}{\log(\sigma'_c / \sigma'_r)} \tag{2.6}$$

where σ'_r is the effective stress state after unloading, e_r is the void ratio after unloading, σ'_c is the pre-consolidated effective stress, and e_c is the void ratio at the pre-consolidated state.

The basic differential equation of Terzaghi's consolidation theory is derived as follows (Terzaghi 1923):

$$\frac{\partial u}{\partial t} = \frac{k}{\gamma_w m_v} \frac{\partial^2 u}{\partial z^2} = C_v \frac{\partial^2 u}{\partial z^2} \tag{2.7}$$

where k is the coefficient of permeability, γ_w is the unit weight of water, u is the pore water pressure, and

$$C_v = \text{coefficient of consolidation} = \frac{k}{\gamma_w m_v} \tag{2.8}$$

$$m_v = \text{coefficient of volumetric compressibility} = \frac{a_v}{1+e} \tag{2.9}$$

$$a_v = \text{coefficient of compressibility} = -\frac{\partial e}{\partial(\Delta\sigma')} \tag{2.10}$$

The void volume change is related to the dissipation of the pore water pressure existing in voids. The pore water pressure distribution inside a soil layer is defined as:

$$u = \sum_{m=0}^{m=\infty} \frac{2u_o}{M} \sin\frac{Mz}{H} e^{\left(-M^2 T_v\right)} \tag{2.11}$$

where m is an integer, u_o is the average pore water pressure, and

$$M = (2m+1)\frac{\pi}{2} \tag{2.12}$$

$$T_v = \text{nondimensional time factor} = \frac{C_v t}{H_{dr}{}^2} \tag{2.13}$$

where H_{dr} is the length of the maximum average drainage path.

The degree of consolidation is defined as the ratio of the amount of excess pore water pressure dissipated due to the initial maximum excess pore water pressure (u_i):

$$U_z = \frac{u_i - u}{u_i} = \frac{\Delta\sigma'}{u_i} \tag{2.14}$$

Meanwhile, in the case of a constant pore water pressure distribution with depth

(u_i=u_o), and upward and downward drain (H=2H_{dr}), the average degree of consolidation for the entire layer is given by

$$U_{av} = \frac{\frac{1}{H}\int_0^H u_i dz - \frac{1}{H}\int_0^H u dz}{\frac{1}{H}\int_0^H u_i dz} \tag{2.15}$$

The average degree of consolidation can be expressed as a function of the time factor (T_v) by combining Eqs. 2.11 and 2.15.

$$U_{av} = 1 - \sum_{m=0}^{m=\infty} \frac{2}{M^2} e^{-M^2 T_v} \tag{2.16}$$

The following equations are used to approximate T_v from Eq. 2.13 (Terzaghi 1943).

For U_{av} = 0 ~ 53 % : $T_v = \frac{\pi}{4}\left(\frac{U_{av}\%}{100}\right)^2$ (2.17)

For U_{av} = 53 ~ 100 % : $T_v = 1.781 - 0.933\left[\log(100 - U_{av}\%)\right]$ (2.18)

The variation of T_v with U_{av} is shown in Table 2.2.

As the time factor is a function of the average degree of consolidation, the coefficient of consolidation can be expressed as a function of the average degree of consolidation by substituting Eqs. 2.17 and 2.18 into Eq. 2.13.

$$C_v = \frac{H_{dr}^{\ 2}}{t} T_v = \frac{H_{dr}^{\ 2}}{t} \cdot \frac{\pi}{4} \left(\frac{U_{av}(\%)}{100} \right)^2 \qquad \text{for } \mathrm{U_{av}} = 0 \sim 53\%$$

$$= \frac{H_{dr}^{\ 2}}{t} \cdot \left[1.781 - 0.933 \{ \log(100 - U_{av}\%) \} \right] \quad \text{for } \mathrm{U_{av}} = 53 \sim 100\% \tag{2.19}$$

Table 2.2 Variation of T_v with U_{av}.

U(%)	T_v	U(%)	T_v	U(%)	T_v	U(%)	T_v
0	0	26	0.0531	51	0.204	76	0.493
1	0.00008	27	0.0572	52	0.212	77	0.511
2	0.0003	28	0.0615	53	0.221	78	0.529
3	0.00071	29	0.0660	54	0.230	79	0.547
4	0.00126	30	0.0707	55	0.239	80	0.567
5	0.00196	31	0.0754	56	0.248	81	0.588
6	0.00283	32	0.0803	57	0.257	82	0.610
7	0.00385	33	0.0855	58	0.267	83	0.633
8	0.00502	34	0.0907	59	0.276	84	0.658
9	0.00636	35	0.0962	60	0.286	85	0.684
10	0.00785	36	0.102	61	0.297	86	0.712
11	0.0095	37	0.107	62	0.307	87	0.742
12	0.0113	38	0.113	63	0.318	88	0.774
13	0.0133	39	0.119	64	0.329	89	0.809
14	0.0154	40	0.126	65	0.304	90	0.848
15	0.0177	41	0.132.	66	0.352	91	0.891
16	0.0201	42	0.138	67	0.364	92	0.938
17	0.0227	43	0.145	68	0.377	93	0.993
18	0.0254	44	0.152	69	0.390	94	1.055
19	0.0283	45	0.159	70	0.403	95	1.129
20	0.0314	46	0.166	71	0.417	96	1.219
21	0.0346	47	0.173	72	0.431	97	1.336
22	0.0380	48	0.181	73	0.446	98	1.500
23	0.0415	49	0.188	74	0.461	99	1.781
24	0.0452	50	0.197	75	0.477	100	∞
25	0.0491						

2.3.2 Mikasa's Consolidation Theory

Terzaghi's governing equation for consolidation (Eq. 2.7) is based on the assumption that the coefficient of volume compressibility (m_v), the coefficient of consolidation (C_v), and the permeability (k) are constant during the consolidation process. However, these assumptions constitute the weak points of Terzaghi's consolidation theory. In reality, the permeability and coefficient of consolidation decrease as the layer thickness decreases. Therefore, Mikasa (1963) suggested an equation in the strain term, considering the permeability and volumetric compressibility change during consolidation:

$$\frac{\partial \varepsilon}{\partial t} = C_v \frac{\partial^2 \varepsilon}{\partial a^2} \tag{2.20}$$

where ε is the compression strain and a is the layer thickness. However, the assumption that the coefficient of consolidation remains constant during consolidation is still made in Mikasa's theory.

The consolidation ratio (ζ) considering the thickness change was derived as:

$$\zeta = \frac{\delta z_i}{\delta z} = \frac{1 + e_i}{1 + e} \tag{2.21}$$

where δz_i is the initial thickness before consolidation, and δz is the present thickness of the layer. Eq. 2.21 is then transformed to a second partial derivative governing equation by substituting Eq. 2.21 into Eq. 2.20:

$$\frac{\partial \zeta}{\partial t} = C_v \zeta^2 \frac{\partial^2 \zeta}{\partial z_o{}^2} \tag{2.22}$$

$\zeta \fallingdotseq 1$ when the amount of consolidation is small, and thus Eq. 2.22 becomes similar to Eq. 2.7. However, the ζ^2 term in Eq. 2.22 shows that Mikasa's theory has good applicability in terms of the nonlinearity behavior of large strain consolidation processes, particularly for weak clay sediments.

The average degree of consolidation is also based on the strain concept. When ε_o is the present strain and ε_f is the final strain, the degree of consolidation is defined as:

$$U_{av} = \frac{\varepsilon_o}{\varepsilon_f} \tag{2.23}$$

The final strain value estimation is important for Mikasa's theory. The non-dimensional time factor (T_v) according to the degree of consolidation is determined when the final strain value is defined. Therefore, the non-dimensional time factor varies with different ε_f values. In other words, the time factor decreases as the final strain level increases. Moreover, the time factor value becomes similar to the values of Terzaghi's theory when the final strain level approaches to zero, which means that the layer is no longer compressible (Ju et al 2003).

2.3.3 One-Dimensional Consolidation Theory for Large Strains

As Mikasa's theory is effectively applicable to the self-weight consolidation process of sedimentation, one-dimensional consolidation theories for large strains can be employed to explain the self-weight consolidation behavior.

Gibson et al (1967) derived a governing equation for large strain consolidation employing the assumptions that the soil particles are homogeneous and time effects such as bonding, cementation, etc. are avoided.

$$\left(\frac{\gamma_s}{\gamma_w}-1\right)\frac{d}{de}\left(\frac{k}{1+e}\right)\frac{\partial e}{\partial z}+\frac{\partial}{\partial z}\left[\frac{k}{\gamma_w(1+e)}\frac{d\sigma'}{de}\frac{\partial e}{\partial z}\right]+\frac{\partial e}{\partial t}=0 \qquad (2.24)$$

where γ_s is the unit weight of solid soils, and γ_w is the unit weight of water. In Eq. 2.24, the permeability (k) and effective stress (σ') are defined as a function of the void ratio:

$$k = k(e) \qquad (2.25)$$

$$\sigma' = \sigma - u = \sigma'(e) \qquad (2.26)$$

The effective stress at a certain depth (z) and time (t) during consolidation is:

$$\sigma'(z,t) = -\frac{1}{\lambda}\ln\left[\frac{e(z,t)-e_f}{e_i-e_f}\right] \qquad (2.27)$$

where e_i is the initial void ratio, e_f is the void ratio when consolidation is finished, *e(z,t)* is the present void ratio, and the relation between the void ratio and effective stress λ is defined as follows (Gibson et al. 1981):

$$\lambda(e) = -\frac{d}{de}\left(\frac{de}{d\sigma'}\right) \tag{2.28}$$

A more general form of the effective stress can be stated as (Pane and Schiffman 1985):

$$\sigma = \beta(e)\sigma' + u \tag{2.29}$$

where the interaction coefficient function $\beta(e)$ is shown in Fig. 2.3. Note that e_m is the maximum void ratio and e_s is the minimum void ratio.

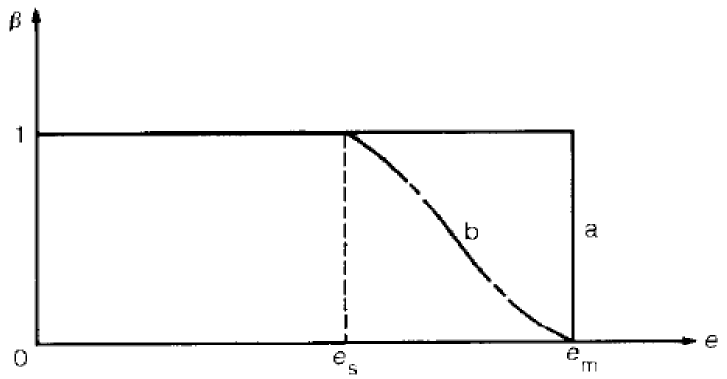

Figure 2.3 Forms of the β constitutive relationship (Pane and Schiffman 1985).

Two kinds of constitutive relations between β and e are shown in Fig. 2.3. The general case (b) shows that the interaction coefficient is a continuous function of e, while case (a) remains constant between e_m and e_s. Therefore, the finite strain governing equation (Eq. 2.24) can be expanded as:

$$\left(\frac{\gamma_s}{\gamma_w}-1\right)\frac{d}{de}\left(\frac{k}{1+e}\right)\frac{\partial e}{\partial z} + \frac{\partial}{\partial z}\left[\frac{k}{\gamma_w(1+e)}\beta\frac{d\sigma'}{de}\frac{\partial e}{\partial z}\right]+\frac{\partial}{\partial z}\left[\frac{k}{\gamma_w(1+e)}\frac{d\beta}{de}\sigma'\frac{\partial e}{\partial z}\right]+\frac{\partial e}{\partial t}=0 \tag{2.30}$$

Most self weight consolidating soils have high initial water content. Thus, the initial void ratio is much larger than e_m:

$$\frac{d\beta}{de}=0 \tag{2.31}$$

The governing equation for sedimentation and self-weight consolidation is then simplified by combining Eqs. 2.30 and 2.31.

$$\left(\frac{\gamma_s}{\gamma_w}-1\right)\frac{d}{de}\left(\frac{k}{1+e}\right)\frac{\partial e}{\partial z}+\frac{\partial e}{\partial t}=0 \tag{2.32}$$

As the permeability is an important parameter in Eq. 2.32, Lee and Sills (1981) suggested a linear void ratio – effective stress – permeability equation as follows:

$$k = \rho_f k_o (1 + e) \tag{2.33}$$

where ρ_f is the fluid density and k_o is constant. Pane and Schiffman (1997) determined the permeability as:

$$k(e) = \frac{v_{si}(1 + e)}{\gamma^*} \tag{2.34}$$

where v_{si} is the initial settling velocity of the solids. The non-dimensional constant γ^* is given by

$$\gamma^* = \frac{\gamma_s - \gamma_w}{\gamma_w} \tag{2.35}$$

Pradhan et al (1995) observed that the void ratio change is significant at the beginning of self-weight consolidation, and abruptly decreases after the yielding point. Therefore, the void ratio should be measured very carefully for reliable evaluation.

The coefficient of consolidation (C_v) is given as (Been and Sills 1981):

$$C_v = -\frac{k}{\rho_f (1 + e)} \frac{d\sigma'}{de} \tag{2.36}$$

2.3.4 Undrained Shear Strength

Empirical equations related to the undrained shear strength (S_u) and overburden effective stress (σ') for normally-consolidated clays were suggested by Skempton (1957) and Chandler (1988).

$$\frac{S_{u(VST)}}{\sigma'} = 0.11 + 0.0037\mathrm{PI} \tag{2.37}$$

$$\frac{S_{u(VST)}}{\sigma'_c} = 0.11 + 0.0037\mathrm{PI} \tag{2.38}$$

where $S_{u(VST)}$ is the undrained shear strength from a vane shear test and σ'_c is the pre-consolidation stress. Jamiolkowski et al (1985) derived an equation for slightly over consolidated clays:

$$\frac{S_u}{\sigma'_c} = 0.23 \pm 0.04 \tag{2.39}$$

Ladd et al (1977) proposed an equation related to the over consolidation ratio (OCR):

$$\frac{(S_u / \sigma')_{\text{Over Consolidated}}}{(S_u / \sigma')_{\text{Normally Consolidated}}} = (OCR)^{0.8} \tag{2.40}$$

However, it is hard to generalize the relation between undrained shear strength and effective stress, because the undrained shear strength differs according to the soil type and material composition. Therefore, empirical methods using experimental results are considered the optimal approach to deriving an equation for the undrained shear strength and effective stress.

2.3.5 Discussions

The critical parameters for the characterization of sedimentation behavior are summarized as follows:

- Initial solid / ionic concentration for the settling behavior.
- Void ratio condition for the self-weight consolidation process.

In the case of kaolinite clay, the settling time is relatively short, and thus the self-weight consolidation process is dominant.

The void ratio is related to the effective stress in soft clay. Therefore, accurate estimation of the void ratio / effective stress is fundamental to the characterization of the in-situ properties.

Settlement observation, pore water pressure measurement, cone penetration test (CPT), etc. are commonly used to estimate the in-situ consolidation behavior. However, Schiffman et al (1984) found that the degree of settlement precedes the degree of pore water pressure dissipation, which means that settlement monitoring overestimates the degree of consolidation of the soft soil. Moreover, conducting pore pressure measurements using cone penetration testing or pore pressure gages precludes several error factors, such as the tidal effect and soil disturbance, that can yield unsatisfactory results. Accordingly, a new and effective technique is required to monitor the effective stress of soft clays.

2.4 Shear Wave Characteristics of Clay

2.4.1 Effective Stress and Shear Wave Velocity

In a continuous medium, the state of confining stress has a minimal effect on the stiffness of the material. On the other hand, the stiffness of a structure in particulate materials is determined by the effective stress condition (Santamarina, et al. 2001).

A shear wave has a good applicability for clays, because it propagates only through the soil skeleton, and its velocity depends on the effective stress of the soil. The shear wave velocity of particulate materials under a zero lateral strain loading (one-dimensional consolidation) can be expressed in terms of the vertical effective stress as follows (Hardin and Richart 1963; Santamarina, et al. 2001):

$$V_s = \alpha_1 \left(\frac{\sigma'_m}{1\text{kPa}} \right)^{\beta} = \alpha_1 \left(\frac{(1+K_o)\sigma'_v}{2\text{kPa}} \right) = \alpha_1 \left(\frac{1+K_o}{2} \right)^{\beta} \left(\frac{\sigma'_v}{1\text{kPa}} \right)^{\beta} = \alpha \left(\frac{\sigma'_v}{1\text{kPa}} \right)^{\beta} \quad (2.41)$$

where V_s is the shear wave velocity, σ'_m is the mean effective stress, σ'_v is the vertical effective stress, K_o is the coefficient of earth pressure at rest, and the parameters α (shear wave velocity at 1kPa) and β are experimentally determined. Generally, in clays, a higher plasticity index is associated with an accordingly higher β exponent and lower α factor. Preloading and aging have the opposite effects (Fig. 2.4). The inverse relationship between α and β is expressed as (Santamarina, et al. 2001):

$$\beta \approx 0.36 - \frac{\alpha}{700} \quad (2.42)$$

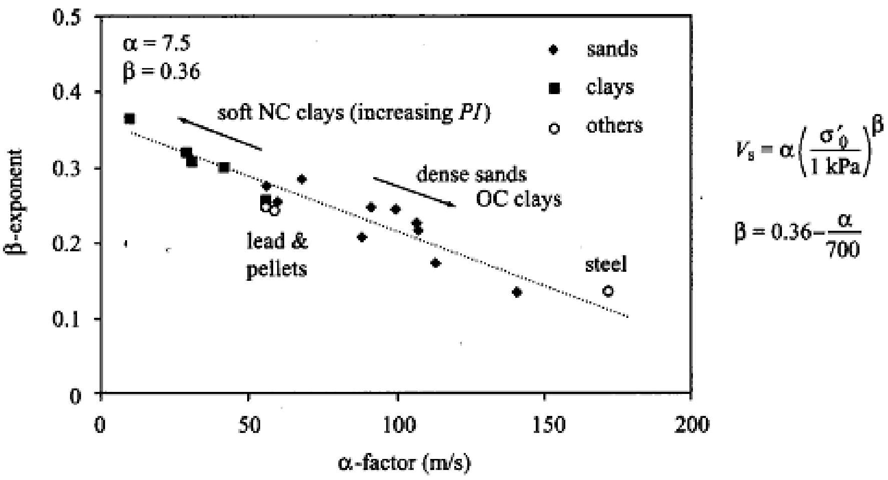

Figure 2.4 Typical values for α and β coefficients (Santamarina, et al. 2001)

2.4.2 Void Ratio and Shear Wave Velocity

The α parameter in Eq. 4.41 involves two different properties: consideration of the grains and the packing effect. The packing effect is related to the void ratio or coordination number of contacts. Therefore, Hardin and Richart (1963), and Hardin and Drnevich (1972) rewrote the shear wave velocity – effective stress equation as:

$$V_s = \alpha\left(\frac{\sigma'_v}{1\text{kPa}}\right)^\beta = AF_e\left(\frac{\sigma'_v}{1\text{kPa}}\right)^\beta \tag{2.43}$$

where the void ratio homogenization factor F_e for sand, which can be expressed as follows:

$$F_e = \frac{(2.17-e)^2}{(1+e)} \quad \text{round particles} \tag{2.44}$$

$$F_e = \frac{(2.97 - e)^2}{(1+e)} \quad \text{angular particles} \tag{2.45}$$

In the case of normally-consolidated clays, the void ratio is intimately related to the effective stress in terms of the compression index. Therefore, F_e itself can be expressed as a function of σ'_v. However, the void ratio – effective stress relation for over-consolidated clays follows the re-compressing curve (slope: swelling index), which differs from the normal compression curve (slope: compression index). Therefore, Eq. 2.43 is modified by eliminating F_e and considering the over consolidation ratio, OCR.

$$\text{OCR} = \frac{\text{pre - consolidated effective stress}}{\text{current effective stress}} = \frac{\sigma'_p}{\sigma'_o} \tag{2.46}$$

$$V_s = A_1 \left(\frac{\sigma'_v}{1\text{kPa}} \right)^{\beta} (\text{OCR})^m \tag{2.47}$$

Correlations between A_1, m and β with the plasticity index can be found in Hardin (1978) and Viggiani and Atkinson (1995).

Fig. 2.5 shows the shear wave velocity data for kaolinite with different void ratio conditions. The figure shows a clear trend for the shear wave velocity – porosity relation during the whole clay phase. Therefore Eq. 2.43 can be expressed in terms of the void ratio rather than F_e.

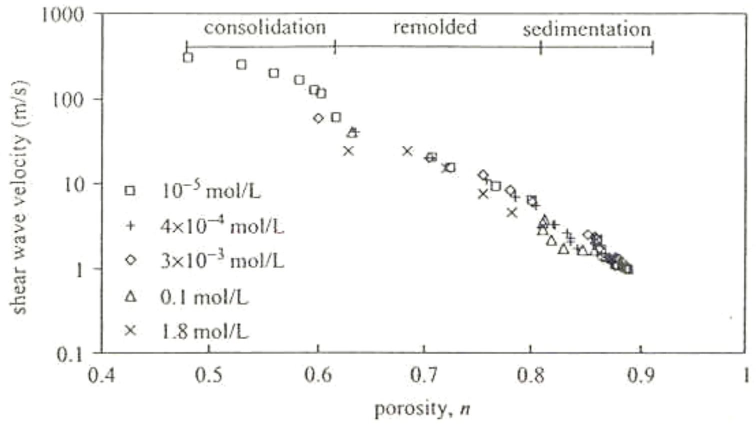

Figure 2.5 Shear wave velocity – porosity relationship for various mixtures of kaolinite clay (Santamarina, et al. 2001).

2.4.3 Bender Element Sensors

The bender element is a double layered piezoelectric transducer that consists of two conductive outer electrodes, two piezoelectric material sheets, and a conductive metal shim at the center (Fig. 2.6(a)). The piezoelectric materials used in bender elements, such as quartz or ceramics, expand or shrink when an electrical potential is applied, depending on their type.

There are two types of bender element operation: series and parallel. In the series type, the bender element is connected at the outer electrodes: thus, each piezoceramic sheet has a different poling direction. Therefore, the bender element has dual direction mobility (Fig. 2.6(b)). The parallel type bender is connected with core wire at the intermediate metal shim, while the outside electrodes are used for grounding. Therefore, the parallel type bender has single mobility (Fig. 2.6(c)).

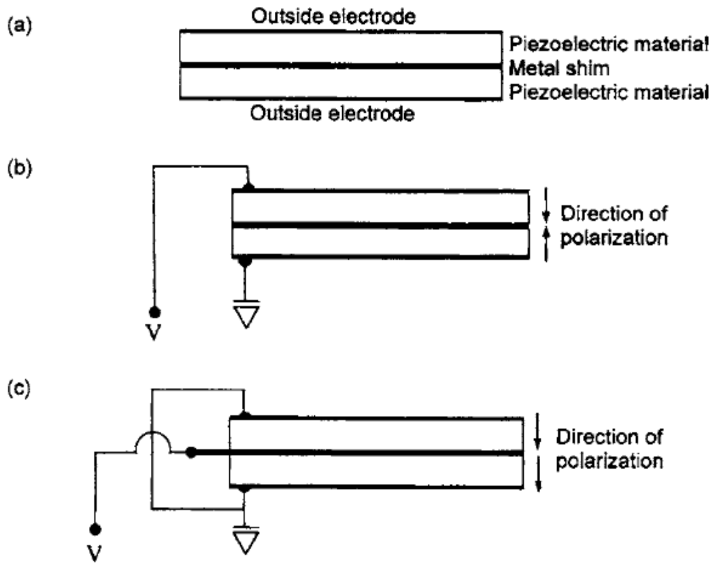

Figure 2.6 Bender elements: (a) schematic representation of bender element, (b) series type, and (c) parallel type (Lee and Santamarina 2005).

For the same applied voltage power, the parallel type provides twice the mobility of the series type connection. Thus, parallel bender elements are recommended for use as the source and the series type as the receiver.

Since Shirley and Hampton (1978) initially applied a bender element to soil testing, bender elements have been widely used in this field, primarily owing to their good coupling with most soils, acceptable directivity, and wide operating frequency range. Dyvik and Madshus (1985) demonstrated the agreement between G_{max} estimated by bender elements and that obtained by resonant column testing. Accordingly, bender elements have been used to characterize various soils using shear wave techniques in the geotechnical engineering field.

CHAPTER III
EVALUATION OF THE CONSOLIDATION STATE OF SOFT SOILS USING SHEAR WAVES

3.1 INTRODUCTION

The stress history of a clay deposit in nature is summarized as a repeating process of loading and unloading. The volumetric strain depending on the stress variation is related to the compression index and swelling index, as discussed in section 2.3.1. However, the selected values for the compression index or swelling index for predicting the deformation that corresponds to additional loading can lead to very different consolidation behaviors of the soil. The inflection point, which divides the effective stress–strain (σ'-ε) curve into a virgin compressing and reloading zone, is defined as the pre-consolidated effective stress (σ'_c). The relationship between the present effective stress state (σ'_o) and the maximum pre-consolidated effective stress (σ'_c) under which the site underwent is defined as the over-consolidated ratio (*OCR*). The in-situ consolidation state can be classified into three states: over-consolidated, normally-consolidated, and under-consolidated.

Casagrande (1936) suggested an iconographic method to determine the pre-consolidation pressure. However, the iconography may render an unreliable result, because it depends on personal judgment by visual observation. Therefore, a more accurate method to evaluate the in-situ pre-consolidated effective stress and consolidation condition is required for reliable predictions and economical construction designs. The relationship between effective stress and shear wave velocity has already been discussed in the literature review (Ch. 2.4).

In this chapter, laboratory consolidation tests using bender element sensors are presented to evaluate the relationship between the effective stress and shear wave velocity for several different clay layers. The shear wave velocity of the in-situ pre-consolidated effective stress state is evaluated by comparing the in-situ density profile with the relationship between the effective stress and the shear wave velocity. Furthermore, the consolidation condition is estimated after a comparison between the in-situ shear wave velocity and the laboratory test results. Likewise, the in-situ void ratio is predicted from the in-situ shear wave velocity.

3.2 EXPERIMENTAL PROGRAM

3.2.1 Site of Interest

Silty kaolinite clay is the most common type of clay deposit observed in Korea. The clays used for this study were sampled from three different sites in Korea. The sampled sites represent the foreshore site, submarine deposit, and thick clay deposit, respectively. Even though the types of the sampled soils were similar, their site formation processes were different. Therefore, each specimen comprised properties of the most typical deposit types in nature. The details of each site are as follows.

Foreshore – Incheon

The site was programmed for coastal road construction. Consistent with the tidal effect, the foreshore site is saturated during the floodtide and is partially unsaturated during ebbtide. A 13m-thick silty clay layer exists between the thin reclaimed surface and the underlying gravel deposit (Fig. 3.1). Therefore, the site evaluation focused on the clay layer.

The density profile shown in Fig. 3.2 is relatively higher than those of the other two sites. This effect is caused by the settling condition of the site. Usually, the foreshore forms near an estuary, where only relatively heavy particles can settle down, while small particles are still affected by the drift. Therefore, the deposit is composed of dense particles. Meanwhile, the drag force during the unsaturated condition by ebbtide, has a densification effect on the particle composition.

The Shelby tube method was used for sampling the 3.0m, 4.5m, 5.5m, and 7.5m point specimens. An in-situ shear-wave velocity profile, measured via a seismic cone penetration test, is shown in Fig. 3.2.

Submarine Deposit – Busan

This natural clay was deposited under the seawater level at the sampled site where a reclamation is planned. The layer and density profile from an in-situ RI-meter test is shown in Fig. 3.3. The N value shows that the soil type under 30m depth may be sand or other type of coarse soil. Therefore, the in-situ consolidation characterization focused on the 30m-thick clay layer existing on the top of the site.

The Shelby tube method was used for sampling the 5.0m, 15.0m, and 28.0m point specimens. An in-situ shear-wave velocity profile, derived via an SPS-logging test, is shown in Fig. 3.3.

Thick Clay Deposit – Busan

This thick clay deposit, which was planned for harbor construction work, required a state evaluation for consolidation, to predict the settling behavior during construction. The in-situ density and shear wave velocity, via an SPS-logging distribution, is shown in Fig. 3.4. Both data show that the soft clay layer was quite thick (30m). Therefore, specimens were sampled from 5.0m, 10.0m, 15.0m, 20.0m, 25.0m, and 30.0m by means of a Shelby tube sampler.

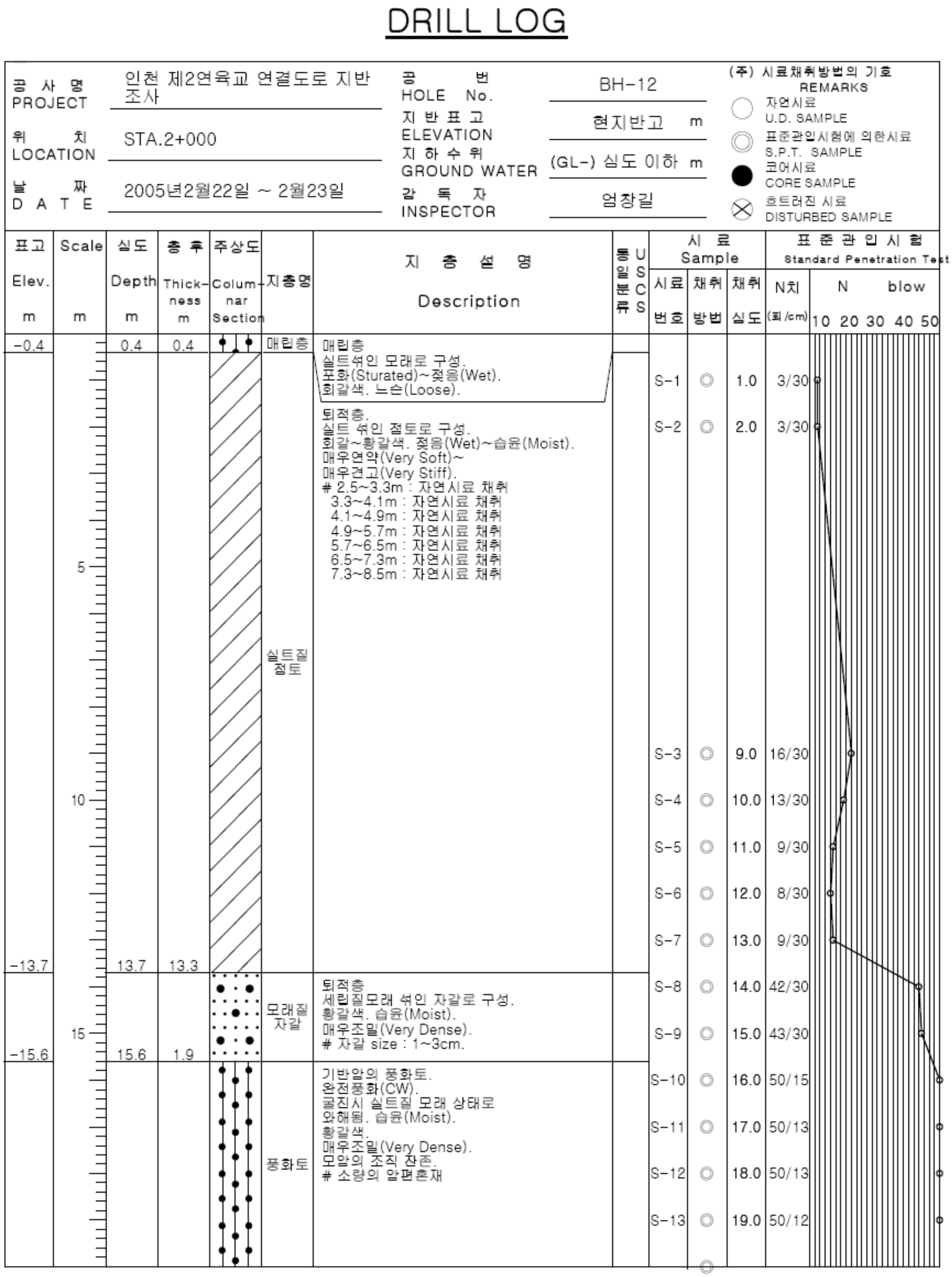

Figure 3.1 Layer profile of the foreshore site in Incheon.

Seismic Cone Penetration Test Result

Project	인천 제2연육교 연결도로 지반조사	Hole No.	SCPT-2
Location	--교	Data	2005-2-2

Depth (m)	Density (ρ)* (g/cm^3)	Vs (m/sec)	Accuracy	Gd** $(tonf/m^2)$
1.0 ~ 2.0	1.79	130	0.86	3.087E+03
2.0 ~ 3.0	1.79	100	0.83	1.827E+03
3.0 ~ 4.0	1.79	110	0.87	2.222E+03
4.0 ~ 5.0	1.79	123	0.89	2.741E+03
5.0 ~ 6.0	1.84	118	0.83	2.592E+03
6.0 ~ 7.0	1.83	140	0.76	3.660E+03
7.0 ~ 8.0	1.83	121	0.71	2.752E+03
8.0 ~ 9.0	1.82	128	0.78	3.043E+03
9.0 ~ 10.0	1.83	135	0.93	3.403E+03
10.0 ~ 11.0	1.82	133	0.94	3.285E+03
11.0 ~ 12.0	1.84	127	0.86	3.028E+03
12.0 ~ 13.0	1.84	135	0.87	3.422E+03
13.0 ~ 14.0	1.84	153	0.72	4.395E+03
14.0 ~ 15.0	1.84	148	0.83	4.113E+03
15.0 ~ 16.0	1.84	155	0.89	4.511E+03
16.0 ~ 17.0	1.89	165	0.70	5.251E+03
17.0 ~ 18.0	1.85	162	0.81	4.954E+03
18.0 ~ 19.0	1.84	160	0.83	4.807E+03
19.0 ~ 20.0	1.84	145	0.86	3.948E+03
20.0 ~ 21.0	1.84	154	0.84	4.453E+03
21.0 ~ 22.0	1.84	158	0.82	4.687E+03
22.0 ~ 23.0	1.84	160	0.87	4.807E+03

Shear wave velocity (m/sec)

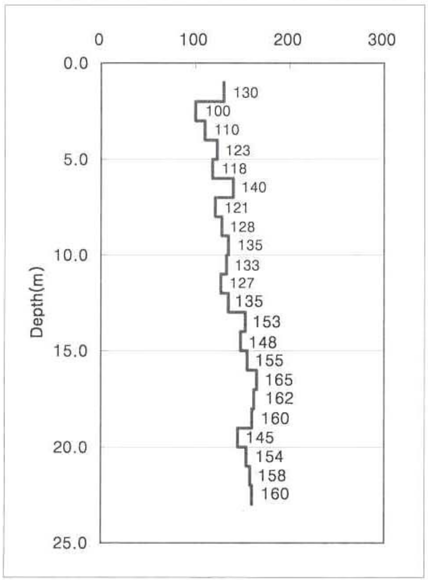

Dynamic shear modulus $(tonf/m^2)$

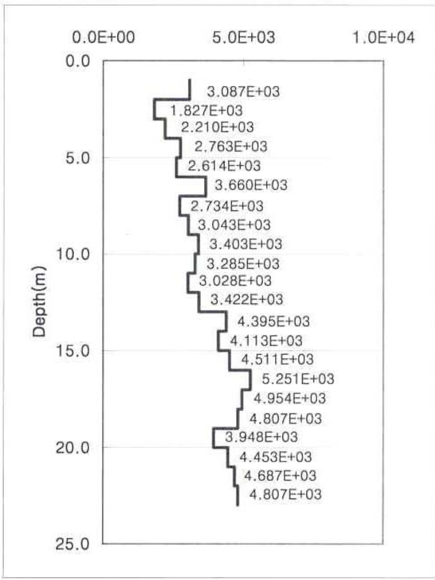

Figure 3.2 Seismic cone penetration test result of the foreshore site, Incheon.

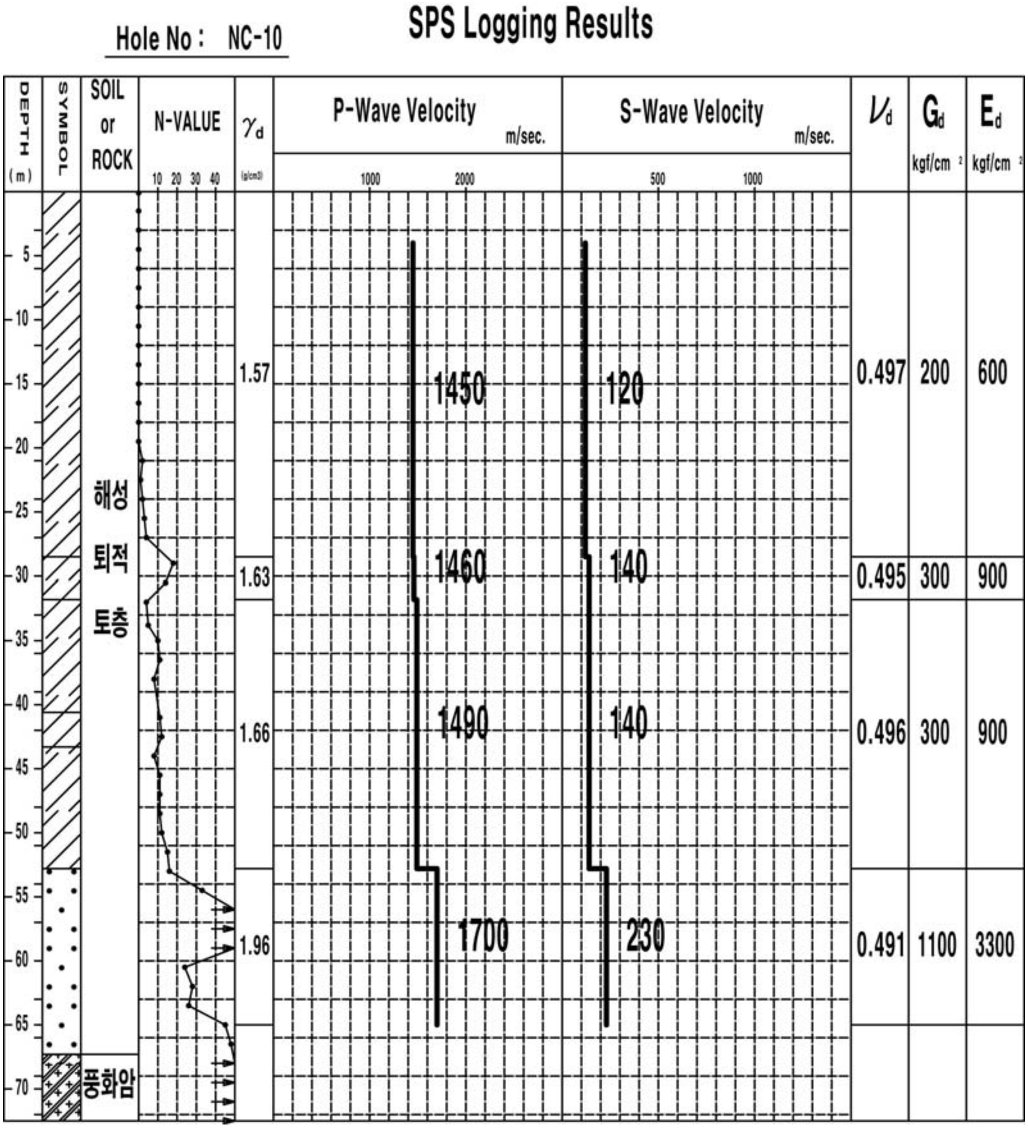

Figure 3.3 Layer profile and SPS-logging result of the submarine deposit, Busan.

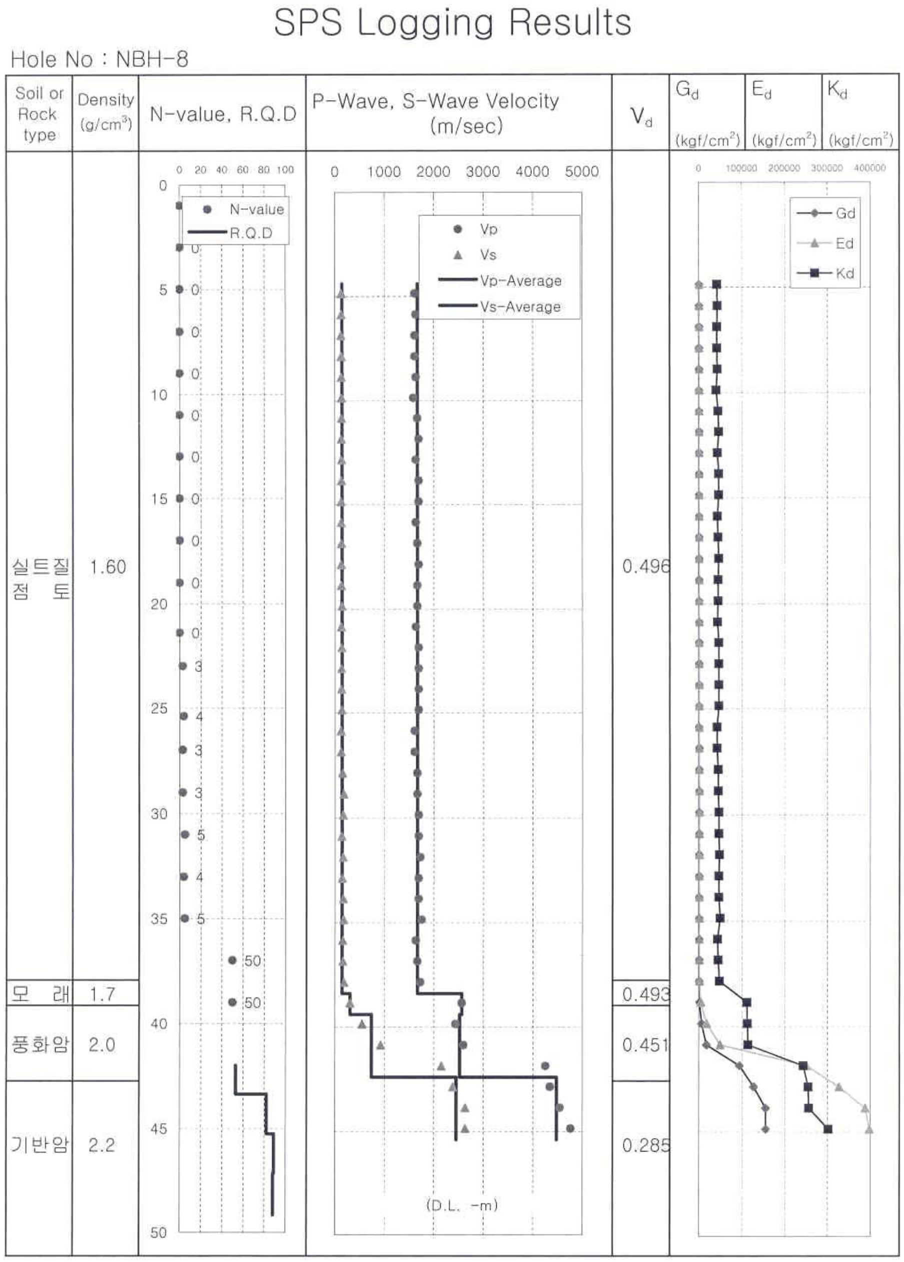

Figure 3.4 Layer profile and SPS-logging result of the thick clay deposit, Busan.

3.2.2 Shelby Tube Consolidation Testing Device

Bender element sensors

The bimorph bender element used in this study was 12mm in length, 8mm in width, and 0.6mm in thickness. The anode and cathode wires of a coaxial cable were soldered to each side of the bender element; therefore, a series type bender element was applied. Polyurethane was coated around the surface of the bender element for waterproofing. Then, a silver paste was layered on the surface to shield against the effect of coupling and cross-talking induced by unwanted electro-magnetism. Finally, the bender elements were mounted on the testing device and fixed with epoxy (Fig. 3.5). Details regarding bender element installation and signal interpretation can be found in Lee and Santamarina (2005).

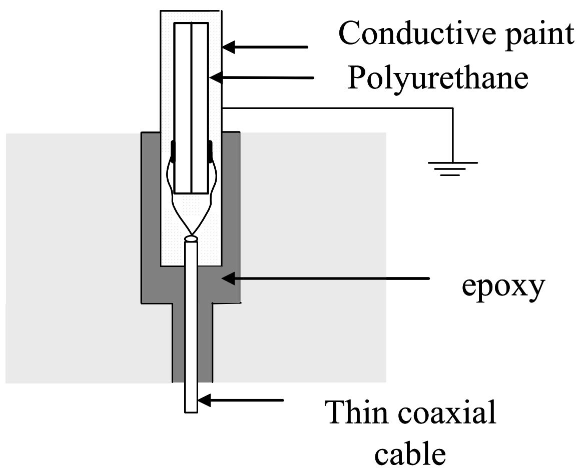

Figure 3.5 Installation of a series type bender element.

Shelby tube oedometric device

An improved oedometric consolidation test type was introduced to characterize the in-situ consolidation behavior. Conventional oedometric consolidation tests can disturb a specimen during both extraction from the Shelby tube and injection into the oedometric cell. Therefore, minimizing specimen disturbance is a key point for accurate in-situ condition simulation in laboratory testing. The Shelby tube for the oedometric cell was used in this study to obtain an undisturbed sample.

With conventional methods, the deformation, or sometimes the pore water pressure, is measured during a consolidation test. However, in this study, piezoelectric bender element sensors were installed at the top and bottom of the specimen to measure the vertical shear wave velocity variation.

A standard Shelby tube is 74mm in diameter. Therefore, the bottom plate was designed for a bottom bender element housing and Shelby tube fixing (Fig. 3.6). The top load cap was designed for two purposes: to apply a uniformly distributed stress to the specimen in the Shelby tube and to fix the bender element sensor. Even though it is recommended to make the cap as light as possible, the acrylic load cap was designed to be 30mm in height for durability and 73mm in diameter for good mobility inside the Shelby tube, with no friction between the tube (Fig. 3.7). Both the bottom plate and top load cap were designed to have vertical drainage holes, which were drilled to allow upward and downward drainage during laboratory consolidation tests. Porous material filters were placed above the drain holes to prevent particle loss.

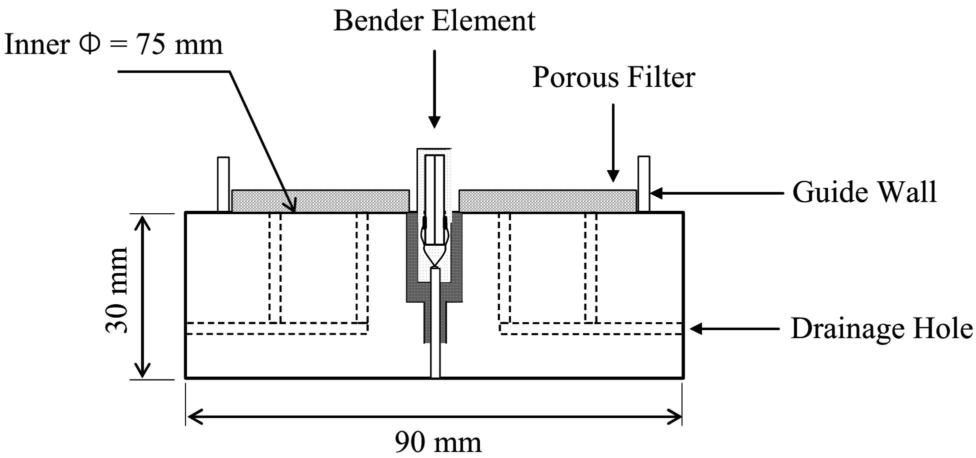

Figure 3.6 Configuration of the bottom plate.

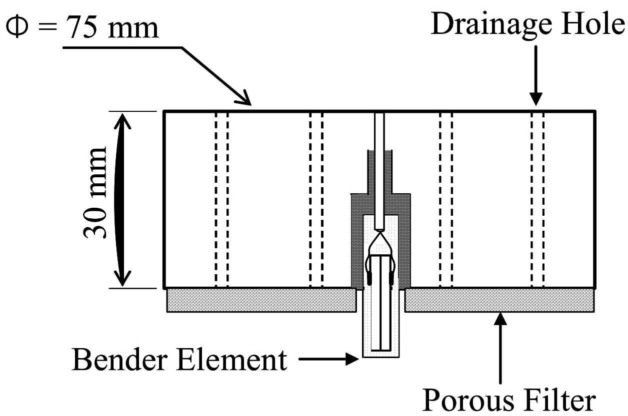

Figure 3.7 Configuration of the top load cap.

Specimen preparation

The main goal of the laboratory test in this study was to minimize sample disturbance. Without extracting the specimen from the Shelby tube, the specimen and the Shelby tube were cut simultaneously using a copper pipe cutter (Fig. 3.8). The cutting process must be performed slowly and carefully, because vibration and local stress caused by blade rotation can disturb the sample.

The initial length of the specimen was decided upon by considering the compressibility and the near field effect. Empirically, the total volumetric strain of natural clay deposits are around 0.25 ~ 0.30. Sufficient space between the source and the receiver is required to avoid the near field effect after loading. Ultimately, the initial specimen length was decided to be 40mm. In conventional consolidation tests, the specimen initial height is usually 2cm. As the drainage time is proportional to the square of the specimen height, the required time for pore pressure dissipation in this study was expected to be four times longer than that of conventional studies.

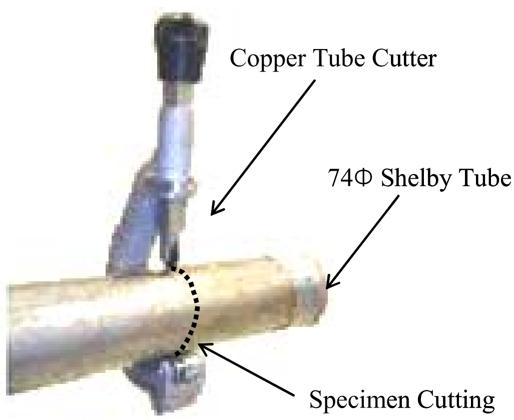

Figure 3.8 Cutting the Shelby tube and specimen together.

Consolidation test setup

To set up the testing system, the Shelby tube specimen was placed on the bottom plate. The top load cap was carefully placed on the specimen to match the direction of the anchored bender element to be parallel with the bottom bender element. Then the device was put into the oedometric tank to maintain the saturated condition of the specimen during the test.

The bottom plate bender element was connected to the signal generator to be used as a source, while the load cap bender element receiver, was connected to the signal conditioner for signal amplification and noise filtering. The experimental devices are shown in Fig. 3.9

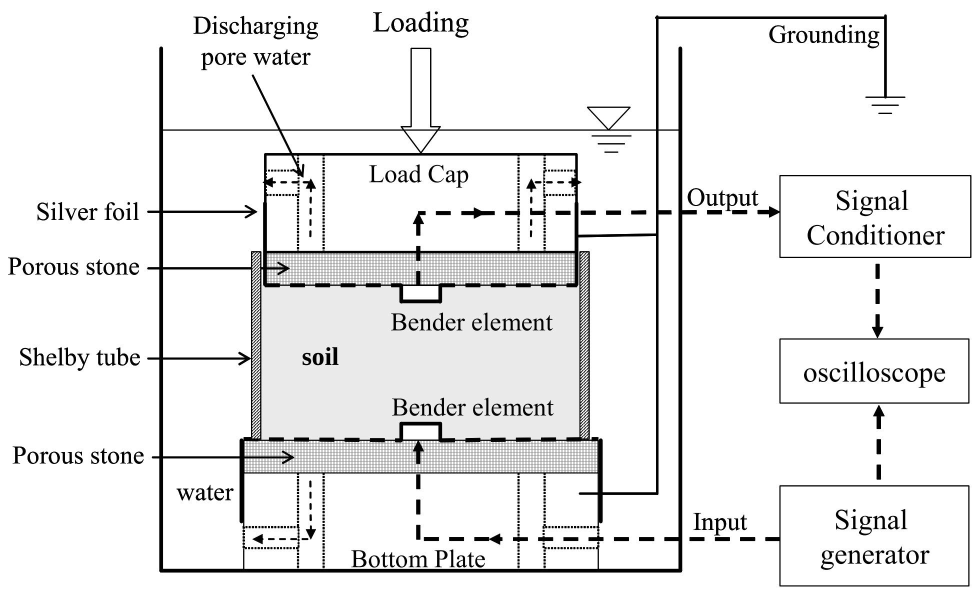

Figure 3.9 Laboratory consolidation test setup.

Electronic peripheral device

The source bender element was connected to the waveform generator (Model: Agilent 33120A) to generate a single step signal with 5 volts amplitude at a 5-kHz frequency. The signal received from the opposite bender element was sent to the multi channel filter (Model: Krohn-Hite 3944) for filtering. A band pass filter (100Hz for a high pass filter, and 50kHz for a low pass filter) was used to avoid unwanted noise caused by electricity and environmental vibration. Both input and output signals were captured with a digital oscilloscope (Model: Agilent 54622D). In this way, the travel time of the shear wave velocity through the specimen was measured. Details of signal interpretation can be found in Lee and Santamarina (2005). The electronic peripheral devices used in this study are shown in Fig. 3.10.

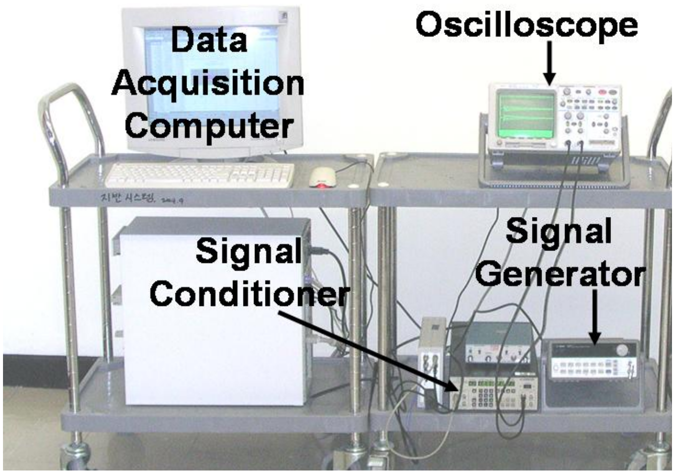

Figure 3.10 Electronic signal processing peripheral devices.

3.2.3 Laboratory Consolidation Test

<u>In-situ effective stress state expected at the end of consolidation</u>

The expected in-situ effective stress state was evaluated from the in-situ density profile, shown in Figs. 3.2, 3.3, and 3.4. Depending on the elevation of the ground water table, the measured density value above the ground water table was assumed to be the dried (solid) density of soil (ρ_d), while the opposite was treated as the saturated density (ρ_s) value. The three sites used in this study were located below the ground water table. Therefore, the density profile from the site investigation was the saturated density distribution. Therefore, the dried density of soil was evaluated as:

$$\rho_d = \rho_s - \rho_w \tag{3.1}$$

where ρ_s is the water density, 1 g/cm^3. After consolidation, the density of soil increases, while the volume decreases. Thus, it was assumed that the total amount of expected effective stress at the end of a consolidation would remain constant in this study, in agreement with Eq. 3.2:

$$\sigma'_v = \int_0^{z_i} \gamma'_i dz = \int_0^{z_o} \gamma'_o dz = \int_0^{z_f} \gamma'_f dz \tag{3.2}$$

In Eq. 3.2, γ' is the average effective unit weight of dried soil (= $\rho_d g$), while i, o, and f represent initial, recent, and final states, respectively. The expected effective stress level for each site and specimen are summarized in Table 3.1.

Table 3.1 In-situ properties.

Site of Interest	Sampled Depth [m]	Average In-situ Density [g/cm3]	Expected Effective Stress [kPa]	In-situ Shear Wave Velocity [m/sec]
Foreshore site (Incheon)	3.0	1.79	23.2	110
	4.5	1.79	34.8	123
	5.5	1.79	42.8	118
	7.5	1.80	59.1	121
Submarine deposit (Busan)	5.0	1.57	28.0	113
	15.0	1.57	83.9	115
	28.0	1.57	156.6	126
Thick clay deposit (Busan)	5.0	1.60	29.4	128
	10.0	1.60	58.9	136
	15.0	1.60	88.3	127
	20.0	1.60	117.7	142
	25.0	1.60	147.2	139
	30.0	1.60	176.6	167

Consolidation test

The step loading method was chosen for the load application of the laboratory consolidation test. Generally, seven or eight steps were applied. Each amount of loading was decided upon by considering the logarithmic scale of the effective stress increment. The effective stress–shear wave velocity relationship (Eq. 2.40) shows that the shear-wave velocity increment is more sensitive under low-stress conditions than under high-stress conditions. Therefore, the extent amount of applying load was decided upon to compare the in-situ expected effective stress value at relatively low stress ranges. Obviously, the upper bound of the loading must be higher than the total amount of stress acting on the point of interest after a field surcharge or other construction. The applied step load for each specimen is presented in Table 3.2.

In this study, a final shear-wave velocity for each load step, when the specimen was fully consolidated, was required to derive a normally-consolidated effective stress–shear wave velocity relationship. Therefore, a subsequent loading was performed after the consolidation according to the previous load step was completely finished.

During loading, a signal wave was generated and was sent to the source bender element. The response of the receiver bender element was recorded. The vertical shear-wave travel time was measured between the top and bottom bender elements. The vertical deformation of the specimen was measured using a dial gage. The vertical shear wave velocity [m/sec] was calculated by dividing the specimen height [m] by the vertical shear wave travel time [sec]. Thus, the shear velocity inside the specimen was measured continuously during consolidation. An example of shear wave travel time determination is shown in Fig. 3.11.

Table 3.2 Load step for consolidation.

Site of Interest	Sampled Depth [m]	In-situ Effective Stress [kPa]	Load Step [kPa]							
			1st	2nd	3rd	4th	5th	6th	7th	8th
Foreshore site (Incheon)	3.0	23.2	6.3	12.5	25.2	50.0	100.4	201.1	402.2	-
	4.5	34.8	9.6	19.1	38.3	76.6	153.1	306.1	612.3	-
	5.5	42.8	9.6	19.1	38.3	76.6	153.1	306.1	612.3	-
	7.5	59.1	9.6	19.1	38.3	76.6	153.1	306.1	612.3	-
Submarine deposit (Busan)	5.0	28.0	5.7	11.4	22.8	45.6	91.2	182.5	-	-
	15.0	83.9	11.4	22.8	45.6	91.2	182.5	365.0	-	-
	28.0	156.6	22.8	45.6	91.2	182.5	365.0	730.0	-	-
Thick clay deposit (Busan)	5.0	29.4	6.4	12.9	25.8	51.6	103.2	206.4	412.7	825.4
	10.0	58.9	6.4	12.9	25.8	51.6	103.2	206.4	412.7	825.4
	15.0	88.3	9.8	19.6	39.2	78.4	156.7	313.4	626.8	1253.5
	20.0	117.7	19.6	39.2	78.4	156.7	313.4	626.8	1253.5	-
	25.0	147.2	19.6	39.2	78.4	156.7	313.4	626.8	1253.5	-
	30.0	176.6	19.6	39.2	78.4	156.7	313.4	626.8	1253.5	-

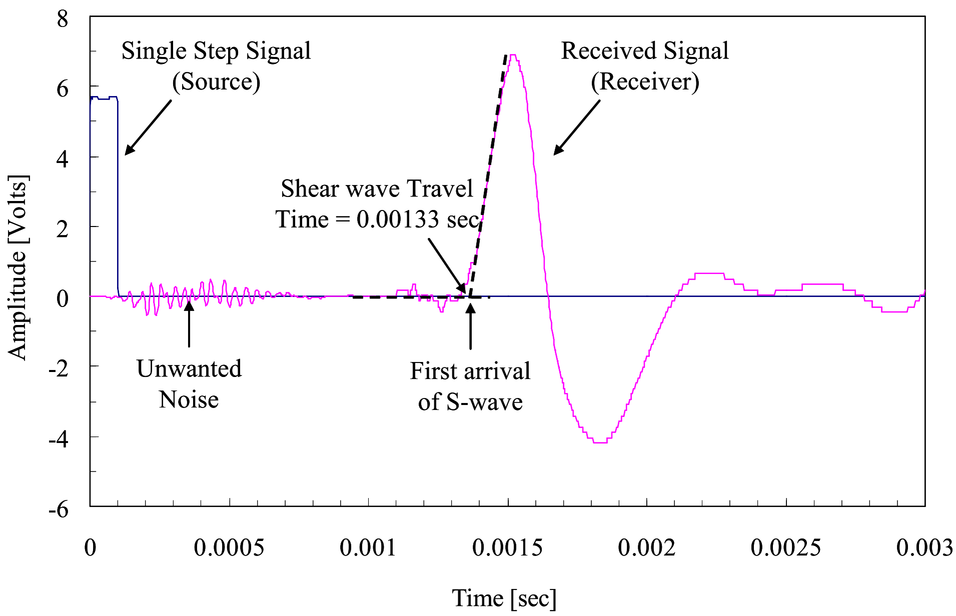

Figure 3.11 Example of shear wave travel time measurement.

3.3 EXPERIMENTAL RESULTS AND ANALYSIS

The merit of shear-wave velocity measurement during consolidation is that estimation of effective stress variation can be performed at the same time. In this study, the effective stress–shear wave velocity relationship was used to characterize the in-situ consolidation state, over consolidation ratio, degree of consolidation, and compressibility.

3.3.1 Shear Wave Velocity and Void Ratio Variation

An example of the shear wave velocity and the void ratio variation during a single load step is shown in Figs. 3.12 and 3.13.

The shear wave velocity showed an abrupt increase between 10min ~ 500min, and converged after 1000min. The shear wave velocity did not increase immediately after the load was applied, in accordance with the drainage path and permeability concepts. When a load was applied, the maximum excess pore water pressure formed inside the specimen. Meanwhile, the relatively long drainage path and low permeability increased the time for drainage. The rate of pore pressure dissipation was initially high and continuously decreased according to the permeability diminution while the soil became denser. This was also in collusion with the effective stress increment.

The void ratio diminution tendency was similar to the time–void ratio curve from conventional consolidation test results. The shear-wave velocity and void ratio variation over time of other specimens were similar to those shown in Figs. 3.12 and 3.13.

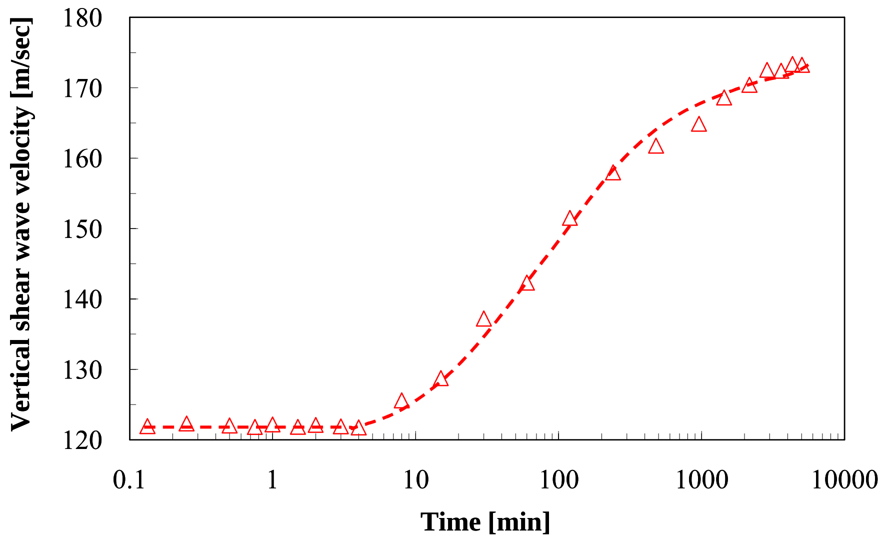

Figure 3.12 Vertical shear wave velocity increase of a single load step.

(5th step, 15m specimen, Submarine deposit, Busan)

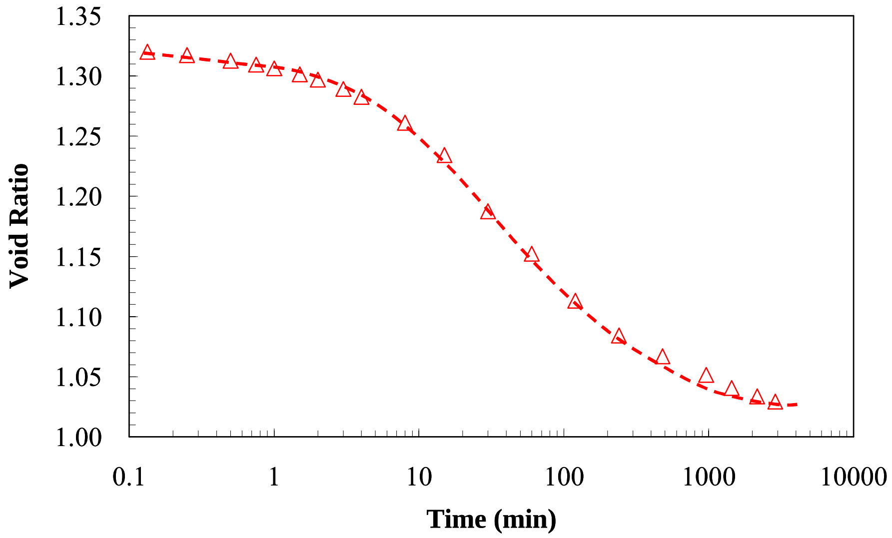

Figure 3.13 Void ratio variation of a single load step (Same to Fig. 3.12).

Foreshore site (Incheon)

The final shear wave velocity and void ratio values for each load step of the foreshore site specimens are summarized in Table 3.3 and shown in Fig. 3.14.

Table 3.3 Experimental results of the Foreshore site, Incheon.

Specimen Depth [m]	Experimental Properties	In-situ Values	Laboratory Results for each Load Step						
			1st	2nd	3rd	4th	5th	6th	7th
3.0	Applied load [kPa]	23.2	6.3	12.5	25.2	50.0	100.4	201.1	402.2
	Shear wave velocity [m/sec]	110	112.3	120.0	140.0	160.0	190.0	225.0	277.9
	Void ratio		0.90	0.87	0.84	0.80	0.76	0.69	0.62
4.5	Applied load [kPa]	34.8	9.6	19.1	38.3	76.6	153.1	306.1	612.3
	Shear wave velocity [m/sec]	123	121.0	143.0	161.6	185.0	220.0	246.9	306.7
	Void ratio		0.83	0.82	0.80	0.78	0.73	0.69	0.63
5.5	Applied load [kPa]	42.8	9.6	19.1	38.3	76.6	153.1	306.1	612.3
	Shear wave velocity [m/sec]	118	100.0	120.0	135.0	170.0	205.0	244.1	311.0
	Void ratio		1.06	1.05	1.02	0.98	0.91	0.84	0.75
7.5	Applied load [kPa]	59.1	9.6	19.1	38.3	76.6	153.1	306.1	612.3
	Shear wave velocity [m/sec]	121	153.1	160.9	187.0	204.7	229.1	253.2	303.8
	Void ratio		0.72	0.70	0.69	0.67	0.65	0.61	0.58

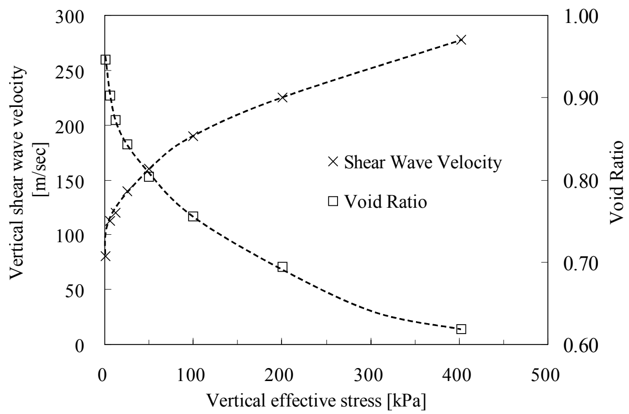

a. 3.0m specimen

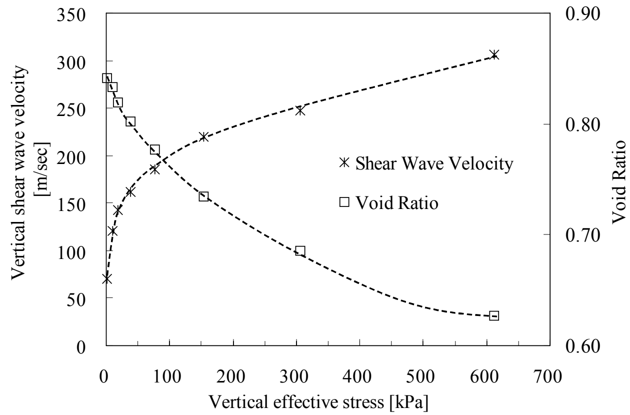

b. 4.5m specimen

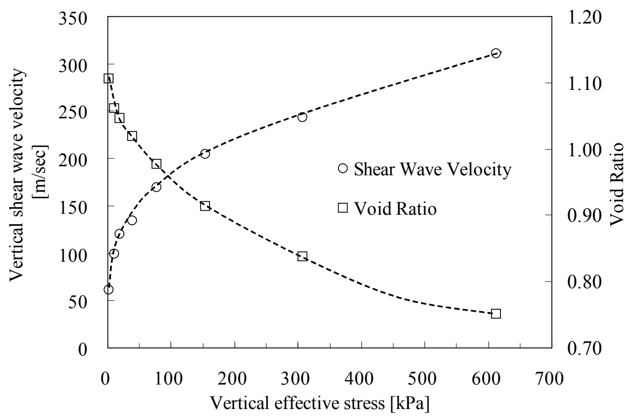

c. 5.5m specimen

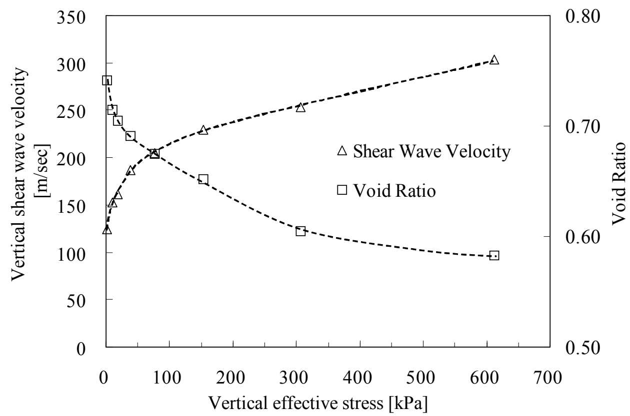

d. 7.5m specimen

Figure 3.14 Vertical shear wave velocity and void ratio variation with time - The foreshore site (Incheon).

<u>Submarine Deposit (Busan)</u>

The final shear-wave velocity and void ratio values for each load step of the foreshore site specimens are summarized in Table 3.4 and shown in Fig. 3.15.

Table 3.4 Experimental results of the Submarine deposit, Busan.

Specimen Depth [m]	Experimental Properties	In-situ Values	Laboratory Results for each Load Step					
			1st	2nd	3rd	4th	5th	6th
5.0m	Applied load [kPa]	28.0	5.7	11.4	22.8	45.6	91.2	182.5
	Shear wave velocity [m/sec]	113	56.4	61.6	73.2	103.8	148.7	207.0
	Void ratio		1.68	1.64	1.56	1.36	1.14	0.94
15.0m	Applied load [kPa]	83.9	11.4	22.8	45.6	91.2	182.5	365.0
	Shear wave velocity [m/sec]	115	69.4	81.2	99.5	123.0	173.3	230.2
	Void ratio		1.72	1.65	1.54	1.33	1.02	0.77
28.0m	Applied load [kPa]	156.6	22.8	45.6	91.2	182.5	365.0	730.0
	Shear wave velocity [m/sec]	126	125.6	162.5	188.9	239.1	300.5	389.1
	Void ratio		1.28	1.24	1.17	1.09	0.98	0.85

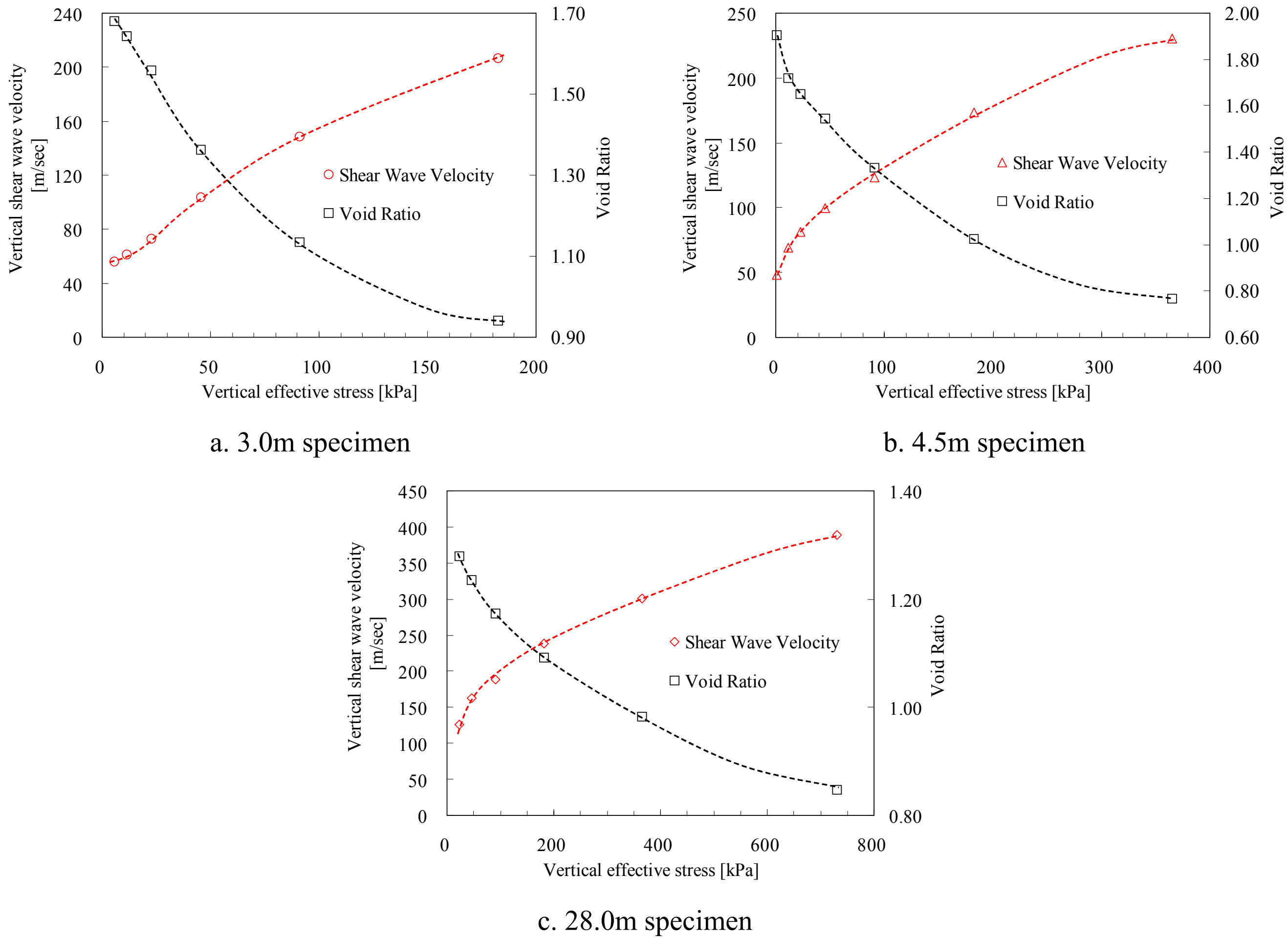

Figure 3.15 Vertical shear wave velocity and void ratio variation with time - The submarine deposit (Busan).

Thick Clay Deposit (Busan)

The final shear-wave velocity and void ratio values for each load step of the thick clay deposit specimens are summarized in Table 3.5 and shown in Fig. 3.16.

Table 3.5 Experimental results of the thick clay deposit, Busan.

Depth [m]	Experimental Properties	In-situ Values	Laboratory Results for each Load Step							
			1^{st}	2^{nd}	3^{rd}	4^{th}	5^{th}	6^{th}	7^{th}	8^{th}
5.0	Applied load [kPa]	29.4	6.4	12.9	25.8	51.6	103.2	206.4	412.7	825.4
	Shear wave velocity [m/sec]	128	57.8	67.8	87.9	104.1	131.3	159.0	198.4	245.7
	Void ratio		1.26	1.23	1.10	1.00	0.87	0.71	0.56	0.50
10.0	Applied load [kPa]	58.9	6.4	12.9	25.8	51.6	103.2	206.4	412.7	825.4
	Shear wave velocity [m/sec]	136	57.5	36.8	71.1	87.3	116.0	155.7	223.5	304.9
	Void ratio		1.23	1.18	1.13	1.05	0.93	0.80	0.64	0.48
15.0	Applied load [kPa]	88.3	9.8	19.6	39.2	78.4	156.7	313.4	626.8	1253.5
	Shear wave velocity [m/sec]	127	60.0	80.0	94.6	115.0	160.0	205.0	270.0	355.8
	Void ratio		1.23	1.20	1.14	1.03	0.90	0.70	0.50	0.41
20.0	Applied load [kPa]	117.7	19.6	39.2	78.4	156.7	313.4	626.8	1253.5	-
	Shear wave velocity [m/sec]	142	70.0	100.0	129.9	170.0	230.0	288.7	396.6	-
	Void ratio		1.21	1.16	1.10	1.00	0.75	0.43	0.27	-

Table 3.5 Continued.

Specimen Depth [m]	Experimental Properties	In-situ Values	Laboratory Results for each Load Step						
			1st	2nd	3rd	4th	5th	6th	7th
25.0	Applied load [kPa]	147.2	19.6	39.2	78.4	156.7	313.4	626.8	1253.5
	Shear wave velocity [m/sec]	139	70.0	95.0	115.1	145.0	210.0	282.8	390.9
	Void ratio		1.14	1.11	1.02	0.90	0.70	0.48	0.36
30.0	Applied load [kPa]	176.6	19.6	39.2	78.4	156.7	313.4	626.8	1253.5
	Shear wave velocity [m/sec]	167	85.8	105.0	123.8	155.4	206.4	256.7	322.9
	Void ratio		1.21	1.16	1.07	0.95	0.70	0.45	0.26

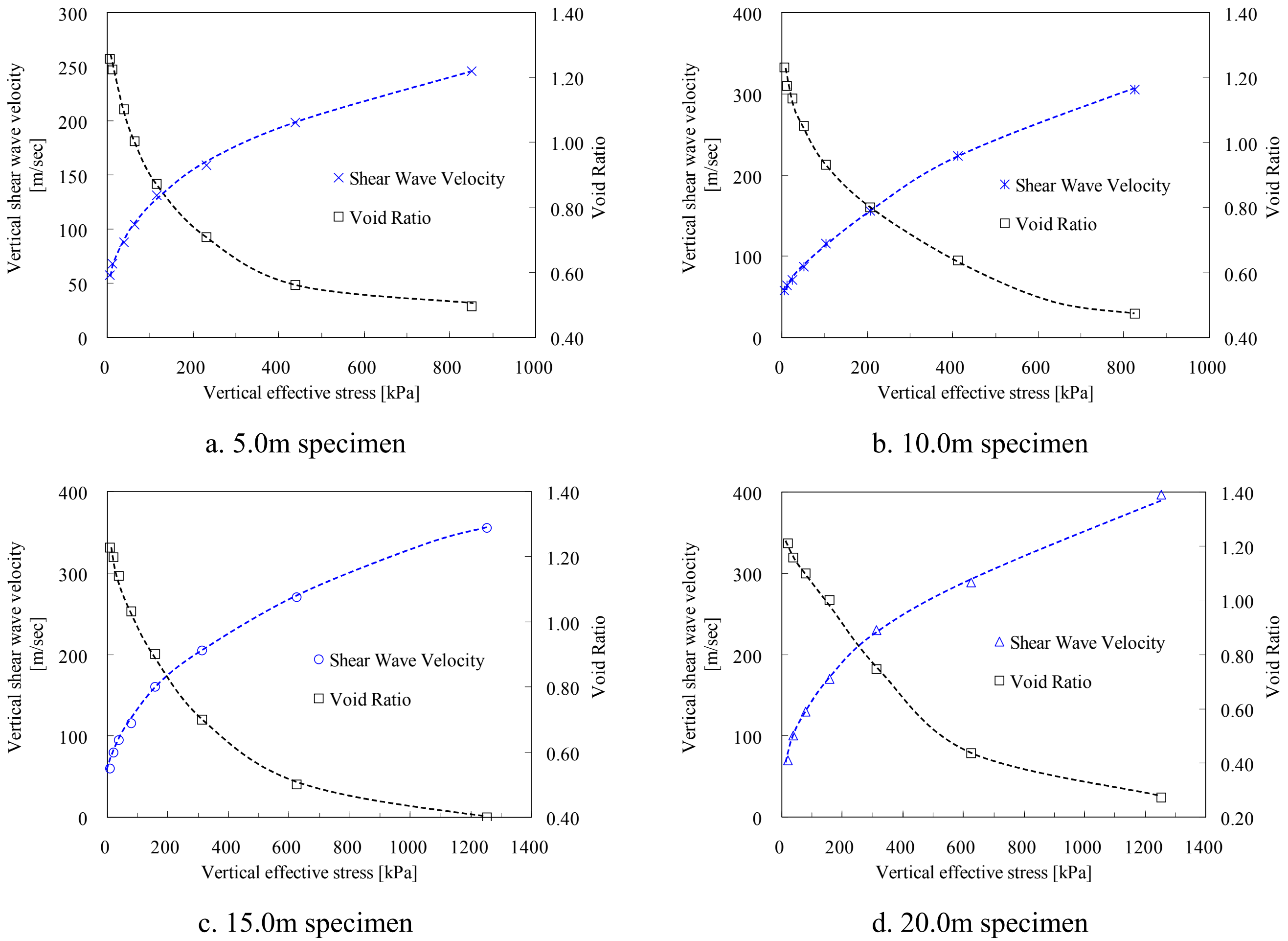

Figure 3.16 Vertical shear wave velocity and void ratio variation with time of the thick clay deposit, Busan.

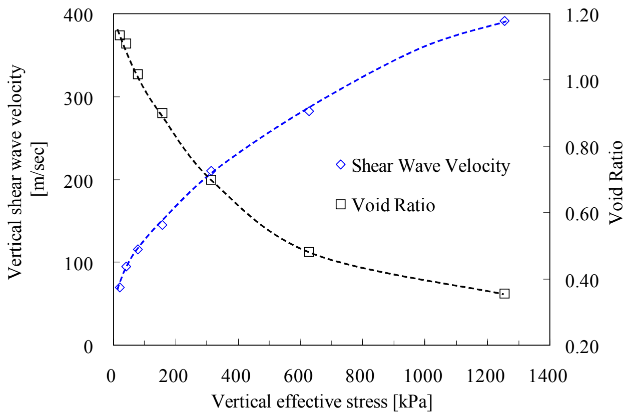

e. 25.0m specimen

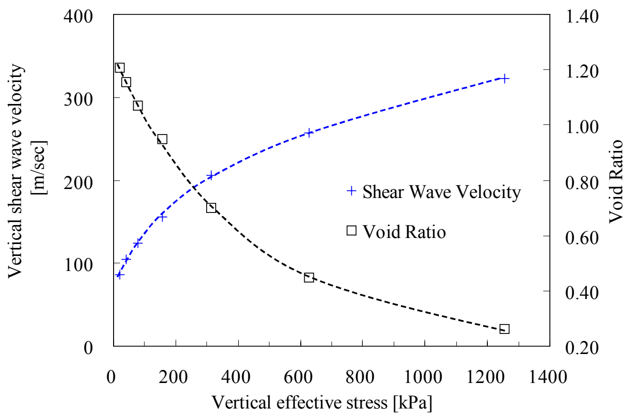

f. 30.0m specimen

Figure 3.16 Continued.

3.3.2 Vertical Effective Stress – Shear Wave Velocity Relationship.

The vertical effective stress variation was derived using the shear wave velocity data and Eq. 2.40. When the load was applied to the specimen, the total stress was resisted by the excess pore water pressure at the initial stage. The hydraulic pressure head difference caused the pore fluid to flow upward and downward through the drainage path; thus, the pore water pressure decreased. The particle packing became denser as the pore water pressure decrement was transferred to the vertical effective stress increment. The rate of pore pressure dissipation was initially high and continuously decreased according to the permeability diminution while the soil became denser. In other words, the effective stress increased with a logarithmic time scale, which was in collusion with the vertical shear-wave velocity variation results.

The vertical effective stress–shear wave velocity relationship of the specimen was derivable by curve fitting the final shear-wave velocity values of each load step. The converged final vertical shear-wave velocity of each step indicated that the excess pore water pressure was completely dissipated; thus, the amount of vertical effective stress inside the specimen was equal to the applying load. The experimentally determined parameters α and β are related to the soil type, and to the particle structure and composition. The in-situ layer profiles (Figs. 3.1, 3.2, 3.3, and 3.4) show that characteristics differ along the depth. Therefore, a vertical effective stress–shear wave velocity equation should be evaluated for each single specimen, respectively.

Curve fitting approximation by MATHCAD (Appendix B.1) was used to derive the equation for the vertical effective stress–shear wave velocity equation for each specimen (Fig 3.17). Evaluated α and β parameters are summarized in Table 3.6.

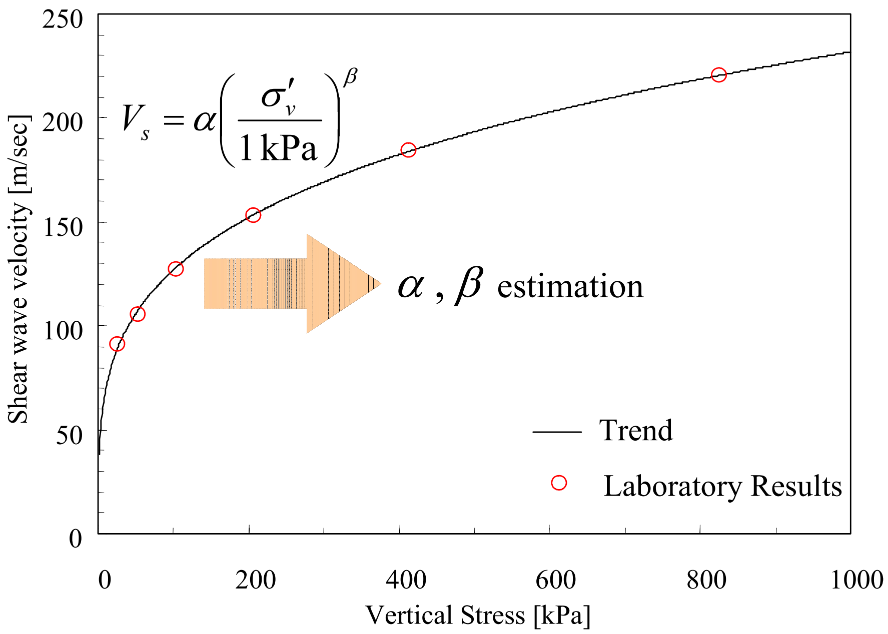

Figure 3.17 Curve fitting of the vertical effective stress – shear wave velocity relation.

Table 3.6 Experimentally determined α and β parameters.

Site of Interest	Sample Depth [m]	α [m/sec]	β
Foreshore Site (Incheon)	3.0	70.42	0.228
	4.5	76.71	0.216
	5.5	54.55	0.274
	7.5	102.99	0.169
Submarine Deposit (Busan)	5.0	21.88	0.44
	15.0	25.58	0.38
	28.0	46.84	0.33
Thick Clay Deposit (Busan)	5.0	28.86	0.32
	10.0	17.87	0.42
	15.0	22.38	0.39
	20.0	24.33	0.39
	25.0	17.32	0.43
	30.0	31.21	0.33

3.3.3 Consolidation State

The consolidation state was evaluated by comparing the estimated trend between the vertical effective stress and shear wave velocity with the in-situ shear wave value. The estimated trend was regarded as characteristic of the shear-wave velocities for a normally-consolidated condition. Therefore, if the in-situ shear-wave velocity approached the trend curve, then the considered site was supposed to be normally-consolidated (NC). A given site was determined to be under-consolidated (UC) when the in-situ shear wave velocity was lower than the estimated trend; a converse case indicated a site as over-consolidated (OC). The flow chart of consolidation state evaluation is shown below (Fig. 3.18).

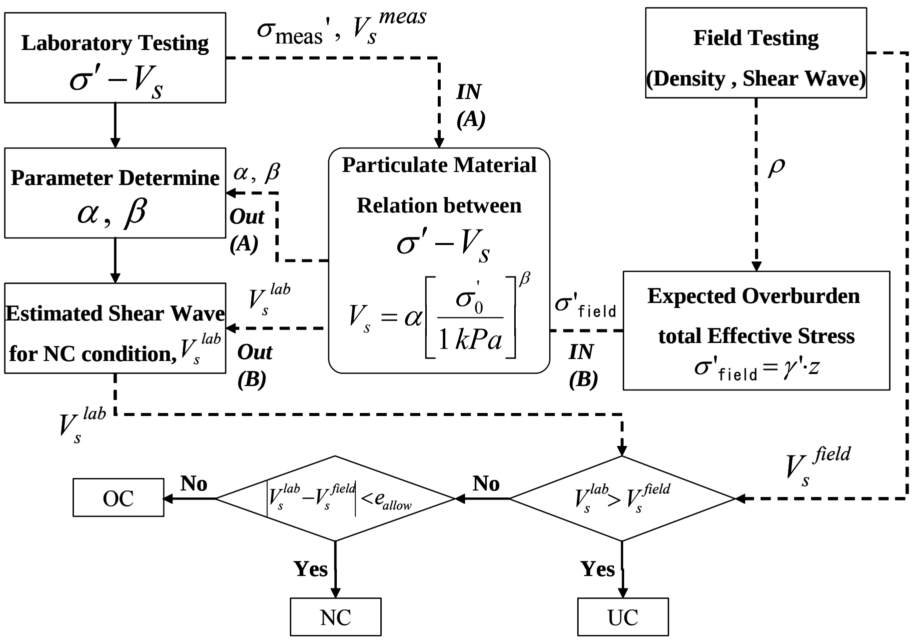

Figure 3.18 Flow chart of consolidation state evaluation.

The degree of consolidation (U_z) was calculated for under-consolidated clays. As the effective stress when the specimen was completely consolidated was already known, the degree of consolidation was evaluated by dividing the recent effective stress value with the final effective stress value (Eq. 2.15). The final effective stress values (σ'_f) are listed in Table 3.1, and the estimated recent effective stress value (σ'_o) of under-consolidated specimens was calculated as:

$$\sigma'_o = \left(\frac{V_s^{field}}{\alpha} \right)^{\frac{1}{\beta}} \tag{3.3}$$

Therefore, the degree of consolidation is derived as:

$$U_z = \frac{\sigma'_o}{\sigma'_f} = \frac{\left(\frac{V_s^{field}}{\alpha} \right)^{\frac{1}{\beta}}}{\sigma'_f} \tag{3.4}$$

The over consolidation ratio (OCR) is defined in Eq. 2.45. The pre-consolidated stress was assumed to be the maximum effective stress value related to the present in-situ shear wave velocity. Moreover, the current in-situ effective stress was the same as the expected in-situ effective stress value (σ'_f).

$$OCR = \frac{\sigma'_c}{\sigma'_o} = \frac{\left(\frac{V_s^{field}}{\alpha} \right)^{\frac{1}{\beta}}}{\sigma'_f} \tag{3.5}$$

<u>Foreshore site (Incheon)</u>

The evaluated vertical effective stress – shear wave velocity equation for each specimen is as:

$$V_{s-v}{}^{3.0m} = 70.4\left(\frac{\sigma'_v}{1\text{kPa}}\right)^{0.23} \quad \text{for 3.0m depth} \tag{3.6}$$

$$V_{s-v}{}^{4.5m} = 76.7\left(\frac{\sigma'_v}{1\text{kPa}}\right)^{0.22} \quad \text{for 4.5m depth} \tag{3.7}$$

$$V_{s-v}{}^{5.5m} = 54.5\left(\frac{\sigma'_v}{1\text{kPa}}\right)^{0.27} \quad \text{for 5.5m depth} \tag{3.8}$$

$$V_{s-v}{}^{7.5m} = 103.0\left(\frac{\sigma'_v}{1\text{kPa}}\right)^{0.17} \quad \text{for 7.5m depth} \tag{3.9}$$

The evaluated vertical effective stress–shear wave velocity relationship is plotted with the in-situ shear wave value in Fig. 3.19 to determine the in-situ consolidation state.

The consolidation states of all four specimens were evaluated to be under-consolidated. Therefore, the estimated degree of consolidation of each specimen is shown in Table 3.7

Table 3.7 Estimated degree of consolidation of the foreshore site, Incheon.

Depth [m]	α [m/s]	β	In-situ shear wave velocity [m/s]	Recent effective stress, σ'_o [kPa]	Final effective stress, σ'_f [kPa]	Degree of Consolidation, U_z
3.0	70.4	0.23	110	7.0	23.2	0.30
4.5	76.7	0.22	123	8.6	34.8	0.25
5.5	54.5	0.27	118	17.5	42.8	0.41
7.5	103.0	0.17	121	2.6	59.1	0.04

Even though the foreshore site appears to consolidate further, the degree of the consolidation remains uncertain if based on the data shown in Table 3.7. In particular, the estimated results may underestimate the in-situ conditions because of unskilled operations, site disturbances, and other factors. Even though in-situ shear-wave velocity measurement is considered the most important factor for field estimation, error factors during field tests can underestimate the in-situ shear wave velocity value. This problem is clearly revealed for the 7.5m specimen. From laboratory testing, α parameter was evaluated as 103.0 m/s, which is very high for clay (Fig. 2.4). This means that the 7.5m specimen was very stiff; thus, the in-situ shear-wave velocity must have been higher than the measurement.

The seismic cone penetration test (S-CPT), used for field testing, also has some problems. The vertical shear wave velocity of the specimen is measured in a laboratory. However, the S-CPT method measures the horizontal shear-wave velocity between two parallel cones. For under-consolidated soils, the vertical shear-wave velocity is generally higher than the horizontal shear-wave velocity. Therefore, the S-CPT method was inappropriate for field testing in this study; instead, the SPS-logging method was adopted.

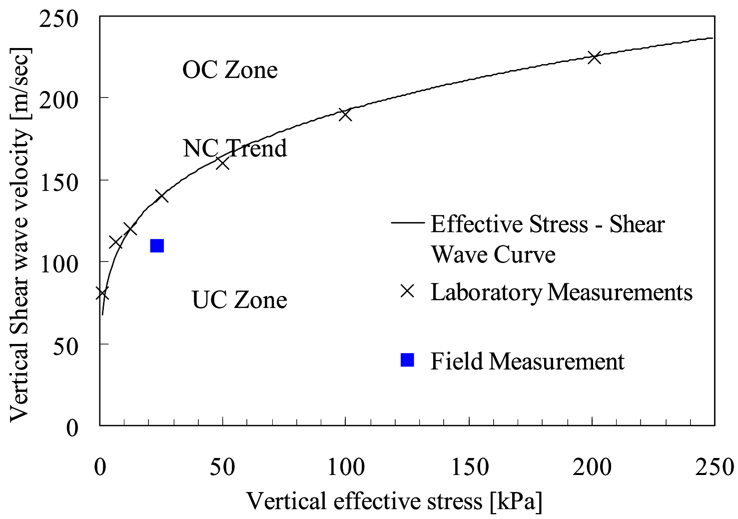

a. 3.0m specimen: Under-consolidated

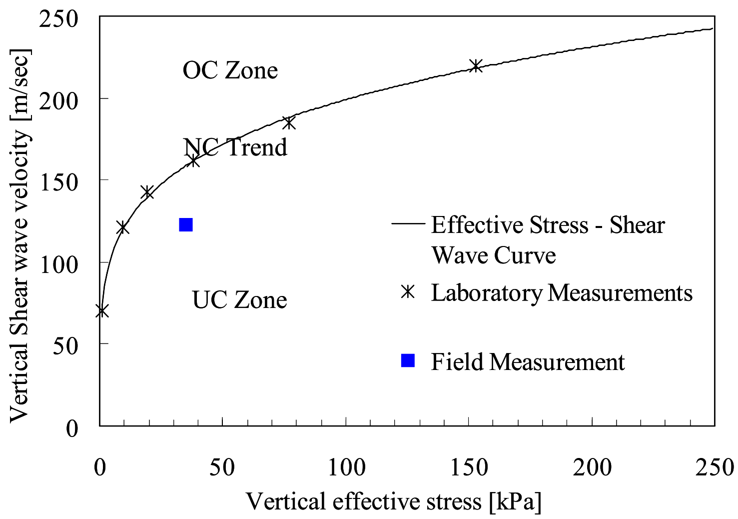

b. 4.5m specimen: Under-consolidated

Figure 3.19 Consolidation state evaluation of the foreshore site, Incheon.

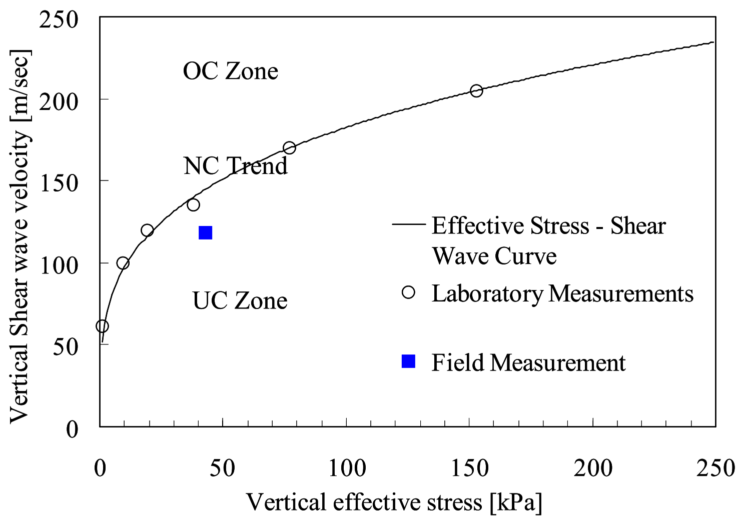

c. 5.5m specimen: Under-consolidated

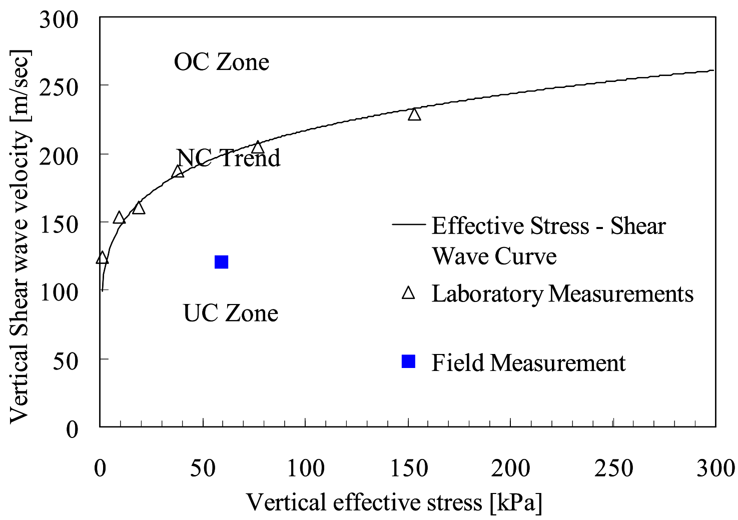

d. 7.5m specimen: Under-consolidated

Figure 3.19 Continued.

<u>Submarine Deposit (Busan)</u>

The evaluated vertical effective stress–shear wave velocity equation for each specimen was as follows

$$V_{s-v}^{\ 5.0m} = 21.9\left(\frac{\sigma'_v}{1\text{kPa}}\right)^{0.44} \qquad \text{for 5.0m depth} \qquad (3.10)$$

$$V_{s-v}^{\ 15.0m} = 25.6\left(\frac{\sigma'_v}{1\text{kPa}}\right)^{0.38} \qquad \text{for 15.0m depth} \qquad (3.11)$$

$$V_{s-v}^{\ 28.0m} = 46.8\left(\frac{\sigma'_v}{1\text{kPa}}\right)^{0.33} \qquad \text{for 28.0m depth} \qquad (3.12)$$

The evaluated vertical effective stress–shear wave velocity relationship was plotted with the in-situ shear wave value, as shown in Fig. 3.20, to determine the in-situ consolidation state.

The consolidation state of the 5.0m specimen was slightly over-consolidated. The OCR was as follows:

$$OCR^{5.0m} = \frac{\left(\dfrac{V_s^{\ field}}{\alpha}\right)^{\frac{1}{\beta}}}{\sigma'_f} = \frac{\left(\dfrac{113}{21.9}\right)^{\frac{1}{0.44}}}{28.0} = 1.5 \qquad (3.13)$$

Over-consolidated behavior of clay layers near the seafloor has been commonly observed. The following reasons have been reported for explaining this behavior: (1) desiccation; (2) tectonic forces causing slumping accompanied by erosion; (3) strengthening of the clay structure brought about by interparticle bonding and/or cementation or even bioturbating animals; (4) release of pressure brought about by the coring process itself (Buchan and Smith 1998).

However, the estimated *OCR* value may not be correct because the α and β parameters of the over-consolidated clay is different from the α and β values of the normal compression conditions.

While the 15.0m specimen was determined as normally-consolidated, the 28.0m specimen was evaluated to be under-consolidated. Thus, the estimated degree of consolidation of the 28.0m specimen was as follows:

$$U_z^{28.0m} = \frac{\left(\dfrac{126}{46.84}\right)^{\frac{1}{0.33}}}{156.6} = 0.13 \tag{3.14}$$

The low degree of consolidation value of the 28.0m point indicates the possibility of an impermeable layer below the 28.0m layer. From Fig. 3.3, the layer around the 30-m depth has a higher Standard Penetration (SPT) Number (N) value than the other layers. Even though it could be an effect of anomalies inside, the possible existence of a low-permeable layer, such as stiff clay or a shale layer, cannot be excluded. The long in-situ drainage path also decreased the degree of consolidation of the 28.0-m-deep layer.

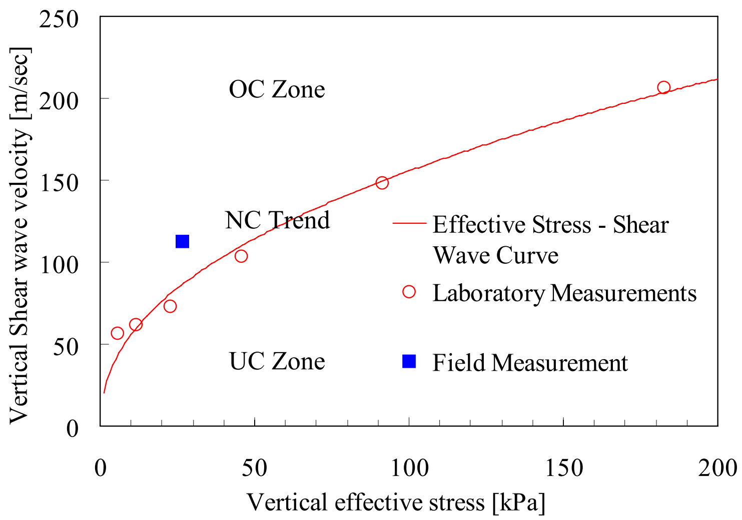

a. 5.0m specimen: Over-consolidated

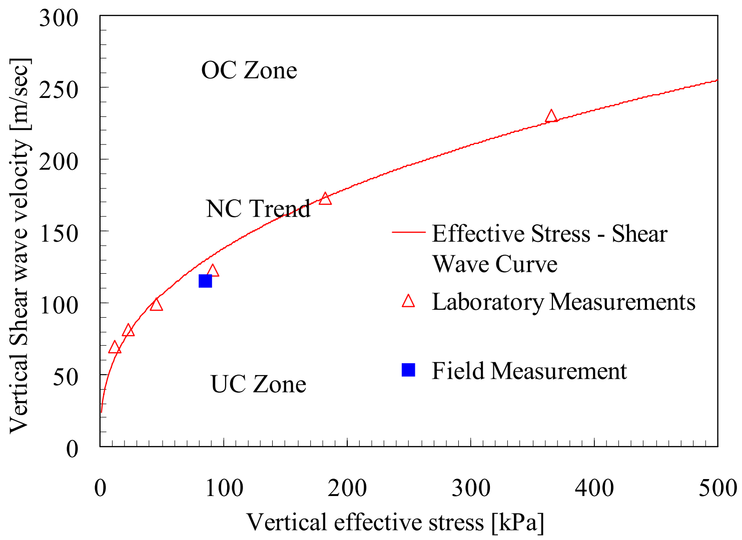

b. 15.0m specimen: Normally-consolidated

Figure 3.20 Consolidation state evaluation of the submarine deposit, Busan.

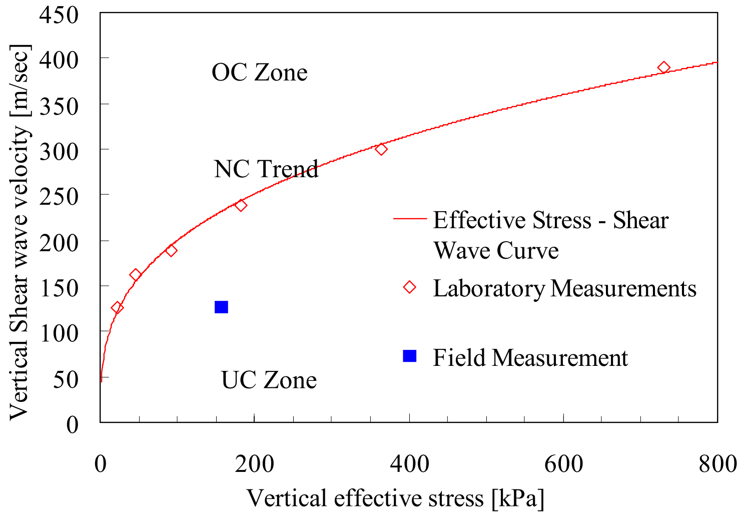

c. 28.0m specimen: Under-consolidated

Figure 3.20 Continued.

Thick Clay Deposit (Busan)

The evaluated vertical effective stress–shear wave velocity equation for each specimen was as follows:

$$V_{s-v}{}^{5.0m} = 28.86\left(\frac{\sigma'_v}{1\text{kPa}}\right)^{0.32} \qquad \text{for 5.0m depth} \tag{3.15}$$

$$V_{s-v}{}^{10.0m} = 17.9\left(\frac{\sigma'_v}{1\text{kPa}}\right)^{0.42} \qquad \text{for 10.0m depth} \tag{3.16}$$

$$V_{s-v}{}^{15.0m} = 22.4\left(\frac{\sigma'_v}{1\text{kPa}}\right)^{0.39} \qquad \text{for 15.0m depth} \tag{3.17}$$

$$V_{s-v}{}^{20.0m} = 24.3\left(\frac{\sigma'_v}{1\text{kPa}}\right)^{0.39} \qquad \text{for 20.0m depth} \tag{3.18}$$

$$V_{s-v}{}^{25.0m} = 17.3\left(\frac{\sigma'_v}{1\text{kPa}}\right)^{0.43} \qquad \text{for 25.0m depth} \tag{3.19}$$

$$V_{s-v}{}^{30.0m} = 31.2\left(\frac{\sigma'_v}{1\text{kPa}}\right)^{0.33} \qquad \text{for 30.0m depth} \tag{3.20}$$

The evaluated vertical effective stress–shear wave velocity relationship was plotted with the in-situ shear wave value, as shown in Fig. 3.21, to determine the in-situ consolidation state.

The states of the 5.0-m and 10.0-m specimens were evaluated as over-consolidated. The states of other specimens, from 15.0m, 20.0m, 25.0m, and 30.0m, were determined to be normally-consolidated. Therefore, the over-consolidation ratios of the 5.0m and 10.0m specimens were as follows:

$$OCR^{5.0m} = \frac{\left(\frac{V_s^{field}}{\alpha}\right)^{\frac{1}{\beta}}}{\sigma'_f} = \frac{\left(\frac{128}{28.9}\right)^{\frac{1}{0.32}}}{29.4} = 3.6 \qquad (3.21)$$

$$OCR^{10.0m} = \frac{\left(\frac{V_s^{field}}{\alpha}\right)^{\frac{1}{\beta}}}{\sigma'_f} = \frac{\left(\frac{136}{17.9}\right)^{\frac{1}{0.42}}}{58.9} = 2.1 \qquad (3.22)$$

The *OCR* value of the thick clay deposit was relatively higher than the *OCR* of the submarine deposit at same depth. This difference corresponds to the different surface conditiond of the thick clay deposit. As the surface of the thick clay deposit was exposed to the air, the effects of desiccation and surface evaporation, which harden the soil structure, were much stronger than those observed for the submerged clay layers.

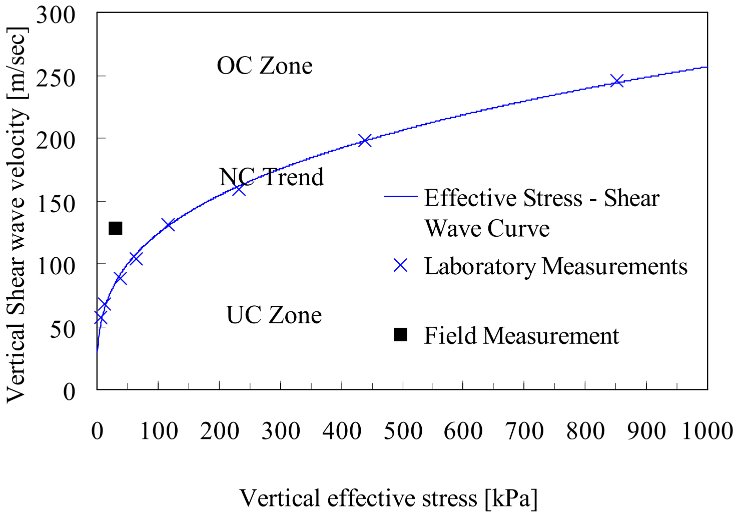

a. 5.0m specimen: Over-consolidated

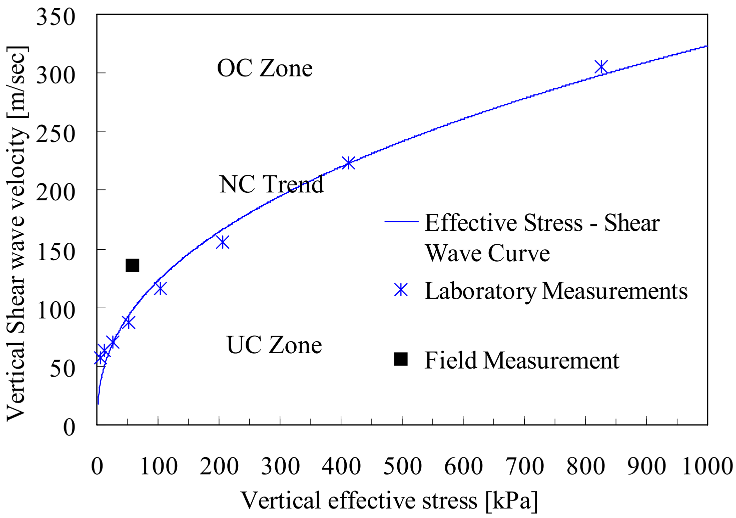

b. 10.0m specimen: Over-consolidated

Figure 3.21 Consolidation state evaluation of the thick clay deposit, Busan.

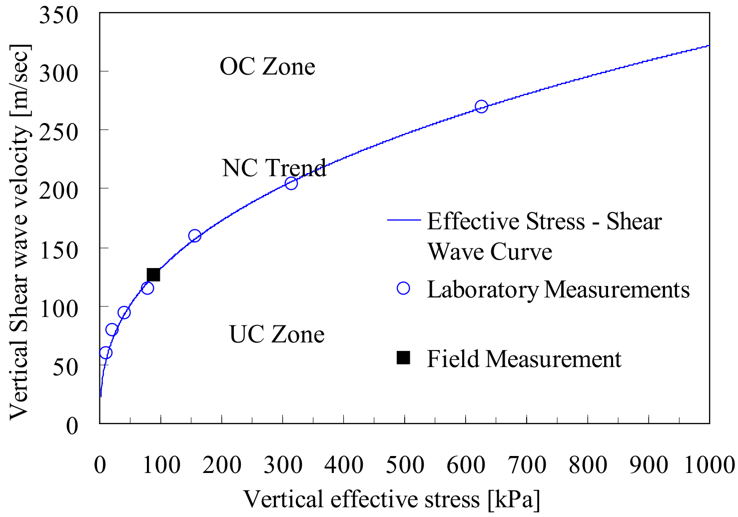

c. 15.0m specimen: Normally-consolidated

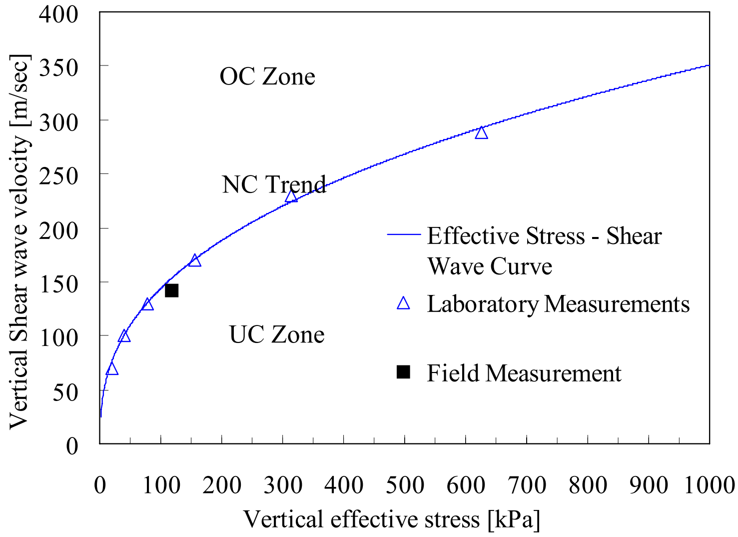

d. 20.0m specimen: Normally-consolidated

Figure 3.21 Continued.

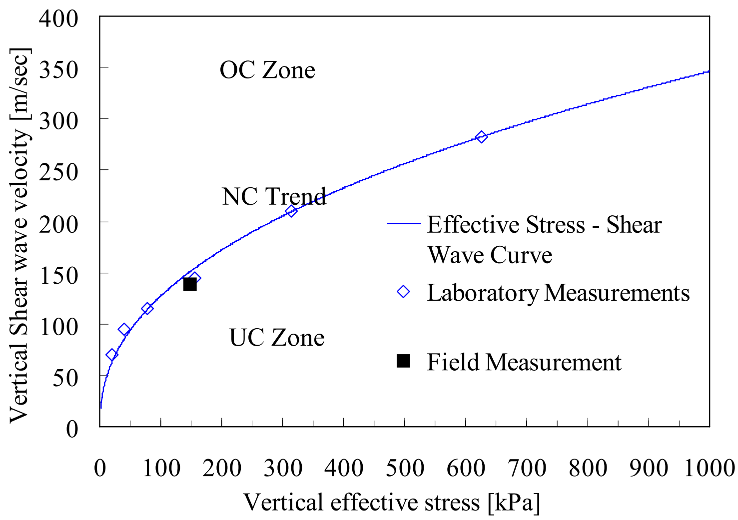

e. 25.0m specimen: Normally-consolidated

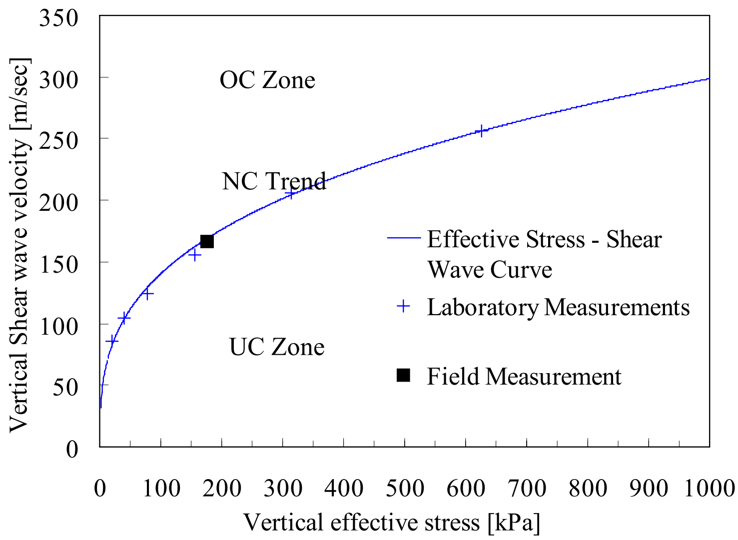

f. 30.0m specimen: Normally-consolidated

Figure 3.21 Continued.

3.3.4 Compressibility

The compressibility of a soil layer is an important parameter by which to predict the amount of settlement corresponding to additional in-situ loads. The final effective stress and void ratio values were plotted on a stress–strain plane, and the stress–strain behavior showed a bilinear curve. The inflection point is the pre-consolidated stress; in this study, it was same as the expected in-situ effective stress value for normally-consolidated condition.

The curve before the pre-consolidation point is related to swelling or reloading. Therefore, the slope of the prior curve becomes the swelling index (C_s) of the specimen. The posterior curve after the pre-consolidation point is the normally consolidating curve. Thus, the slope is equal to the compression index (C_c) of the specimen.

The swelling index and compression index of each specimen is shown in Figs. 3.22, 3.23, and 3.24.

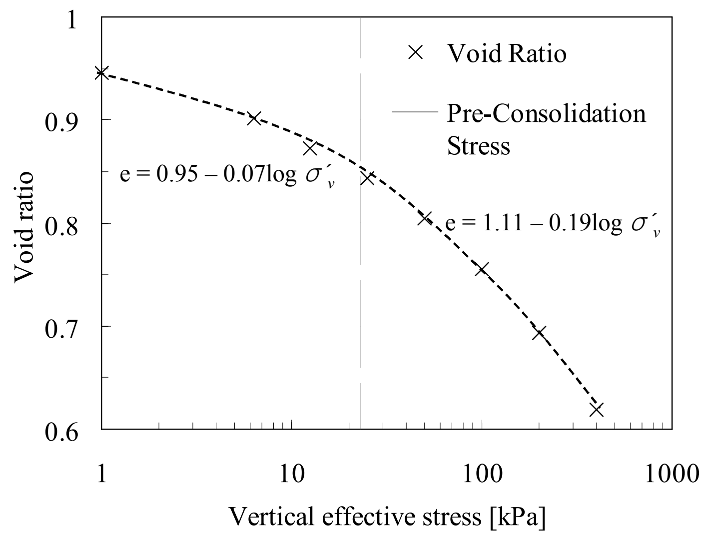

a. 3.0m specimen: $C_s = 0.07$, $C_c = 0.19$

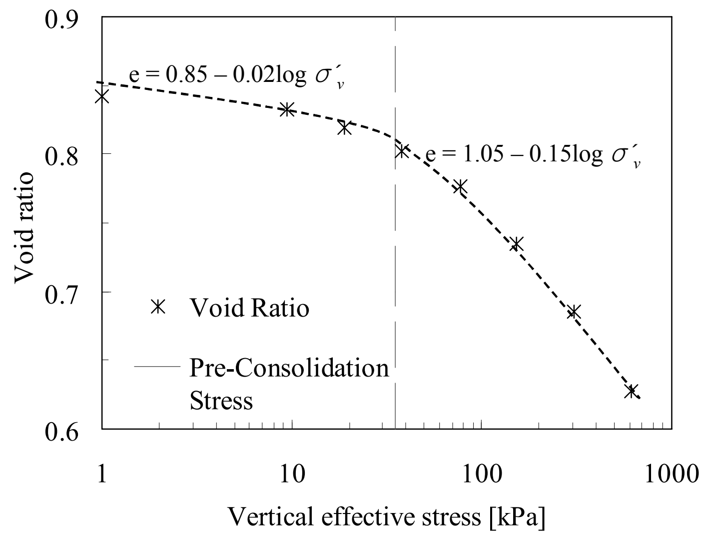

b. 4.5m specimen: $C_s = 0.02$, $C_c = 0.15$

Figure 3.22 Stress – strain curve of the foreshore site, Incheon.

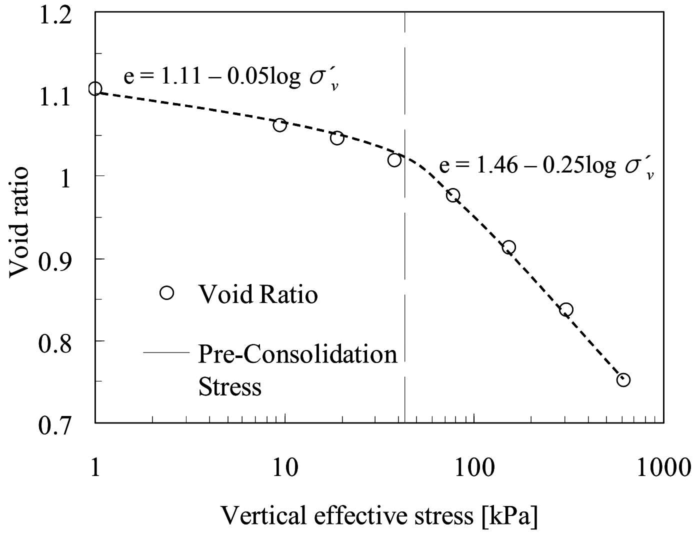

a. 5.5m specimen: $C_s = 0.05$, $C_c = 0.25$

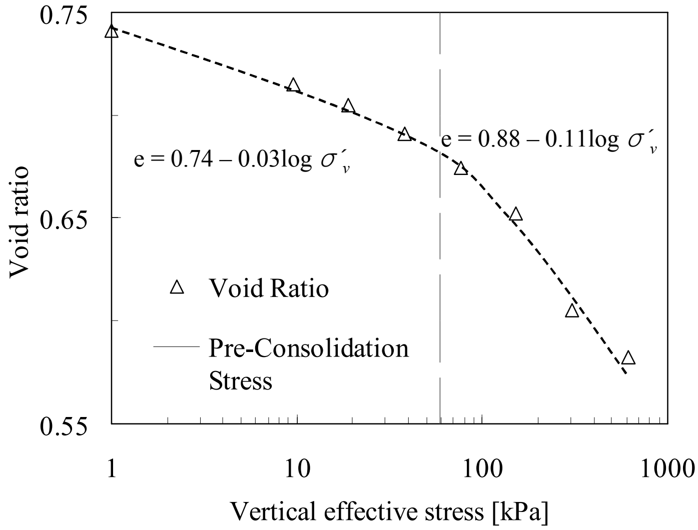

b. 7.5m specimen: $C_s = 0.03$, $C_c = 0.11$

Figure 3.22 Continued.

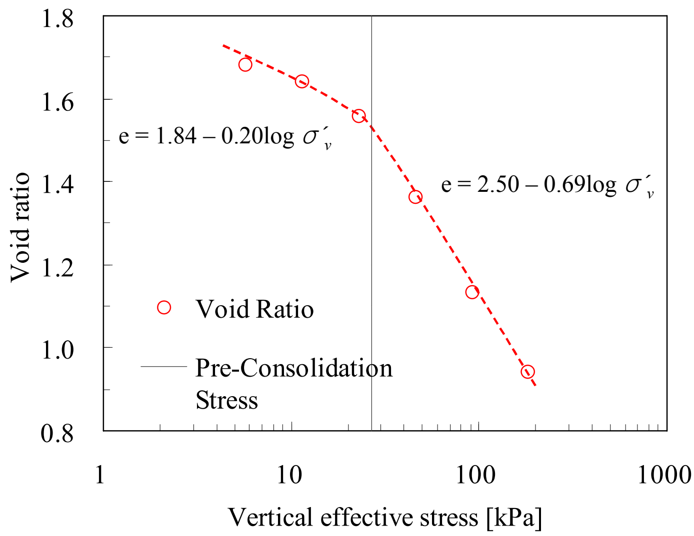

a. 5.0m specimen: $C_s = 0.20$, $C_c = 0.69$

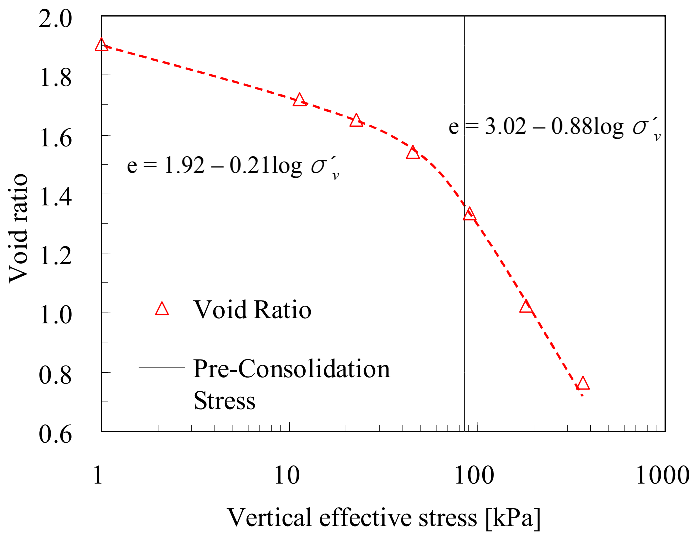

b. 15.0m specimen: $C_s = 0.21$, $C_c = 0.88$

Figure 3.23 Stress – strain curve of the submarine deposit, Busan.

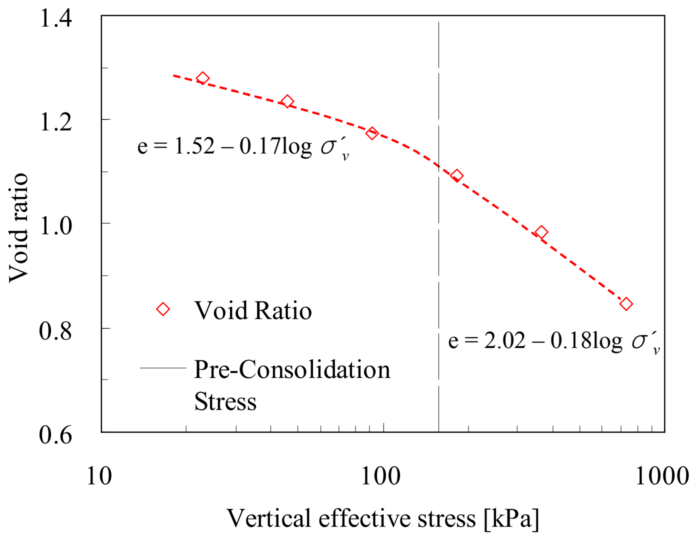

a. 28.0m specimen: $C_s = 0.17$, $C_c = 0.18$

Figure 3.23 Continued.

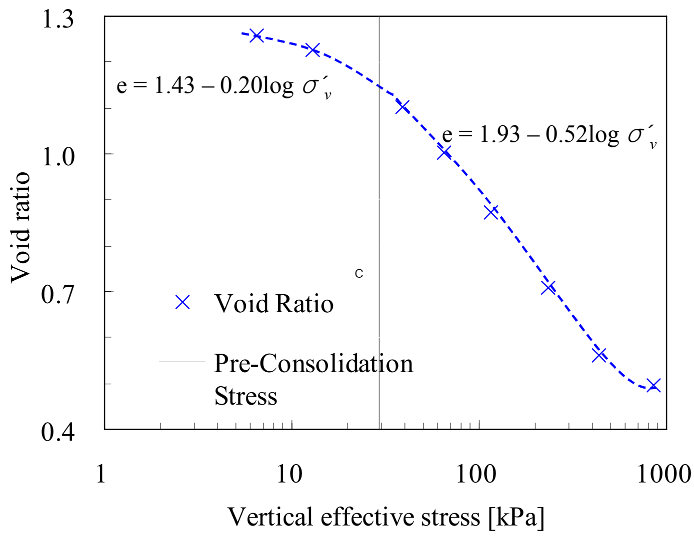

a. 5.0m specimen: $C_s = 0.20$, $C_c = 0.52$

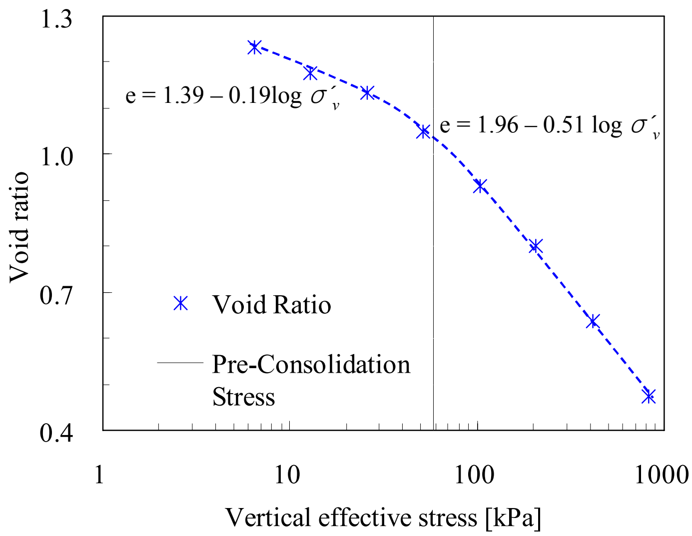

b. 10.0m specimen: $C_s = 0.19$, $C_c = 0.51$

Figure 3.24 Stress – strain curve of the thick clay deposit, Busan.

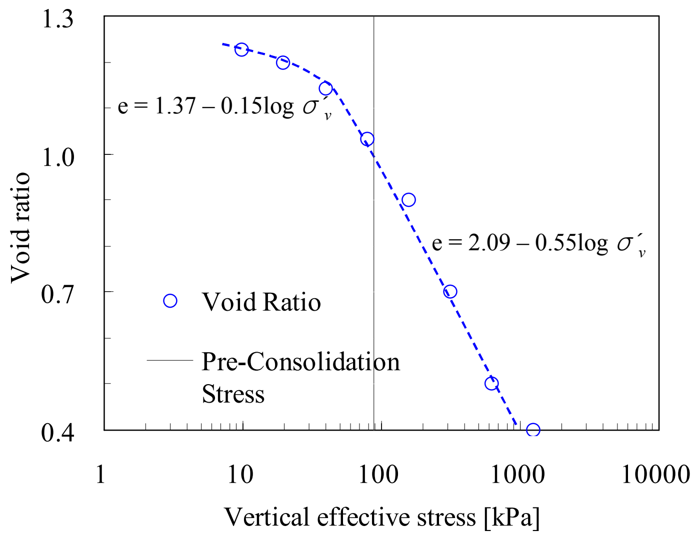

a. 15.0m specimen: $C_s = 0.15$, $C_c = 0.55$

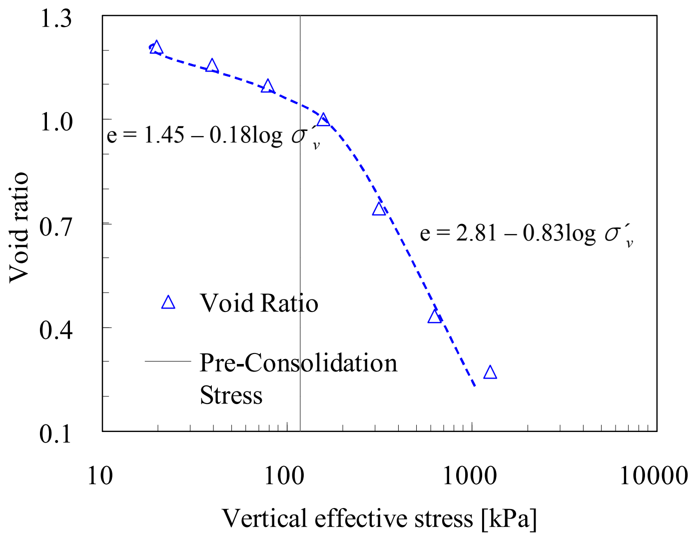

b. 20.0m specimen: $C_s = 0.18$, $C_c = 0.83$

Figure 3.24 Continued.

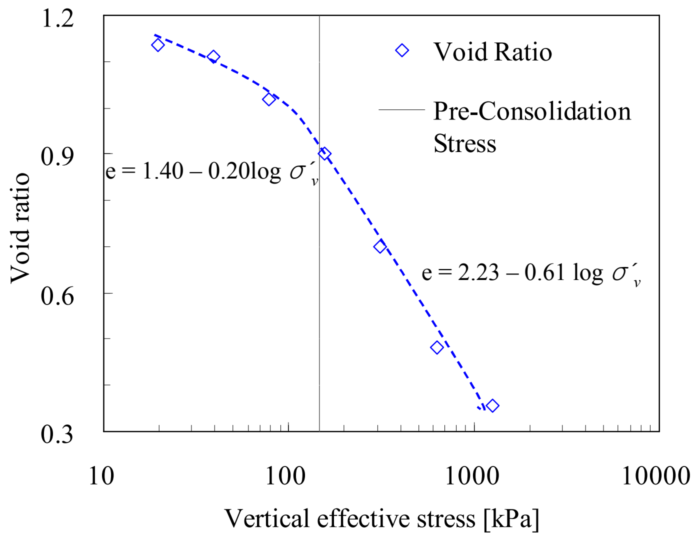

a. 15.0m specimen: $C_s = 0.20$, $C_c = 0.61$

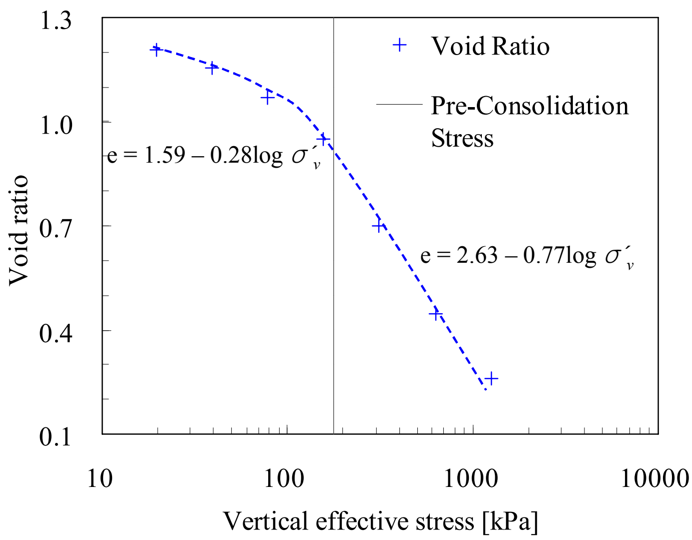

b. 20.0m specimen: $C_s = 0.28$, $C_c = 0.77$

Figure 3.24 Continued.

3.4 FIELD APPLICATION

The in-situ properties evaluated from the shear-wave-based laboratory tests are summarized in Table 3.8:

Table 3.8 Evaluated in-situ soil consolidation properties.

Site	Depth [m]	V_s^{field} [m/s]	σ'_o [kPa]	σ'_c [kPa]	Consolidation State	C_s	C_c
Foreshore Site (Incheon)	3.0	110	7.0	23.2	UC	0.07	0.19
	4.5	123	8.6	34.8	UC	0.02	0.15
	5.5	118	17.5	42.8	UC	0.05	0.25
	7.5	121	2.6	59.1	UC	0.03	0.11
Submarine Deposit (Busan)	5.0	113	41.7	28.0	OC	0.20	0.69
	15.0	115	83.9	83.9	NC	0.21	0.88
	28.0	126	20.1	156.6	UC	0.17	0.41
Thick Clay Deposit (Busan)	5.0	128	104.65	29.4	OC	0.20	0.52
	10.0	136	124.99	58.9	OC	0.19	0.51
	15.0	127	88.3	88.3	NC	0.14	0.55
	20.0	142	117.7	117.7	NC	0.18	0.83
	25.0	139	147.2	147.2	NC	0.20	0.61
	30.0	167	176.6	176.6	NC	0.28	0.77

The one-dimensional consolidation settlement (S_c) corresponding to an additional in-situ load ($\Delta\sigma$) for each condition was found to be as follows:

Normally / Under-consolidated layers

$$S_c = \frac{C_c H}{1+e_o} \log \frac{\sigma'_o + \Delta\sigma}{\sigma'_o} \tag{3.23}$$

Over-consolidated layers ($\sigma'_o + \Delta\sigma < \sigma'_c$)

$$S_c = \frac{C_s H}{1+e_o} \log \frac{\sigma'_o + \Delta\sigma}{\sigma'_o} \tag{3.24}$$

Over-consolidated layers ($\sigma'_o + \Delta\sigma < \sigma'_c$)

$$S_c = \frac{C_s H}{1+e_o} \log \frac{\sigma'_c}{\sigma'_o} + \frac{C_c H}{1+e_o} \log \frac{\sigma'_o + \Delta\sigma}{\sigma'_c} \tag{3.25}$$

Finally, the settlement of each layer was predictable when the quantity of an additional load was available.

3.5 SUMMARY AND CONCLUSIONS

The consolidation state and properties of clay deposits in nature were characterized through a study of shear-wave-based laboratory tests. Bender element sensors were used to measure the shear-wave velocity of the experimental specimens during the laboratory consolidation process.

The consolidation states of three sites were evaluated. A foreshore site was evaluated to be under-consolidated. A submarine deposit and a thick clay deposit had similar distributions: the top layer showed an over-consolidated condition, while the deep layers were normally or under-consolidated. However, the surface layer *OCR* value of the thick clay deposit was larger than that of the submarine deposit. The in-situ consolidation state distribution of each site is summarized in Fig. 3.25.

However, as discussed in section 3.3.3, the accuracy of an in-situ consolidation state evaluation depends on the accuracy of the in-situ shear-wave velocity data. A small error can cause highly inaccurate results. Therefore, reliable in-situ shear wave velocity testing is one of the most important prerequisites for a reliable in-situ consolidation state evaluation.

The consolidation state of clay deposits in nature can be evaluated by following the procedures as:

(1) Non-disturbed in-situ soil specimens may be sampled, using Shelby tube sampler.

(2) In-situ density profile and shear wave velocity distribution has to be evaluated

by field testing.

(3) Shelby tube oedometric device (Fig 3.9) is setup in laboratory.

(4) Laboratory consolidation test, measuring the shear wave velocity using piezoelectric bender element sensors, are performed.

(5) Vertical effective stress – shear wave velocity relationship is evaluated, using the final shear wave velocity of each load step.

(6) In-situ consolidation state is evaluated by comparing the in-situ shear wave velocity with the estimated effective stress – shear wave velocity trend. The site is evaluated as over-consolidated, if the in-situ shear wave velocity is higher than estimated value from laboratory, and is determined as under-consolidated for the opposite. The site is normally-consolidated when the in-situ shear wave velocity is close to the laboratory result.

(7) The degree of consolidation of under-consolidated specimens, and the over consolidation ratio of over-consolidated samples can be calculable by comparing the in-situ present stress state with the expected amount of effective stress of the normally compressed condition.

(8) The compressibility parameters, C_s and C_c of each sample are evaluated from the effective stress – void ratio curve from the laboratory data. The inflection

point shows a good accuracy matching with the estimated pre-consolidated stress value. Using the compressibility parameters, the in-situ settlement according to additional loads is predictable.

Following the descriptions, the consolidation states of three concerned sites were evaluated. The foreshore site was evaluated to be under-consolidated. The submarine deposit and thick clay deposit has a similar distribution, in which the top layer shows an over-consolidated condition, while the deep layers become normally or under-consolidated. Though, the surface layer *OCR* value of the thick clay deposit is bigger than the submarine deposit. The in-situ consolidation state distribution of each site is summarized in Fig. 3.25.

However, as discussed in section 3.3.3, the accuracy of in-situ consolidation state evaluation depends on the in-situ shear wave velocity data. A small error can give totally different results. Therefore reliable in-situ shear wave velocity testing is one of the most important prerequisite for reliable in-situ consolidation state evaluation in this study.

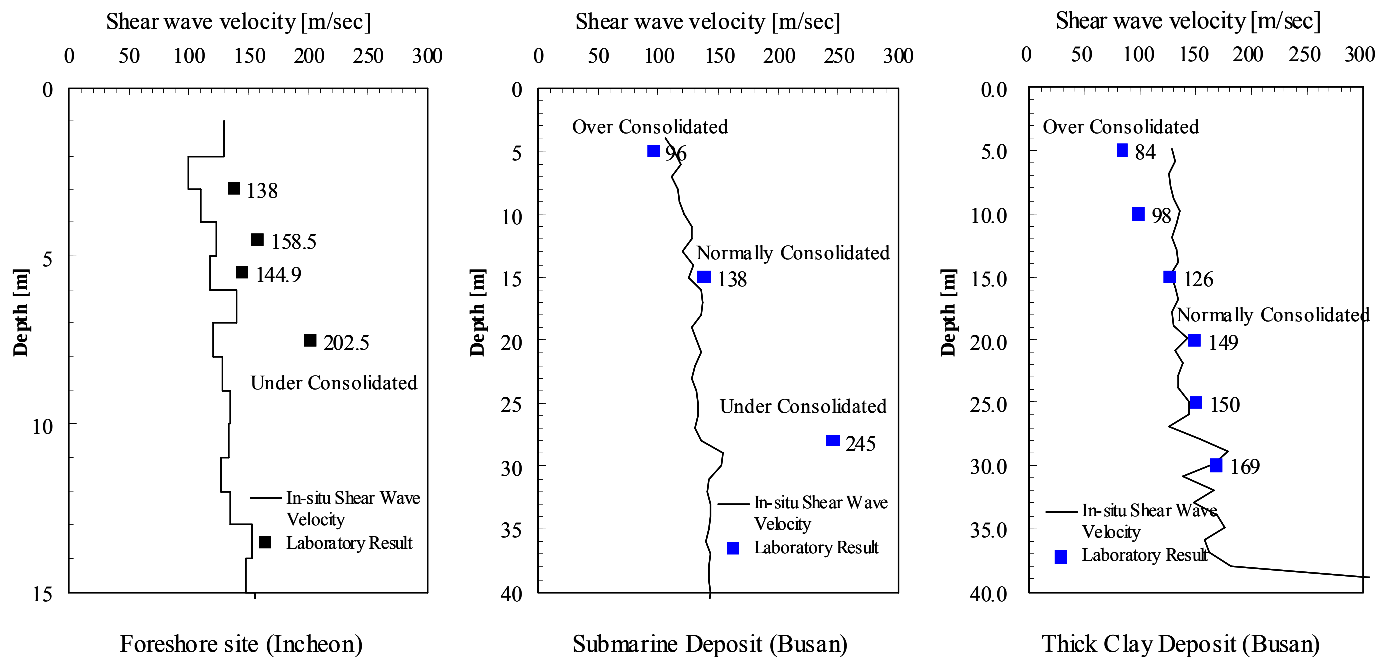

Figure 3.25 In-situ consolidation state and shear wave velocity distribution.

CHAPTER Ⅳ
EVALUATION OF THE CONSOLIDATION STATE OF DREDGED AND RECLAIMED CLAY USING SHEAR WAVES

4.1 Introduction

The characterization of dredged and reclaimed clay deposits is important to the prediction of their permanent settlement and strength as an additional load induced by offshore structure construction is applied in-situ. The strength condition of a reclaimed deposit is generally weak, and thus field improvement is required in order to accelerate the drainage of excess pore water pressure and thereby increase the in-situ density.

In general, reclamation follows sedimentation and self-weight consolidation processes. However, the free fall settling process is negligibly short in the case of kaolinite clay. Thus, the self-weight consolidation process is particularly meaningful in the characterization of most reclaimed deposits in Korea. The most widely used method to characterize the consolidation process in the laboratory is a large tank sedimentation test. However, the efficiency of this approach is low and it is also impossible to represent large stress conditions of deep soil elements. Meanwhile, field tests focus on settlement monitoring and pore pressure measurement. However, the settlement tendency is discordant with the degree of pore pressure dissipation (Schiffman et al., 1984), and the pore pressure measurement has several error factors, leading to unsatisfactory results. Accordingly, a non-destructive technique is required for monitoring the effective stress change during the self-weight consolidation of dredged clay. A shear wave propagates only through the soil skeleton, and its velocity depends on the effective stress of the soil (Santamarina et al., 2001). Therefore, shear wave velocities can accurately characterize the consolidation behavior based on effective stress variation.

In this chapter, a laboratory test method to simulate in-situ sedimentation and self-weight consolidation of dredged and reclaimed deposits is introduced. Because it is difficult to obtain undisturbed soil samples from reclaimed sites, a laboratory sedimentation test is required to remold the in-situ soil composition. Meanwhile, a laboratory consolidation test is performed to reproduce the in-situ self-weight consolidation process, even for deep conditions in a small specimen scale. Shear wave velocity is measured continuously inside the soil specimen so as to directly evaluate the effective stress behavior during sedimentation and self-weight consolidation.

4.2 Experimental Program

4.2.1 Site of Interest

The soil sample used in this study was collected from a reclaimed site near Kwang-Yang, Korea. The site of interest was reclaimed by dredged kaolinite slurry having 300% initial water content, and therefore the settling type is consolidation settling (Imai 1980). The effect of gravity on sedimentation is greater than that of the electric attraction when the water content of kaolinite slurry is below 500% (Imai. 1980). Thus, the effect of ionic concentration should be negligible. The soil sample from the field was totally disturbed. Therefore, average values were used to characterize the in-situ soil properties, as shown in Table 4.1. The in-situ drill log profile is shown in Fig. 4.1.

Table 4.1 Properties of the in-situ soil sample.

Specific Gravity , G_s	Average Water Content, w [%]	Degree of Saturation [%]	Average Void Ratio	Soil Type	Percent finer #200 sieve [%]
2.68	72	98	2.1	CL / CH	92
D_{50} [mm]	Water Salt Concentration [%]	Average Density [g/cm^3]	Average Liquid Limit, LL [%]	Average Plastic Limit , PL [%]	Average Plasticity Index , PI [%]
0.015	0.3	1.63	60	29	32

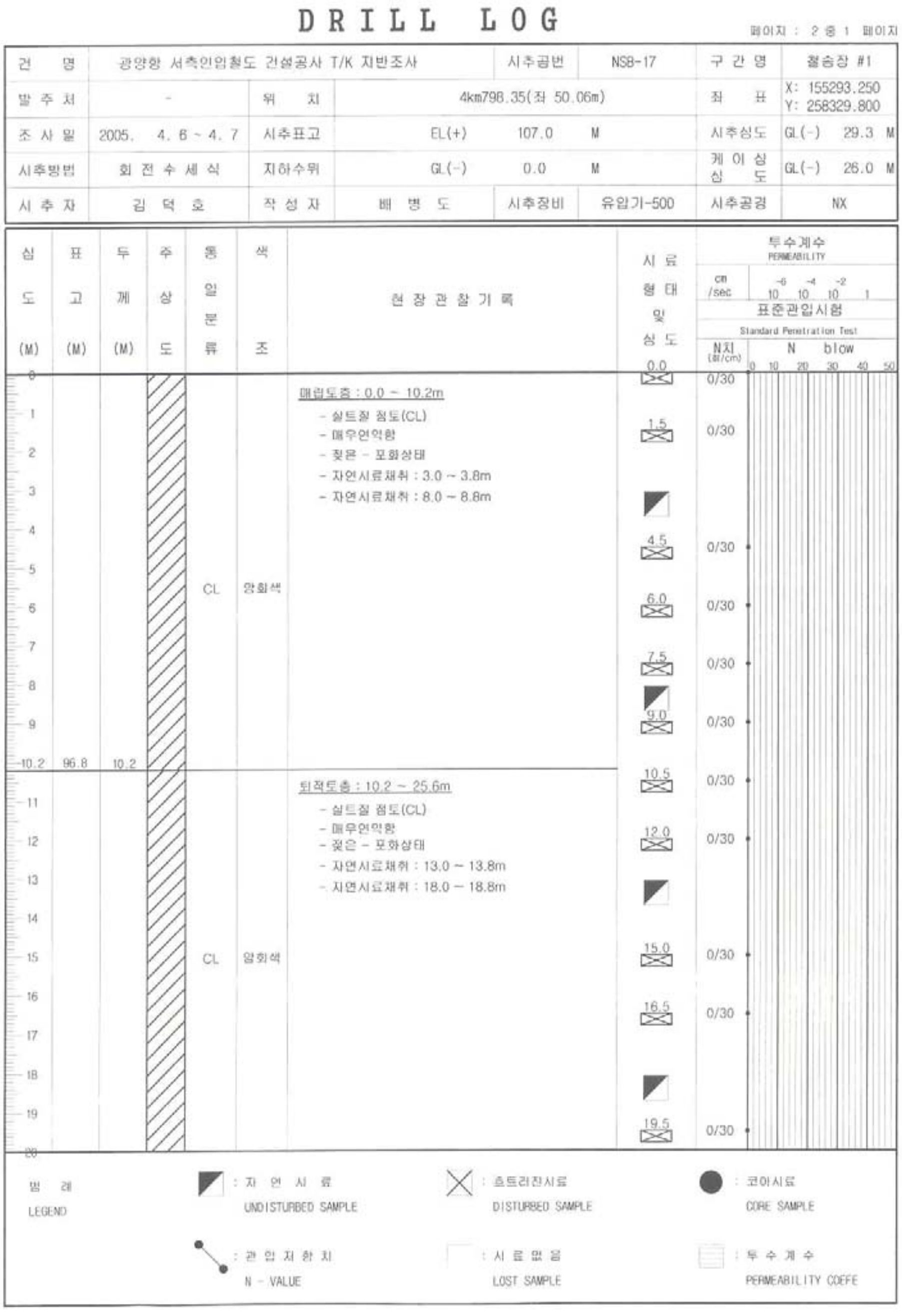

Figure 4.1 Drill log profile of the site of interest, Kwangyang.

4.2.2 Sedimentation Testing Device

In-situ dredged soil follows sedimentation and self-weight consolidation processes to form reclaimed sites. A sedimentation tube device was made to simulate the in-situ sedimentation and self-weight consolidation process of reclamation in the laboratory. A laboratory sedimentation test was performed to represent the in-situ particle composition and soil fabric, while a consolidation test was applied to simulate the in-situ self-weight consolidation process of various depths.

The acrylic tube is 400mm in height and 80mm in diameter. The tube has the special feature of a separable oedometric cell at its bottom (Fig. 4.2). The separable oedometric cell is 80mm in height and 80mm in diameter. A piezoelectric bender element sensor is installed at the center of the bottom (Fig. 4.3). The guide tube and separable oedometric cell were screwed together, and vacuum grease was lubricated on the screw to prevent leakage from the joints. Drainage paths were drilled at the bottom to allow downward drainage during the laboratory consolidation test (Fig. 4.4). However, the drainage holes were closed during the sedimentation test.

A load cap was designed for two purposes: to apply uniformly distributed stress to the specimen in the oedometric cell and to fix the bender element sensor, which will receive the generated signal from the bottom bender element. While it is recommended to make the cap as light as possible, the acrylic cap was designed to be 30mm in height and 79mm in diameter for durability consideration. Vertical drainage holes were also drilled to allow upward drainage during the laboratory consolidation test. Top and bottom views of the load cap are shown in Fig. 4.5.

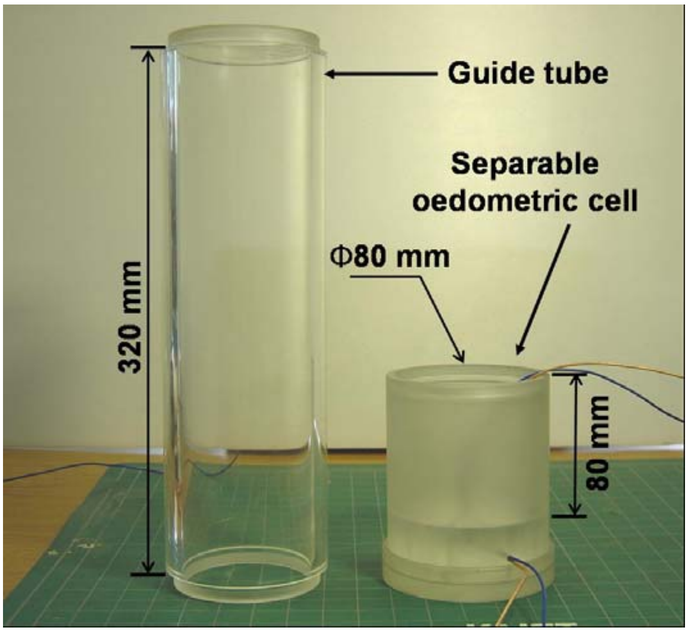

Figure 4.2 Guide tube and separable oedometric cell of the sedimentation test device.

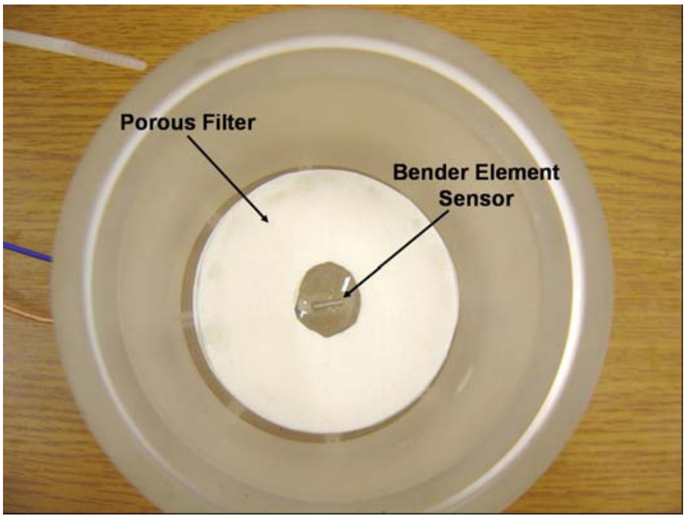

Figure 4.3 Top view of the separable oedometric cell.

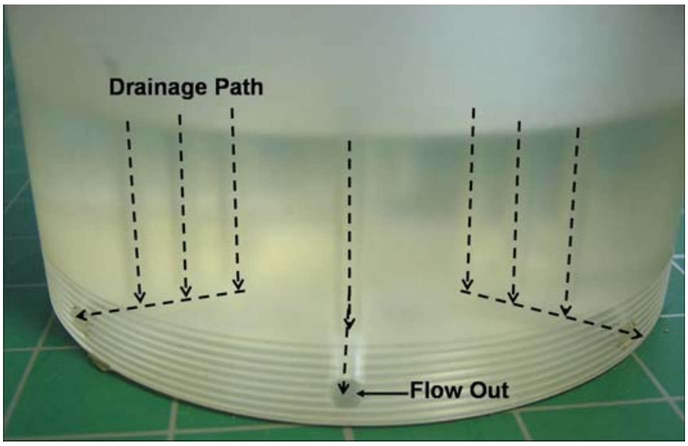

Figure 4.4 Drainage system of the oedometric cell.

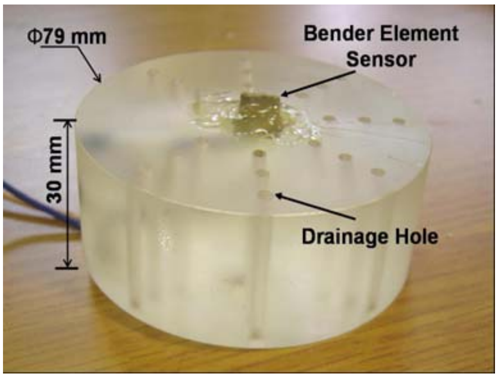

a. Sensor installed load cap.

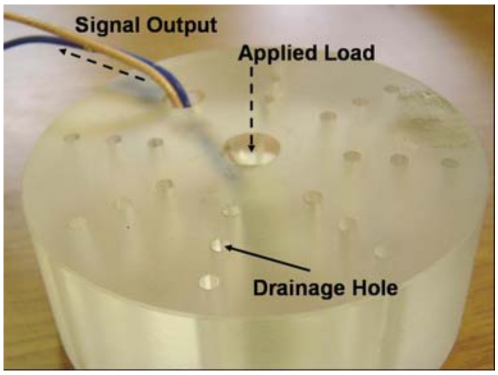

b. Top view of the load cap.

Figure 4.5 Load cap.

4.2.3 Electronic Peripheral Device

Piezoelectric bender element sensors were used to measure the shear wave velocity variation during laboratory testing. Details of bender element used in this study are provided in section 3.2.2.

The bender is installed in the cell and connected to a signal generator to be used as a source. Meanwhile, the load cap bender – receiver is connected to a signal conditioner for signal amplification and noise filtering. The signal generation devices, i.e. a wave form generator, a multi channel filter, and a digital oscilloscope, are shown in Fig. 3.10.

4.3 Sedimentation Test - Specimen Remolding

It is impossible to take undisturbed samples from the dredged and reclaimed field because its soil is weak. Thus specimen remolding is one of the most important requirement for simulating the in-situ sedimentation in laboratory. The sedimentation and self-weight consolidation process of dredged and reclaimed soil is affected by several factors, such as the soil type, initial water content, local concentration of particles, and ionic concentration of the dredged slurry (Imai, 1980).

The sampled clay was washed and dried under 120℃ temperature to remove any organic matters. Distilled water has been used as a solvent to control the salt concentration of the mixed slurry. A 300g dry soil and 900g distilled water were mixed together to make a 300% water content slurry, which is the same as the in-situ initial water content for consolidation settling behavior. Salt minerals were added to equilibrate the ionic concentration with the in-situ condition.

The prepared slurry was poured into the set-up sedimentation tube for sedimentation test. Four different specimens were prepared at the same time. After the settlement converges, weak sediment which represents the in-situ soil composition is formed at the bottom, actually, inside the separable oedometric cell of the sedimentation tube. Fig. 4.6 shows photographic images taken during the sedimentation test and Fig. 4.7 shows the measured volume change of the soil with time.

After the sedimentation process, the separable oedometric cell was dismantled from the tube. The basic element specimen reconstituted in the oedometric cell represents the initial state of the in-situ self-weight consolidation process (Fig. 4.8).

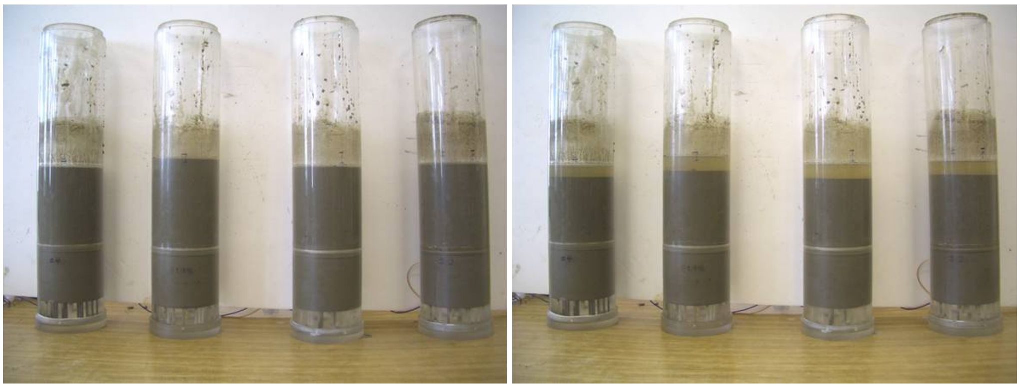

a. Initial (t=0). b. 2 hours later.

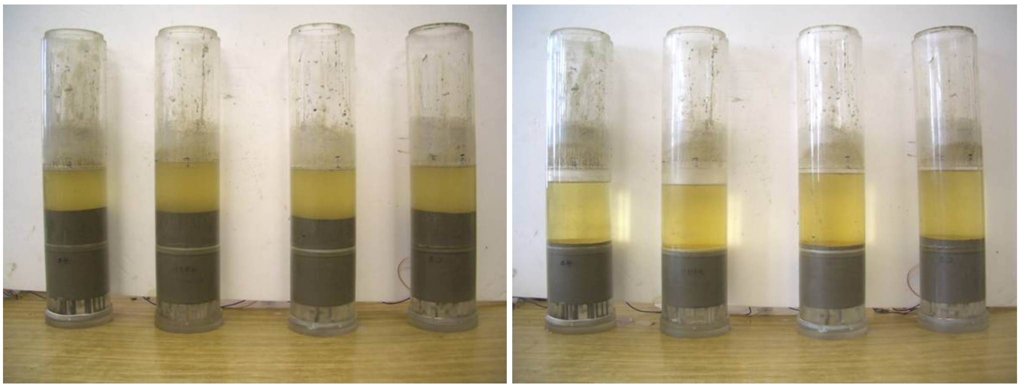

c. One day later. d. Final (t = 3 days).

Figure 4.6 Photographic images taken during the sedimentation test.

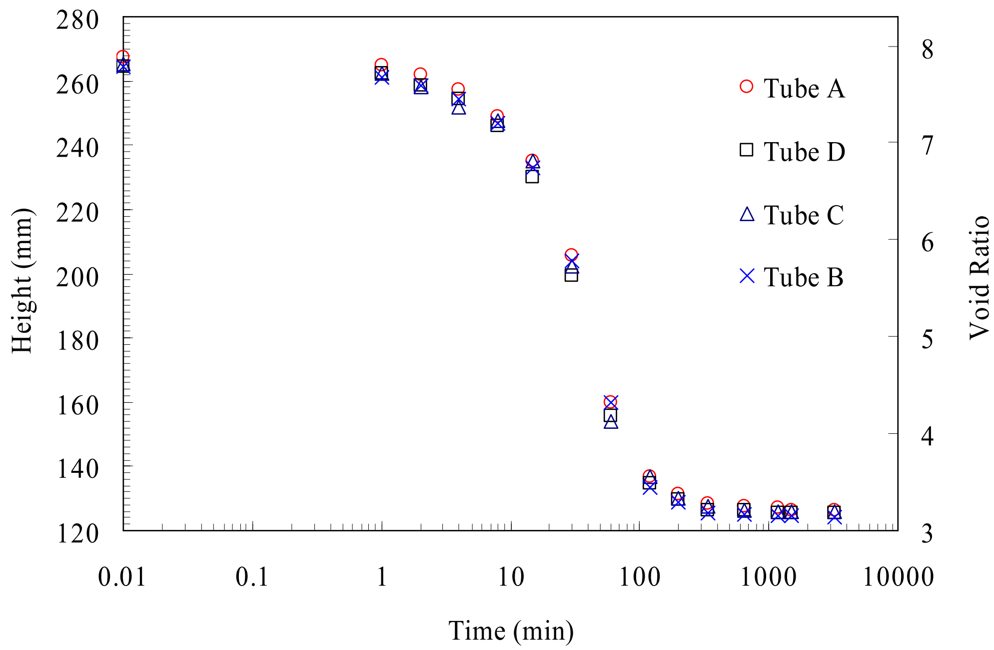

Figure 4.7 The measured volume change of the soil with time.

Figure 4.8 Reconstituted basic element specimens.

4.4 Consolidation Test

4.4.1 Basic Concept

The in-situ self-weight consolidation process was reproduced in a laboratory setting by applying the expected total amount of effective stress to the oedometric cell specimen obtained from the sedimentation tube. The validity of this experimental configuration is based on the attribute that the total amount of stress that an in-situ soil element receives under sedimentation is determined by its initial location at the beginning of soil structure formation, rendering the constant total stress condition. After the specimens are subjected to their corresponding additional loading, the excessive pore-water pressure dissipates and the effective stress increases with time.

4.4.2 Testing Sequence

The separated oedometric cell specimen was placed on an oedometric testing device and porous materials were placed both at the top and bottom of the specimen in order to allow the water to drain in two directions during loading. The bender element anchored load cap was placed on the top of the specimen immediately prior to loading.

The self-weight consolidation of the in-situ sedimentation process was simulated by applying the expected total effective overburden stresses to the load cap placed on the oedometric cell specimen. This is practicable because the relative positions between soil particles are irreversible during sedimentation and consolidation. Therefore, even though the volume of the overlying layer decreases, the effective density increases, and thus the expected effective stress value is calculable at any phase of the self-weight consolidation process.

During loading, a signal wave was generated and sent to the source bender element. The response of the receiver bender element was recorded. The vertical shear wave travel time was measured between the top and bottom bender elements. As all four specimens were available to measure the vertical shear wave travel time, one oedometric cell has a pair of bender elements installed at the side wall in order to measure the horizontal shear wave velocity during the consolidation process. The vertical deformation of the specimen was measured from a dial gauge. The vertical shear wave velocity [m/sec] was calculated by dividing the specimen height [m] with the vertical shear wave travel time [sec]. As horizontal displacement is not allowed in the oedometric cell, the horizontal shear wave velocity could be calculated by dividing the fixed specimen width with the horizontal shear wave travel time (Fig. 4.9).

The thickness of the in-situ reclaimed deposit is around 12m. Therefore, the specimens were selected such that they represent different depths: 2.5m, 5.0m, 7.5m, and 10.0m. In particular, the 7.5m specimen was related to the oedometric cell, which has horizontal bender elements installed inside. The applied load of each specimen was determined by the in-situ density profile (Fig. 4.1). The experimental properties are summarized in Table 4.2.

Table. 4.2 Summary of experimental properties.

Site of Interest		2.5 m	5.0 m	7.5 m	10.0 m
Average In-situ Density [g/cm^3]		1.63	1.63	1.63	1.63
Sedimentation Test	Dry Soil [g]	300	300	300	300
	Initial Void Ratio	7.80	7.80	7.80	7.80
Consolidation Test	Applied Load [kPa]	15.4	30.8	46.2	61.7
	Initial Void Ratio	2.47	2.56	2.54	2.61

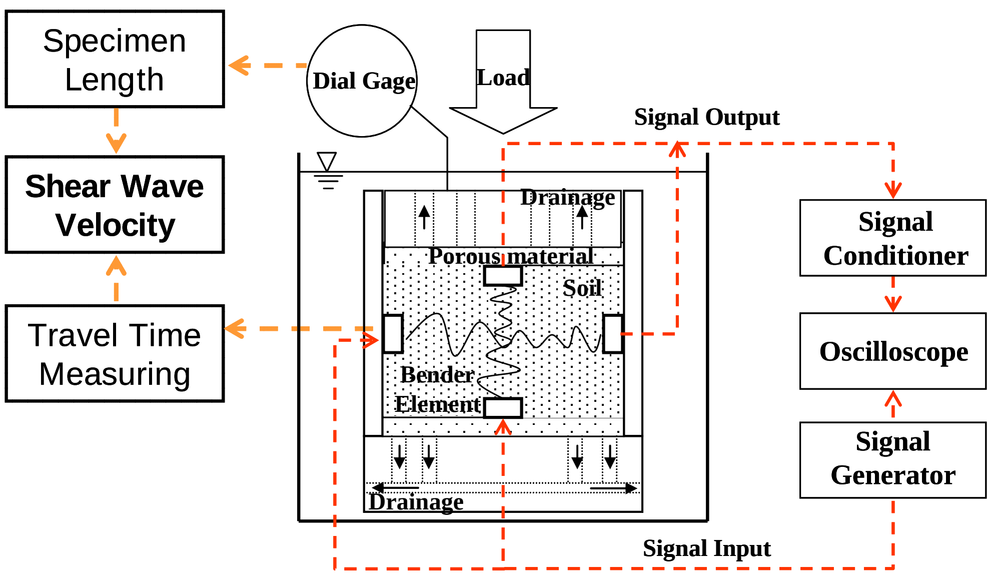

Figure 4.9 Self-weight consolidation testing system.

4.5 Experimental Results and Analysis

4.5.1 Shear Wave Velocity and Void Ratio Variation

The shear wave velocity increment and void ratio diminution of each specimen are shown in Fig. 4.10. The shear wave velocity variation shows an S-shape curve with a logarithmic time scale, while the void ratio trend is overturned. The period where the shear wave velocity increases rapidly appears earlier, as the applied load increases.

Even though the specimen volume shows an abrupt decrease, the shear wave velocity does not increase rapidly at the beginning of loading. This is attributed to the time delay of the excess pore water pressure dissipation. However, the delay time is brief, and thus the shear wave velocity increases 1 minute after loading.

The results of the laboratory consolidation test are presented in Table 4.3.

Table 4.3 Results of the consolidation test.

Site of Interest		2.5 m	5.0 m	7.5 m	10.0 m
Applied Load [kPa]		15.4	30.8	46.2	61.7
Final Void Ratio		1.68	1.55	1.51	1.41
Vertical Shear Wave Velocity	Before Load [m/sec]	22.6	22.0	19.5	20.1
	After Load [m/sec]	68.0	106.3	124.0	153.0

The initial vertical shear wave velocity of the soft clay sediment is low because its particle packing is loose. In the case of one-dimensional consolidation, when the load that represents the total overburden weight for the self-weight consolidation process is applied to the specimen, the total stress is resisted by the excess pore water pressure. The hydraulic pressure head difference causes the pore fluid to flow upward and downward through the drainage path, and thus the pore water pressure decreases. The particle packing thereupon becomes denser as the pore water pressure decrement transfers to the vertical effective stress increment. The rate of pore pressure dissipation is initially high and continuously decreases according to the permeability diminution as the soil becomes denser. In other words, the effective stress increases on a logarithmic time scale, which agrees with the vertical shear wave velocity variation results shown in Fig. 4.10.

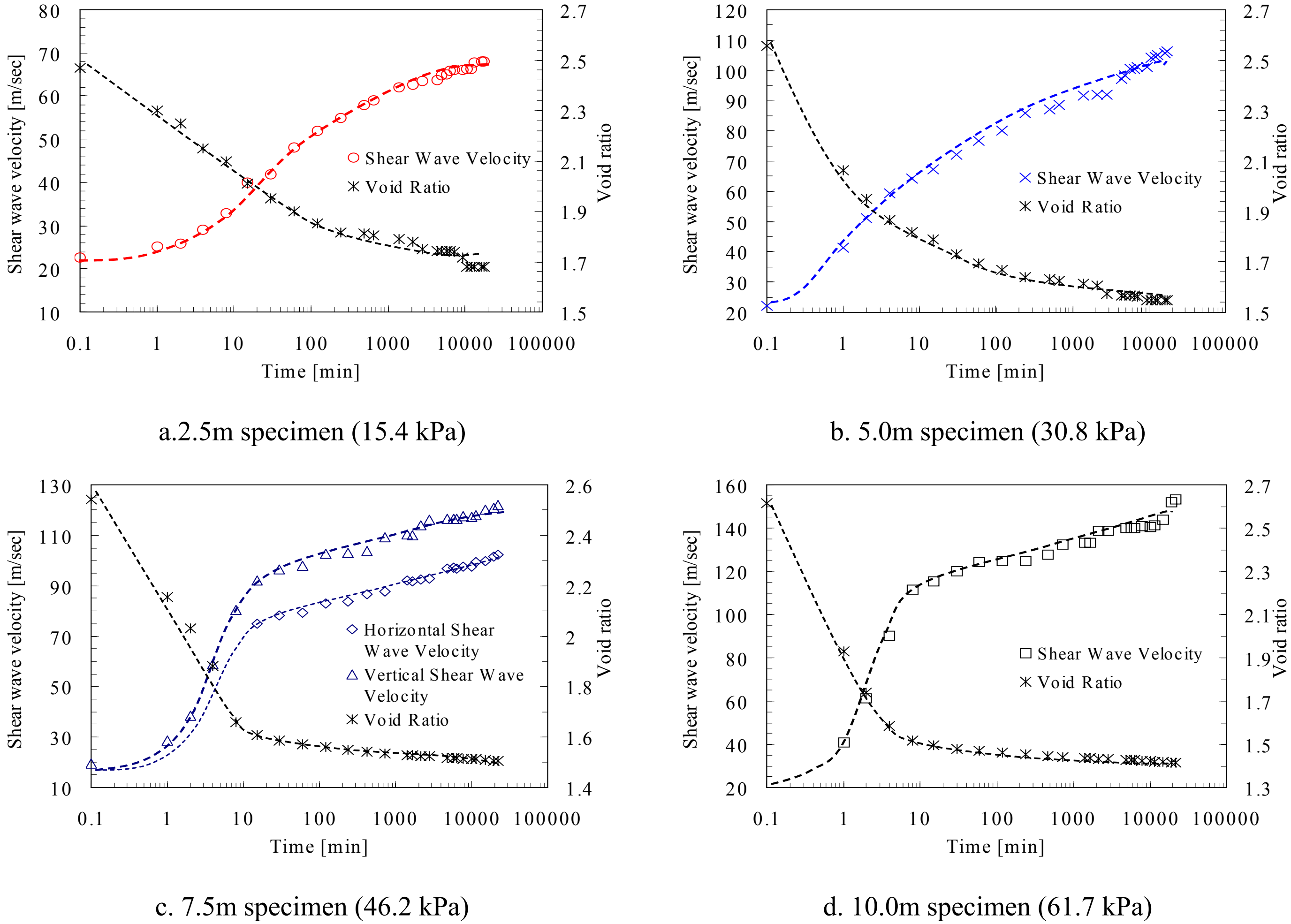

Figure 4.10 Shear wave velocity and void ratio variation during laboratory consolidation test.

4.5.2 Vertical Effective Stress – Shear Wave Velocity Relation

The vertical effective stress – shear wave velocity relationship of the specimen can be derived by curve fitting the converged shear wave velocity results. The convergence of the vertical shear wave velocity means that the excess pore water pressure is completely dissipated, and thus the amount of vertical effective stress inside the specimen becomes equal to the applied load. In chapter 3, different vertical effective stress – shear wave velocity equations were derived for each specimen. However, as the soil type of a single dredged site and that of a reclaimed site are the same, it can be assumed that even though the density varies with depth, the particle arrangement and composition are similar. This means that the effective stress state is the only independent variable for normally-consolidated reclaimed deposits.

Curve fitting approximation by MATHCAD (Appendix B.2) was used to derive the vertical effective stress – shear wave velocity equation from the experimental results. The converged vertical effective stress and shear wave velocity data were plotted on an effective stress – shear wave velocity plane for curve fitting (Fig. 4.11). The parameters α and β can then be determined with a least square solution, rendering:

$$\alpha = 16.47\mathrm{m/sec} \quad , \quad \beta = 0.56 \tag{4.1}$$

Finally, the vertical effective stress – shear wave velocity equation for the laboratory specimens was estimated by substituting the parameter values ($\alpha = 16.47\mathrm{m/sec}$, $\beta = 0.56$) into Eq. 2.41, thus yielding the following:

$$V_{s-v} = 16.5\left(\frac{\sigma'_v}{1\text{kPa}}\right)^{0.56} \tag{4.2}$$

where $V_{s\text{-}v}$ is the vertical shear wave velocity and σ'_v is the vertical effective stress.

Therefore, the vertical effective stress – shear wave relation for each specimen (2.5m, 5.0m, 7.5m, 10.0m) can be plotted by substituting the experimental shear wave velocity measurement results into Eq. 4.2 (Fig. 4.12). Moreover, Eq. 4.2 shows that a normally / under-consolidated dredged reclaimed site has a one-to-one relationship of vertical effective stress versus shear wave velocity.

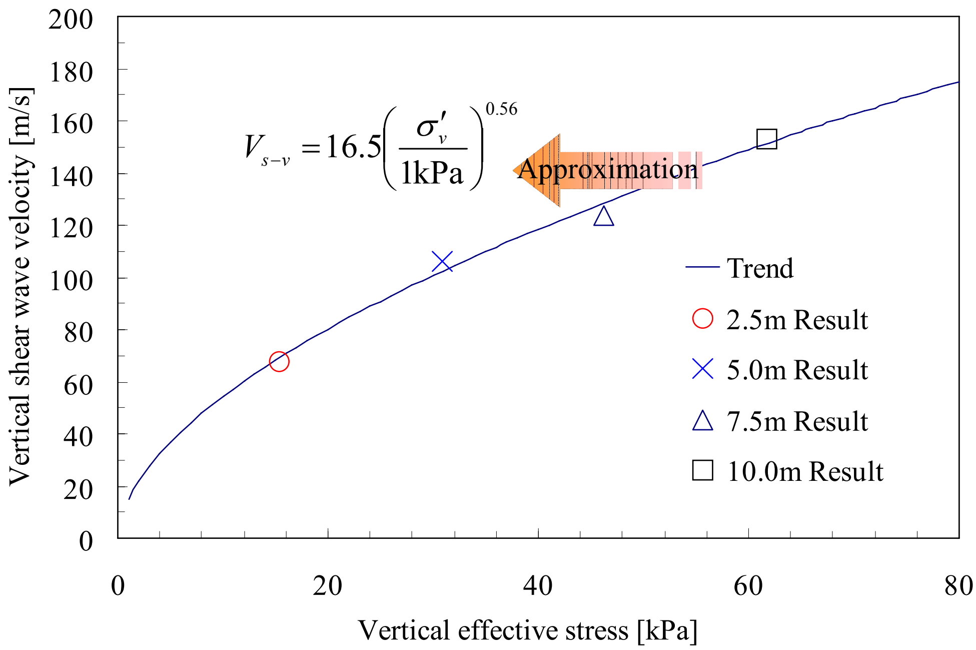

Figure 4.11 Curve fitting of the vertical effective stress – shear wave velocity relation.

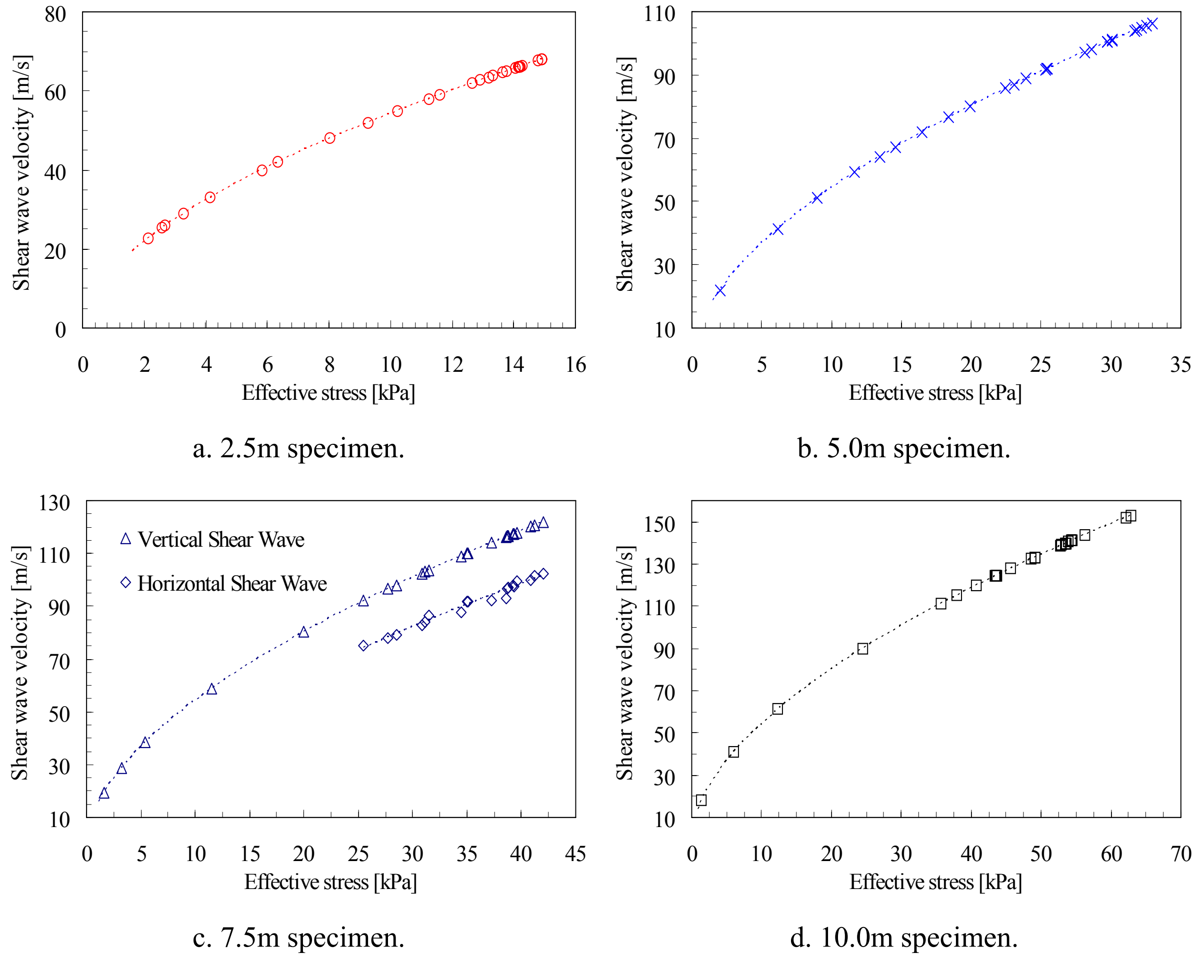

Figure 4.12 Vertical effective stress – shear wave velocity relationship for each specimen.

4.5.3 Degree of Consolidation

The degree of consolidation at any depth z is defined as:

$$U_z = \frac{\text{Excess pore water pressure dissipated}}{\text{Initial excess pore water pressure}} = \frac{u_i - u}{u_i} = 1 - \frac{u}{u_i} = \frac{\Delta\sigma'}{u_i} \tag{4.3}$$

where u_i is the initial maximum excess pore water pressure and $\Delta\sigma'$ is the increase of effective stress due to consolidation. In reality, u_i is equal to the final effective stress value (σ'_f) for each specimen, and $\Delta\sigma'$ is the vertical effective stress state. As the vertical effective stress is a function of shear wave velocity, Eq. 4.2 can be re-written as:

$$\left(\frac{\sigma'_v}{1kPa}\right) = \left(\frac{V_{s-v}}{16.5}\right)^{\frac{1}{0.56}} \tag{4.4}$$

Therefore, the degree of consolidation becomes a function of shear wave velocity by combining Eq. 4.3 and Eq. 4.4.

$$U_z = \frac{1}{\sigma'_f}\left(\frac{V_{s-v}}{16.47}\right)^{\frac{1}{0.56}} \tag{4.5}$$

The relationship between the degree of consolidation and vertical shear wave velocity is plotted in Fig. 4.13. The shear wave velocity can be approximately related to the degree of consolidation for each specimen as follows:

$$V_{s-v}^{2.5m} = 68.0U^{0.56} \qquad \text{for 2.5m depth} \qquad (4.6)$$

$$V_{s-v}^{5.0m} = 106.3U^{0.56} \qquad \text{for 5.0m depth} \qquad (4.7)$$

$$V_{s-v}^{7.5m} = 122.0U^{0.56} \qquad \text{for 7.5m depth} \qquad (4.8)$$

$$V_{s-v}^{10.0m} = 153.1U^{0.56} \qquad \text{for 10.0m depth} \qquad (4.9)$$

The estimated degree of consolidation values does not take into consideration the excess pore water distribution inside the soil specimen during consolidation. This is because the shear wave velocity used in the evaluation is the average shear wave velocity between the bottom and top of the specimen. Thus, the evaluated degree of consolidation is the average degree of consolidation of the specimen (U_z=U_{av}). However, as the specimen size is relatively small compared to the in-situ deposit thickness, the evaluated degree of consolidation can be considered as a point value.

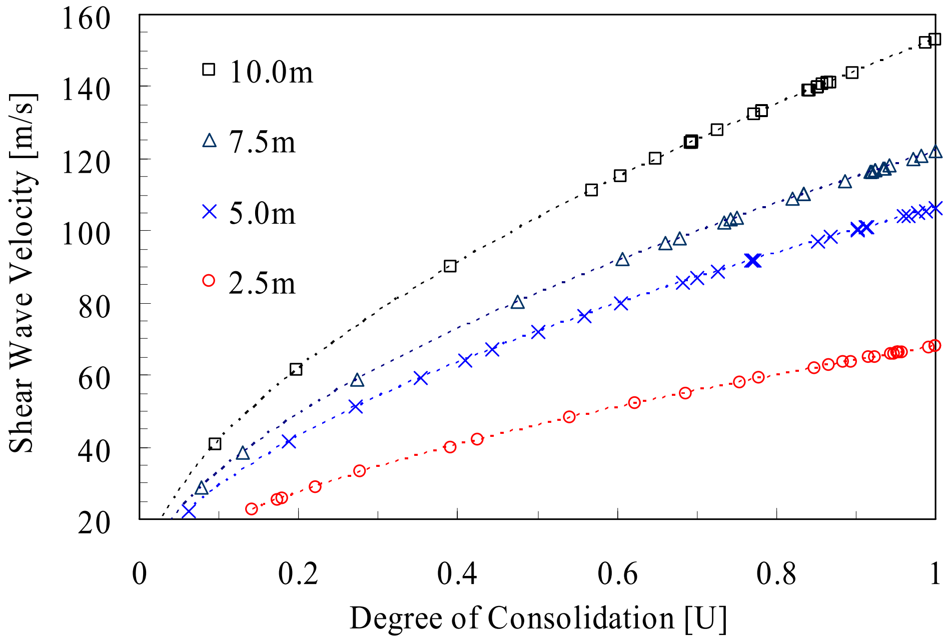

Figure 4.13 Degree of consolidation – vertical shear wave velocity relationship.

4.5.4 Coefficient of Consolidation

In classical soil mechanics, the coefficient of consolidation (C_v) for soil deposits is assumed to be constant. However, the permeability decreases as the density increases during consolidation and the drainage ability of pore water decreases. Therefore, the coefficient of consolidation must decrease as the degree of consolidation increases.

The coefficient of consolidation during laboratory testing can be evaluated using the specimen height variation (H-t), and the degree of consolidation – vertical shear wave velocity relationship (U-$V_{s\text{-}v}$) from section 4.5.3.

As both upward and downward drainage are allowed, the length of the maximum drainage path (H_{dr}) of the specimen is

$$H_{dr} = \frac{H}{2} \tag{4.10}$$

where H is the specimen height. The time factor (T_v) can be expressed in terms of U_{av} (Eqs. 2.17, 18, and 19). Considering Eq. 4.5,

$$T_v = f(U_{av}) = f(V_{s-v}) \tag{4.11}$$

Thus, the coefficient of consolidation can be defined as follows:

$$C_v = \frac{{H_{dr}}^2 T_v}{t} = \frac{{H_{dr}}^2 \cdot f(V_{s-v})}{t} \tag{4.12}$$

As H_{dr} and t are known and measured during consolidation tests, the coefficient of consolidation becomes a function of the vertical shear wave velocity. The coefficient of consolidation is plotted against the vertical shear wave velocity in Fig. 4.14 (Details of the calculation can be found in Appendix B.3)

The coefficient of consolidation decreases as the vertical shear wave velocity increases. This accounts for the decrease of permeability caused by densification during consolidation.

The coefficient of consolidation is plotted against the degree of consolidation in Fig. 4.15. The coefficient of consolidation decreases with the increase in the degree of consolidation and has a unique relation with the degree of consolidation regardless of the applied vertical stresses. An approximate equation for the $U - C_v$ relationship is:

$$C_v \, (\mathrm{m}^2 / \mathrm{min}) = 0.17 \cdot \exp(-12.1 \cdot U) \tag{4.13}$$

This equation is applicable for all depths of reclaimed soil. That is, the coefficient of consolidation is a function of the degree of consolidation for normally and under-consolidated soft clay deposits.

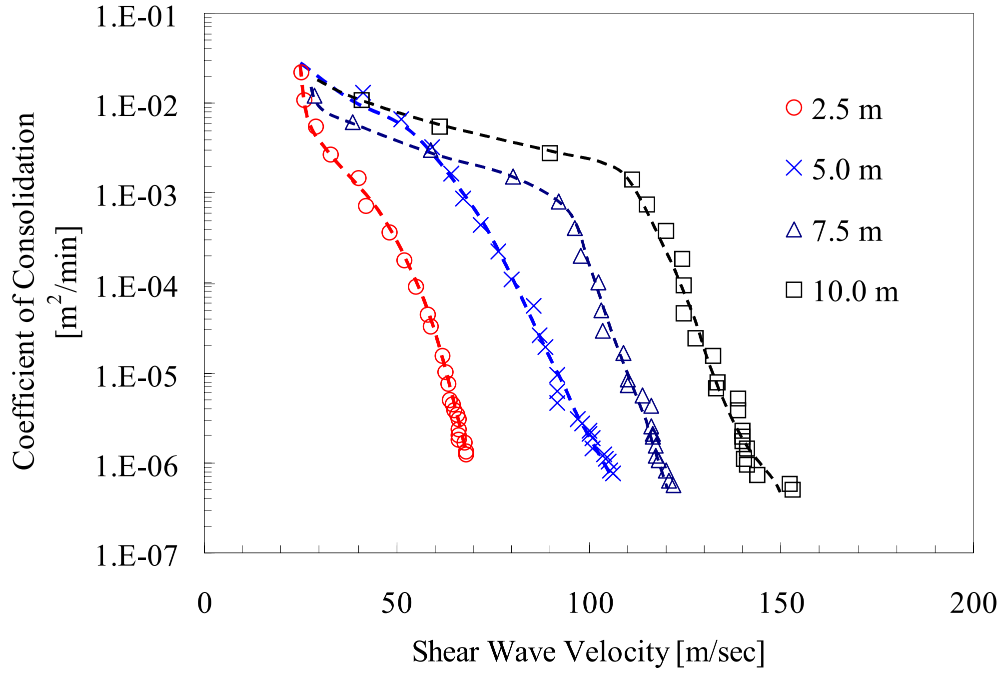

Figure 4.14 The variation of the coefficient of consolidation with the vertical shear wave velocity.

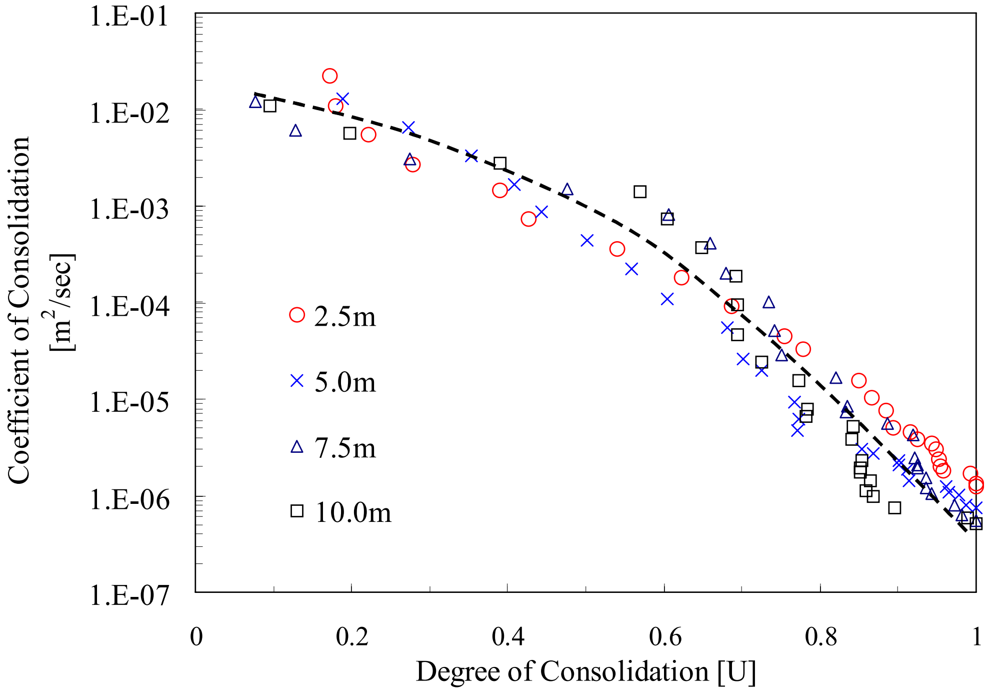

Figure 4.15 Degree of consolidation and coefficient of consolidation relationship.

4.5.5 Coefficient of Earth Pressure at Rest

The horizontal shear wave velocity was also measured for the 7.5m specimen (Fig. 4.10(c)). The result demonstrates the high accuracy of the bender element sensors for horizontal shear wave monitoring. The vertical effective stress – horizontal shear wave velocity relationship is approximated from data in Fig. 4.12(c) as:

$$V_{s-h} = 9.7\left(\frac{\sigma'_v}{1\text{kPa}}\right)^{0.56} \tag{4.14}$$

where V_{s-h} is the horizontal shear wave velocity.

The ratio of the horizontal stress to the vertical stress, when horizontal strain is not allowed, is called the coefficient of earth pressure at rest, K_o (Das 1998). Thus, the horizontal shear wave represents the K_o condition of the in-situ process. The horizontal shear wave velocity and vertical effective stress are related as follows (Santamarina, et al. 2001):

$$V_{s-h} = \alpha_1\left(\frac{K_o\sigma'_v}{1\text{kPa}}\right)^{\beta_1} = \alpha_1 K_o{}^{\beta_1}\left(\frac{\sigma'_v}{1\text{kPa}}\right)^{\beta_1} \tag{4.15}$$

β_1 corresponds with $\beta = 0.56$ from Eq. 4.14, and thus Eq. 4.15 can be written:

$$V_{s-h} = \alpha_1 K_o{}^{0.56}\left(\frac{\sigma'_v}{1\text{kPa}}\right)^{0.56} = 9.71\left(\frac{\sigma'_v}{1\text{kPa}}\right)^{0.56} \tag{4.16}$$

The vertical shear wave velocity and effective stress relationship (Eq. 2.41) is writeen as follows:

$$V_{s-v} = \alpha_1 \left(\frac{(1+K_o)\sigma'_v}{2\text{kPa}} \right) = \alpha_1 \left(\frac{1+K_o}{2} \right)^{\beta} \left(\frac{\sigma'_v}{1\text{kPa}} \right)^{\beta} \tag{4.17}$$

The ratio between vertical and horizontal shear wave velocity is expressed from Eqs. 4.15 and 17:

$$\frac{V_{s-v}}{V_{s-h}} = \frac{\alpha_1 \left(\frac{1+K_o}{2} \right)^{\beta} \left(\frac{\sigma'_v}{1\text{kPa}} \right)^{\beta}}{\alpha_1 K_o{}^{\beta} \left(\frac{\sigma'_v}{1\text{kPa}} \right)^{\beta}} = \left(\frac{1+K_o}{2K_o} \right)^{\beta} \tag{4.18}$$

Finally, the coefficient of earth pressure at rest K_o can be defined:

$$K_o = \left\{ 2\left(\frac{V_{s-v}}{V_{s-h}} \right)^{\frac{1}{\beta}} - 1 \right\}^{-1} \tag{4.19}$$

As β=0.56, Eq. 4.19 shows that K_o varies during the self-weight consolidation process. From the analysis, the initial value of K_o is estimated to be 0.5 and increases during consolidation, finally approaching 0.6 (Fig. 4.16).

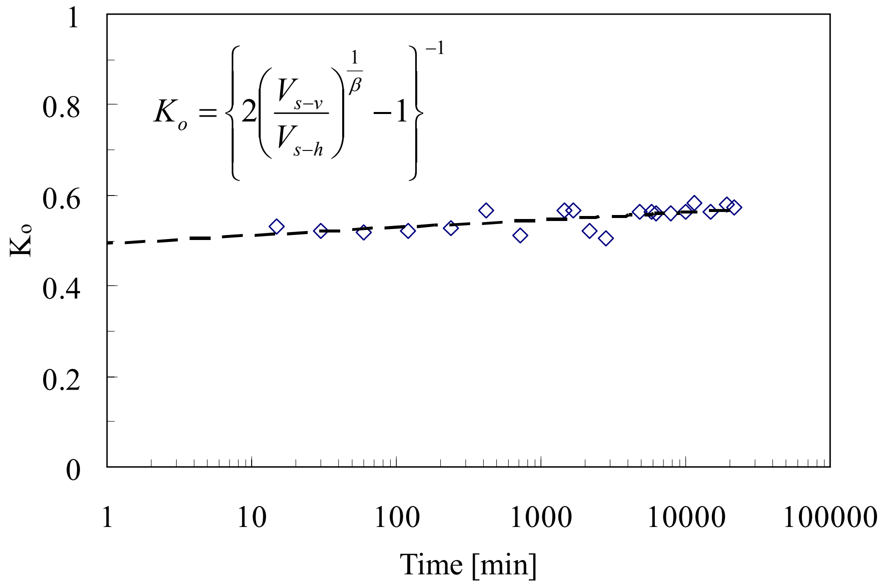

Figure 4.16 Coefficient of earth pressure variation with time.

The evaluated K_o is plotted against the vertical shear wave velocity in Fig. 4.17. The K_o and vertical shear wave velocity relationship is approximated as:

$$K_o = 0.36 \log V_{s-v} - 0.16 \tag{4.20}$$

The result shows that K_o increases as the soil density increases. As the excess pore water pressure dissipates, the particle packing becomes denser. However, the approximated trend shows that the K_o value has an upper bound of around 0.6. This case is only valid in one-dimensional normally compressed loading.

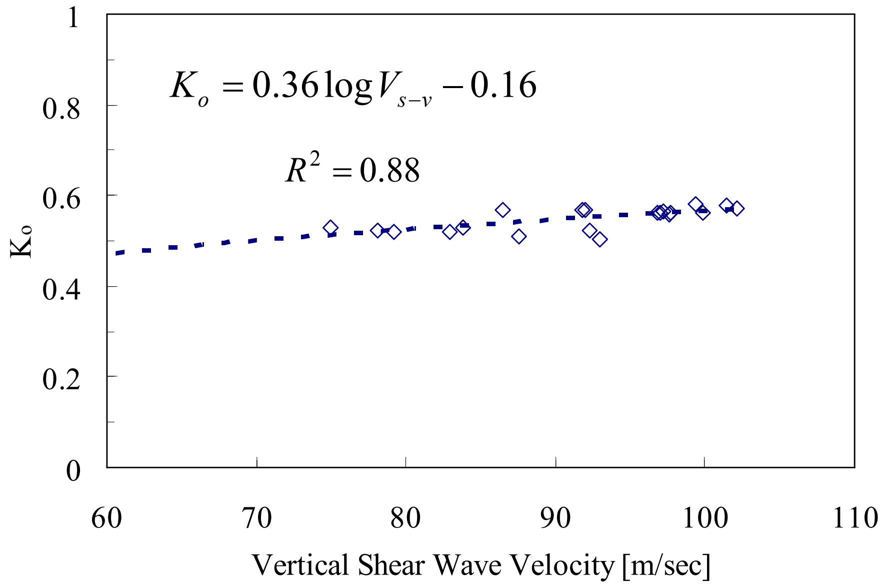

Figure 4.17 K_o – vertical shear wave velocity relationship.

4.5.6 Void Ratio – Shear Wave Velocity Relationship

The α parameter from Eq. 2.41 is the shear velocity at 1kPa confinement. Thus, α is related to the density of soil. This relationship provides the basic concept for estimating the void ratio – shear wave velocity relationship. The void ratio variation with time is shown in Fig. 4.10, and the vertical shear wave velocity variation at the corresponding time (Fig. 4.10) is plotted in Fig. 4.18.

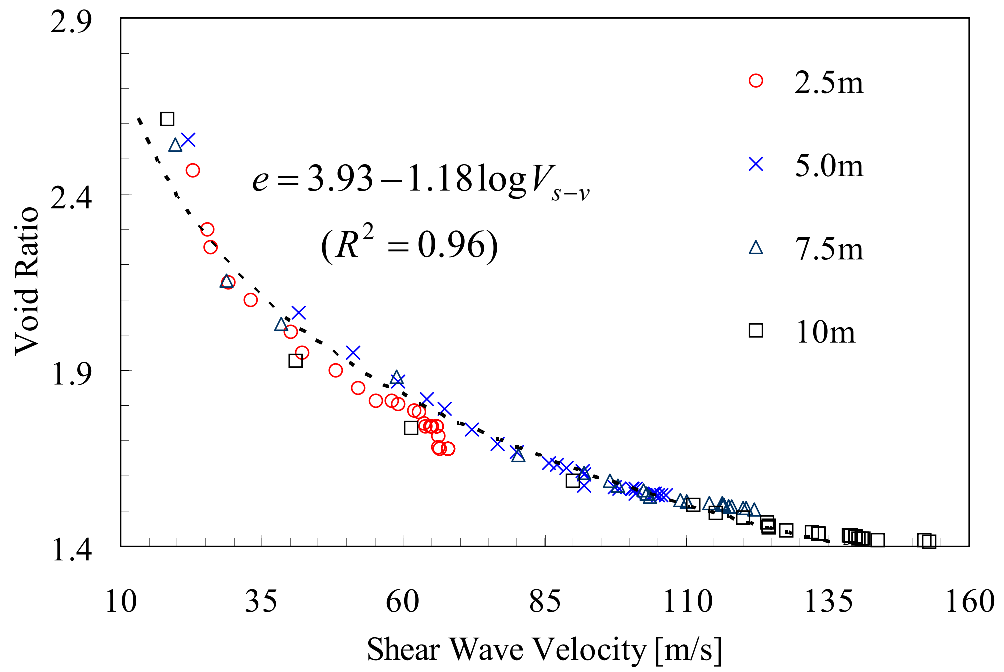

Figure 4.18 Vertical shear wave velocity – void ratio relationship.

The results show a strong relationship between the vertical shear wave velocity and the void ratio. It should be noted that the general trend is unique for different depths. This demonstrates the one-to-one relation between void ratio and shear wave velocity for normally-consolidated deposits. The approximate equation of the trend in Fig. 4.18 is as follows:

$$e = 3.93 - 1.17 \cdot \log V_{s-v} \tag{4.21}$$

This relationship presents a useful approach for the estimation of the in-situ void ratio in reclaimed sites.

Fig. 4.19 shows the relation of the void ratio to vertical effective stress. Fig. 4.19 shows that the relationship curve is bilinear, which means the slope differs before and after the 3kPa effective stress point. The void ratio – effective stress equation can also be derived by combining Eqs. 4.2 and 4.21 (Fig. 4.19):

$$e = 2.77 - 1.56 \log \sigma'_v \qquad \text{for } \sigma'_v \leq 3 \text{ kPa} \tag{4.22}$$

$$e = 2.40 - 0.57 \log \sigma'_v \qquad \text{for } \sigma'_v \geq 3 \text{ kPa} \tag{4.23}$$

According to its low stress state, the 3kPa stress point can be regarded as the trade zone between sedimentation and self-weight consolidation. This explains the phase velocity difference between settling soil and consolidating soil. The slope value of 0.66 from Eq. 4.22 is considered as the compression index, defined in Eq. 2.5.

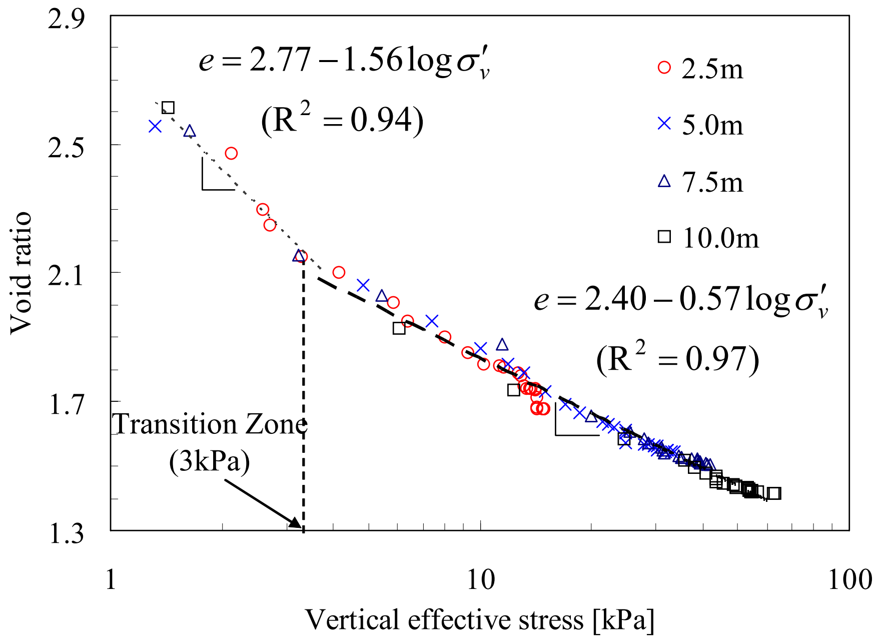

Figure 4.19 Vertical effective stress – void ratio relationship.

4.5.7 Permeability Estimation

The permeability –void ration relationship is linear according to Eq. 2.33. Thus, the effective stress and permeability relationship is considered to be non-linear in order to maintain a constant coefficient of consolidation, as shown in Eq. 2.36. However, Figs. 4.14 and 15 show that the coefficient of consolidation is not constant during large strain consolidation of weak clays. From Eq. 2.36, the permeability can be expressed as:

$$k = -\frac{\rho_f (1+e) C_v}{\frac{d\sigma'}{de}} \tag{4.24}$$

From Eq. 4.23, the void ratio derivative of the effective stress is written as:

$$\frac{d\sigma'}{de} = -\frac{\sigma'}{0.25} \tag{4.25}$$

Therefore, Eq. 4.24 is re-written as:

$$k = \frac{0.25\rho_f (1+e) C_v}{\sigma'} \tag{4.26}$$

while ρ_f is the pore fluid density, and the e, C_v, σ' variations are already known. Therefore, the permeability of each specimen is evaluative.

The evaluated effective stress – permeability relationship is shown in Fig. 4.20. The approximated equation of Fig. 4.20 is:

$$k\,[\mathrm{m/s}] = 0.035 \cdot \left(\sigma'_v\right)^{-1.13} \tag{4.27}$$

The non-linear effective stress – permeability relationship reflects the results of previous studies. However, the difference in this study is that the non-linearity is based on the variation of the coefficient of consolidation.

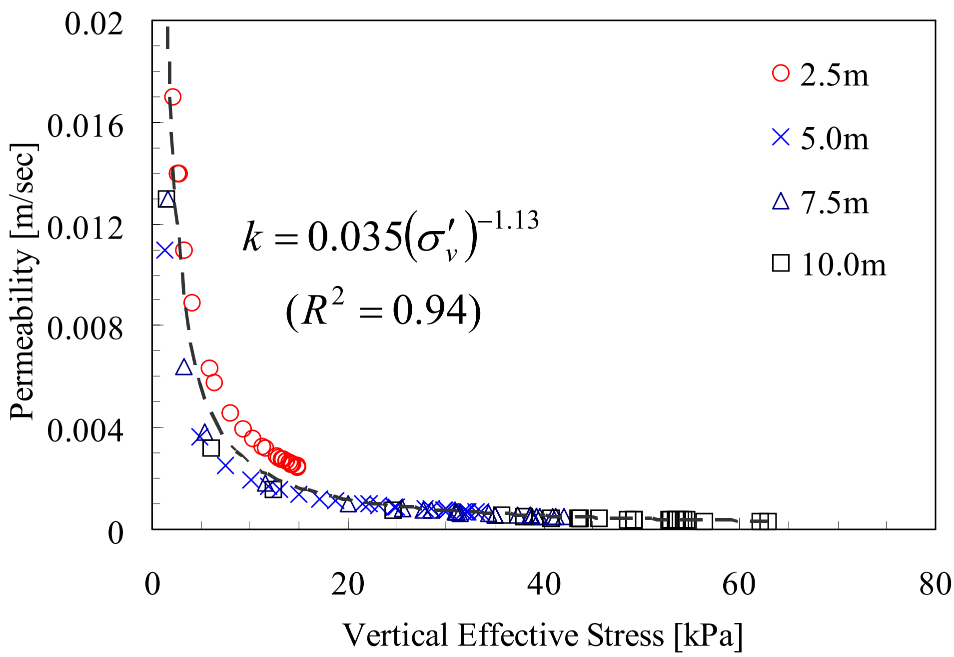

Figure 4.20 Vertical effective stress and permeability relationship.

4.6 Field Application

In section 4.5, the vertical effective stress state, degree of consolidation, coefficient of consolidation, and void ratio of dredged and reclaimed deposits were evaluated using the shear wave velocity. In this section, design parameters related to in-situ conditions are estimated using the in-situ shear wave velocity and laboratory test results.

As the vertical shear wave velocity is used to evaluate the state of consolidation in laboratory testing, the in-situ shear wave velocity should be obtained in the vertical direction. While various methods for in-situ shear wave velocity measurement have been developed, the SPS-logging method is preferred for correspondence. The field suspension (SPS) -logging test results for the site of interest are summarized in Table 4.4.

Table 4.4 In-situ vertical shear wave velocity.

Site of Interest - Depth	2.5 m	5.0 m	7.5 m	10.0 m
Vertical Shear Wave Velocity [m/sec]	75	70	100	120

4.6.1 Effective Stress State

The in-situ vertical effective stress condition is estimated by substituting the in-situ shear wave velocity value into Eq. 4.2. The estimated value for each depth is as follows:

$$\sigma_v'^{\,2.5m} = \left(\frac{V_{s-v}^{\;2.5m}}{\alpha}\right)^{\frac{1}{\beta}} = \left(\frac{75}{16.47}\right)^{\frac{1}{0.56}} = 14.6\,\text{kPa} \tag{4.28}$$

$$\sigma_v'^{\,5.0m} = \left(\frac{V_{s-v}^{\;5.0m}}{\alpha}\right)^{\frac{1}{\beta}} = \left(\frac{70}{16.47}\right)^{\frac{1}{0.56}} = 12.9\,\text{kPa} \tag{4.29}$$

$$\sigma_v'^{\,7.5m} = \left(\frac{V_{s-v}^{\;7.5m}}{\alpha}\right)^{\frac{1}{\beta}} = \left(\frac{100}{16.47}\right)^{\frac{1}{0.56}} = 24.4\,\text{kPa} \tag{4.30}$$

$$\sigma_v'^{\,10.0m} = \left(\frac{V_{s-v}^{\;10.0m}}{\alpha}\right)^{\frac{1}{\beta}} = \left(\frac{120}{16.47}\right)^{\frac{1}{0.56}} = 33.8\,\text{kPa} \tag{4.31}$$

The converged shear wave velocities shown in Table 4.3 are the shear wave velocities when the element receives the total amount of expected overburden effective weight (stress), (i.e., the complete dissipation of excess pore water pressure). Therefore, the consolidation state can be determined by the same method as in section 3.3.3. The in-situ consolidation state is shown in Fig. 4.21.

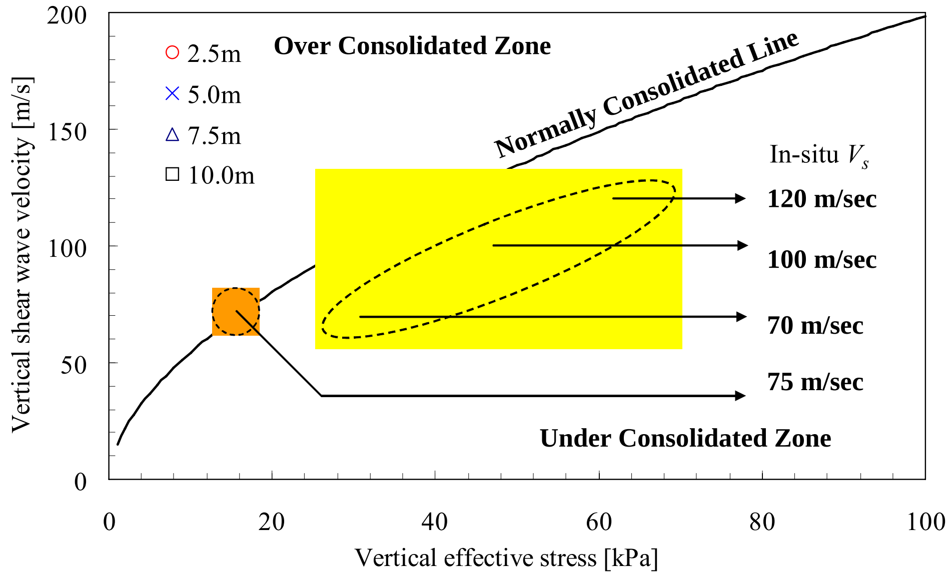

Figure 4.21 The in-situ consolidation state.

<u>2.5m specimen</u>

The in-situ shear wave velocity is 75 m/sec while the expected shear wave velocity for the normally-consolidated condition is 68 m/sec. Therefore, the in-situ consolidation state can be categorized as a slightly over consolidation state. However, the probability for a normally-consolidated condition cannot be ignored because of the potential for error factors in the in-situ shear wave measurement.

The over-consolidated condition is generally observed near the top surface of reclaimed sites. Desiccation and surface moisture evaporation decrease the water content of the surface soils. Thus, a bonding effect and capillary force between particles increase inter-particle forces without global load increment (Cargill 1985, Znidarcic 1989).

<u>5.0m specimen</u>

The in-situ shear wave velocity is 70 m/sec while the expected shear wave velocity for the normally-consolidated condition is 106 m/sec. Therefore, the in-situ consolidation state can be categorized as an under consolidation state. This means that the layer is still being consolidated with a certain amount of excess pore water pressure existing inside the voids. The degree of consolidation should be evaluated.

<u>7.5m specimen</u>

The in-situ shear wave velocity is 100 m/sec while the expected shear wave velocity for the normally-consolidated condition is 124 m/sec. Therefore, the in-situ consolidation state can be categorized as an under consolidation state. The degree of consolidation should be evaluated.

<u>10.0m specimen</u>

The in-situ shear wave velocity is 120 m/sec while the expected shear wave velocity for the normally-consolidated condition is 153 m/sec. Therefore, the in-situ consolidation state can be categorized as an under consolidation state. The degree of consolidation should be evaluated.

4.6.2 Degree of Consolidation

The estimation of the degree of consolidation is required to predict the hereafter settlement and to choose the drainage method for improving the under-consolidated layers. As the 2.5m depth sample was determined to be slightly over- consolidated, the degree of consolidation is estimated for 5.0m, 7.5m, and 10.0m specimens.

The in-situ shear wave velocity value (Table 4.4) and the evaluated degree of consolidation – shear wave velocity equations (Eqs. 4.7, 4.8, 4.9) are combined to estimate the degree of consolidation at the depths of interest at the test sites.

<u>Place at 5.0m depth</u>

From Eq. 4.7 the degree of consolidation is estimated as (Fig. 4.22):

$$U_{field}^{5.0m} = \left(\frac{V_{s-v}^{5.0m}}{106.3} \right)^{\frac{1}{0.56}} \approx 48\,\% \qquad (4.32)$$

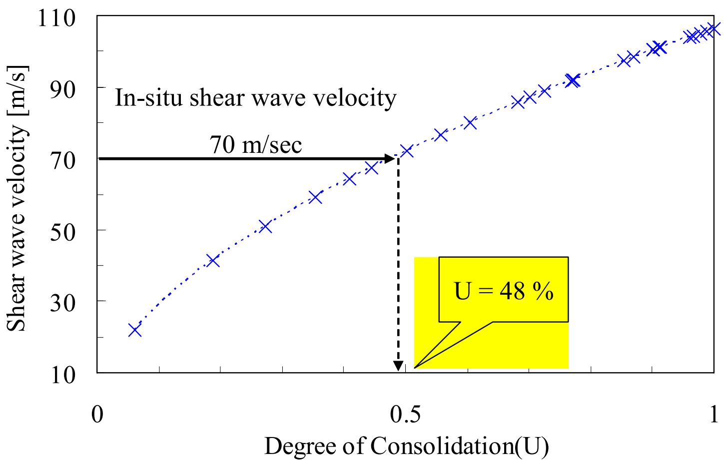

Figure 4.22 Estimated degree of consolidation of the 5.0m in depth.

<u>Place at 7.5m depth</u>

From Eq. 4.8 the degree of consolidation is estimated as (Fig. 4.23):

$$U_{field}^{7.5m} = \left(\frac{V_{s-v}^{7.5m}}{122.0}\right)^{\frac{1}{0.56}} \approx 70\,\% \qquad (4.33)$$

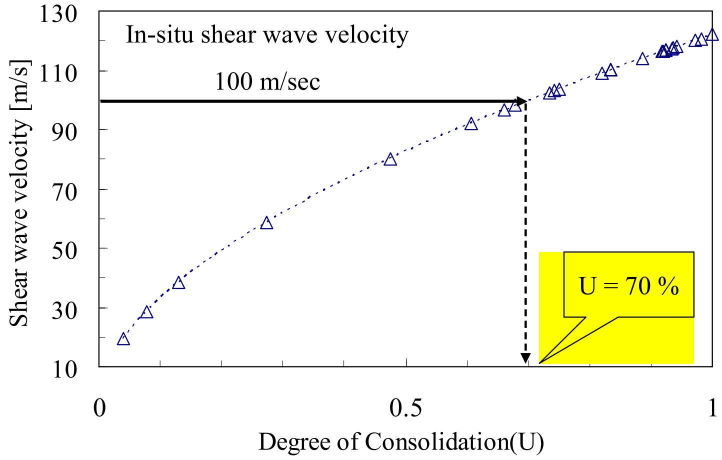

Figure 4.23 Estimated degree of consolidation of the 7.5m in depth.

<u>Place at 10.0m depth</u>

From Eq. 4.9 the degree of consolidation is estimated as (Fig. 4.24):

$$U_{field}^{10.0m} = \left(\frac{V_{s-v}^{10.0m}}{153.0} \right)^{\frac{1}{0.56}} \approx 65\,\% \tag{4.34}$$

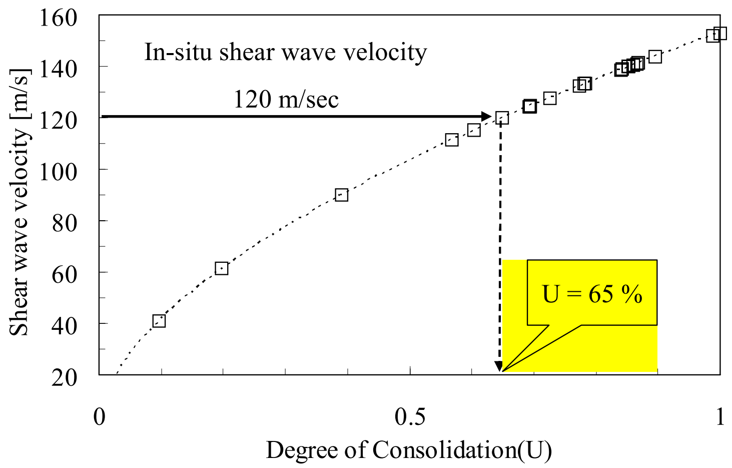

Figure 4.24 Estimated degree of consolidation of the 10.0m in depth.

The expected profile of the degree of consolidation in-situ is shown in Fig. 4.25. The degree of consolidation of under-consolidated layers shows a parabolic distribution. This result is attributed to the low permeable dried crust on the surface and the underlying low permeable stiff clay deposit in the field, which obstruct the outward drainage at the boundaries. Clay particle segregation can result in low permeability of the surface layer, because the surface region contains more fine particles than the bottom layer. Meanwhile, the middle zone has relatively better drainage conditions for pore water pressure dissipation. Therefore, even though the density is higher at the bottom, the external degree of consolidation is lower than the middle zone of the reclaimed deposit.

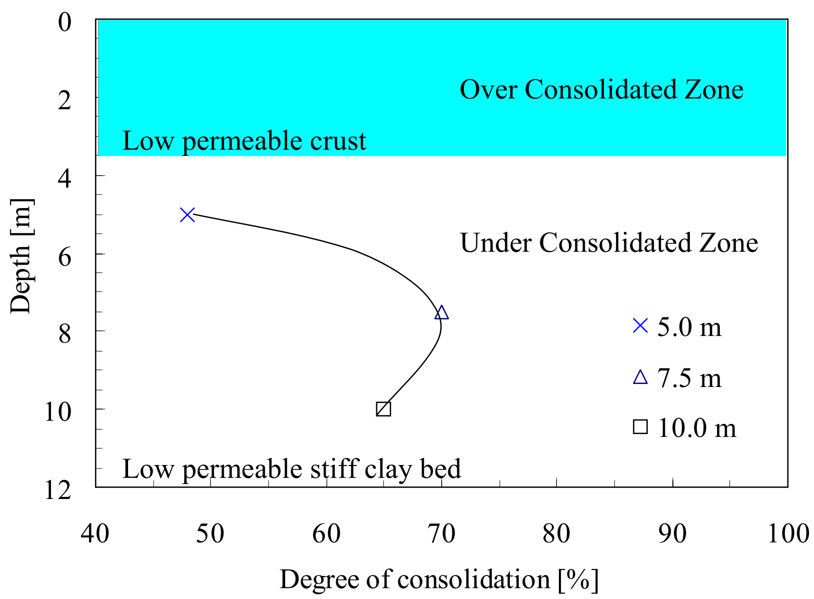

Figure 4.25 Predicted profile of the degree of consolidation in situ.

4.6.3 Void Ratio

The in-situ void ratio condition is estimated by combining Eq. 4.21 and the in-situ shear wave velocity value (Table 4.4). However, it was noted previously that Eq. 4.21 can only be applied to normally / under-consolidated places. Thus, the void ratios for 5.0m, 7.5m, and 10.0m are calculable in this study.

Place at 5.0m depth

$$e_{field}^{5.0m} = 3.93 - 0.51 \cdot \ln V_{s-v}^{5.0m} = 3.93 - 0.51 \cdot \ln 70 = 1.76 \qquad (4.35)$$

Place at 7.5m depth

$$e_{field}^{7.5m} = 3.93 - 0.51 \cdot \ln V_{s-v}^{7.5m} = 3.93 - 0.51 \cdot \ln 100 = 1.58 \qquad (4.36)$$

Place at 10.0m depth

$$e_{field}^{10.0m} = 3.93 - 0.51 \cdot \ln V_{s-v}^{10.0m} = 3.93 - 0.51 \cdot \ln 120 = 1.49 \qquad (4.37)$$

Void ratio is an important parameter to estimate the density and strength of clay deposits. Therefore, the undrained shear strength is also predictable using the shear wave velocity. The most general method to measure the undrained shear strength in field is the vane test. However, the vane shear test disturbs the soil, and is limited with respect to the application depth. The shear wave velocity technique, conversely, minimizes soil disturbance and is applicable to deep depths. Thus, the undrained shear strength value of a deep point is available without excavation through the use of the shear wave velocity technique.

4.6.4 Settlement Prediction

The one-dimensional consolidation settlement of a clay layer having a thickness H is calculated as:

$$S = \frac{\Delta e}{1 + e_o} H \tag{4.38}$$

where e_o is the present void ratio value and Δe is the additional void ratio change.

The additional settlement of an under-consolidated layer is related to the void ratio decrease during the residual consolidation process until the consolidation condition approaches the normal consolidated condition. Therefore, the settlement prediction is important for understanding the soil behavior after drainage installation or other structural upgrades.

The present void ratio condition is calculated by Eqs. 4.35, 36, and 37. The values of the anticipated final void ratio when the layer is perfectly normally-consolidated are listed in Table 4.3. The expected void ratio change is given in Table 4.5.

As the in-situ reclaimed deposit thickness is around 12m and the top layer, i.e. at least 2.5m from the surface, is over-consolidated, the layers under 3m depth were considered for settlement prediction.

Table 4.5 Expected additional void ratio change.

Site of Interest	5.0 m	7.5 m	10.0 m
Current Void Ratio	1.76	1.58	1.49
Final Void Ratio	1.55	1.51	1.41
Expected Void Ratio Change	0.21	0.07	0.08

The layers were divided into three zones, 3.0m ~ 6.0m, 6.0m ~ 9.0m, and 9.0m ~ 12.0m. The void ratio values shown in Table 4.5 were assumed to replace the average void ratio conditions for each of the three zones. Thus, the void ratio values at the 5.0m point represent the average values of the 3.0m ~ 6.0m zone. In the same way, the 7.5m point represents the 6.0m ~ 9.0m zone, and 10.0m is for the deepest zone. Therefore, the average additional settlement for each zone is as follows:

Zone 1 (3.0m ~ 6.0m)

$$S_1 = \frac{\Delta e_1}{1 + e_{o<1>}} H_1 = \frac{0.21}{1 + 1.76} \times 3\,\mathrm{m} = 0.23\,\mathrm{m} \tag{4.39}$$

Zone 2 (6.0m ~ 9.0m)

$$S_2 = \frac{\Delta e_2}{1 + e_{o<2>}} H_2 = \frac{0.07}{1 + 1.58} \times 3\,\mathrm{m} = 0.08\,\mathrm{m} \tag{4.40}$$

Zone 3 (9.0m ~ 12.0m)

$$S_3 = \frac{\Delta e_3}{1 + e_{o<3>}} H_3 = \frac{0.08}{1 + 1.49} \times 3\,\mathrm{m} = 0.10\,\mathrm{m} \tag{4.41}$$

Finally, the additional total settlement expected is as follows:

$$S_{total} = \sum_i S_i = S_1 + S_2 + S_3 = 0.23 + 0.08 + 0.10 = 0.41\,\mathrm{m} \tag{4.42}$$

This means that the elevation of the surface decreases by 0.41m when all layers are normally-consolidated (Fig. 4.26). Under the assumption that all layers are normally-consolidated, the average properties of each zone are summarized in Table 4.6.

Table 4.6 Stress – strain properties for the normally-consolidated condition.

Zone of layer	1	2	3
Initial zone thickness [m]	3.00	3.00	3.00
Settlement for NC condition [m]	-0.23	-0.08	-0.10
Final zone thickness [m]	2.76	2.92	2.90
Void Ratio for NC state, e_o	1.55	1.51	1.41
Effective Stress for NC state, p_o [kPa]	30.8	46.2	61.7

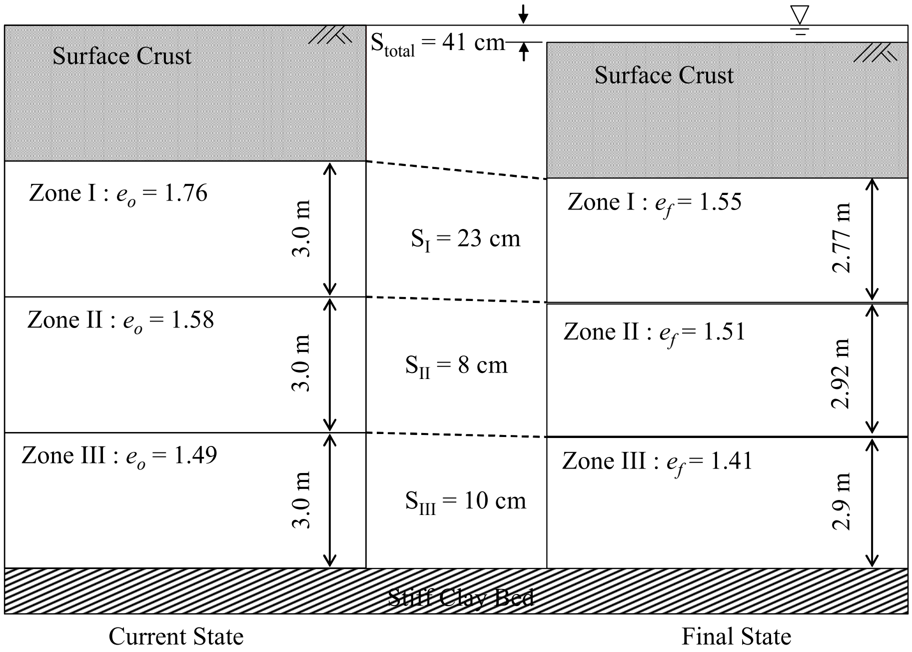

Figure 4.26 Total settlement of the in-situ layer.

The extra settlement caused by additional load application is predictable. As the compression index was evaluated as C_c=0.57 from Eq. 4.23, the settlement caused by an additional load, Δp, is calculated as follows:

Zone 1

$$S_1 = \frac{C_c H_1}{1+e_o^{\,1}} \log \frac{p_o^{\,1} + \Delta p}{p_o^{\,1}} = \frac{0.57 \times 2.76}{1+1.55} \log \frac{30.8 + \Delta p}{30.8} \tag{4.43}$$
$$= 0.62\left(\log(30.8+\Delta p) - 1.49\right) = 0.62\log(30.8+\Delta p) - 0.92$$

Zone 2

$$S_2 = \frac{C_c H_2}{1+e_o{}^2}\log\frac{p_o{}^2+\Delta p}{p_o{}^2} = \frac{0.57\times 2.92}{1+1.51}\log\frac{46.2+\Delta p}{46.2}$$
$$= 0.66\left(\log\left(46.2+\Delta p\right)-1.66\right) = 0.66\log\left(46.2+\Delta p\right)-1.10 \tag{4.44}$$

Zone 3

$$S_3 = \frac{C_c H_3}{1+e_o{}^3}\log\frac{p_o{}^3+\Delta p}{p_o{}^3} = \frac{0.57\times 2.90}{1+1.41}\log\frac{61.7+\Delta p}{61.7}$$
$$= 0.69\left(\log\left(61.7+\Delta p\right)-1.79\right) = 0.69\log\left(61.7+\Delta p\right)-1.24 \tag{4.45}$$

Therefore, the total settlement occurred by an extra load, Δp, is predicted as:

$$S_{total} = \sum_i S_i = S_1 + S_2 + S_3$$

$$= \log(30.8+\Delta p)^{0.62} + \log(46.2+\Delta p)^{0.66} + \log(61.7+\Delta p)^{0.69} - 3.26 \tag{4.46}$$

$$= \log\left\{\frac{(30.8+\Delta p)^{0.62}\cdot(46.2+\Delta p)^{0.66}\cdot(61.7+\Delta p)^{0.69}}{10^{3.26}}\right\}$$

4.6.5 In-situ Permeability

The in-situ permeability for each point of depth is evaluated by comparing the estimated in-situ effective stress values (Eqs. 4.28, 29, 30, and 31) with the evaluated permeability – effective stress relationship (Eq. 4.27). The permeability of the 2.5m depth point is not available because Eq. 4.27 is applicable to under and normally consolidation states only. However, the permeability values of other points are shown as:

$$k^{5.0m} = 0.035\sigma_v'^{-1.13} = 0.035 \times 12.9^{-1.13} = 0.0019 \text{ m/s} \tag{4.47}$$

$$k^{7.5m} = 0.035\sigma_v'^{-1.13} = 0.035 \times 24.4^{-1.13} = 0.00095 \text{ m/s} \tag{4.48}$$

$$k^{10.0m} = 0.035\sigma_v'^{-1.13} = 0.035 \times 33.8^{-1.13} = 0.00066 \text{ m/s} \tag{4.49}$$

The required time for 99% consolidation can be estimated via the estimated coefficient of consolidation and permeability relationship.

4.7 Summary and Conclusions

The sedimentation and self-weight consolidation behavior of dredged and reclaimed kaolinite deposits were characterized through a series of shear wave based laboratory tests. Bender element sensors were used to measure the shear wave velocity of the experimental specimens during laboratory consolidation tests, which represented the in-situ self-weight consolidation process. The main findings are summarized as follows:

1. The vertical effective stress – shear wave velocity relationship was evaluated using the converged shear wave velocity value for each applied load. As the soil compositions and particle arrangement of a reclaimed deposit are treated as being unique, the derived vertical effective stress – shear wave velocity equation is applicable for any depth of a given site.
2. The degree of consolidation was estimated from the shear wave velocity by combining the vertical effective stress – shear wave velocity equation and shear wave velocity data obtained from the consolidation test. The results show that the degree of consolidation increases with increased shear wave velocity.
3. The evaluated coefficient of consolidation, considering the change of specimen size and degree of consolidation, shows a decreasing trend with increased shear wave velocity and degree of consolidation. However, the degree of consolidation is more uniquely related to the coefficient of consolidation than the shear wave velocity.

4. The coefficient of earth pressure at rest, K_o, was evaluated using the horizontal shear wave data. From the results, K_o shows an increasing tendency during the consolidation test. Thus, in reclaimed sites, the coefficient of earth pressure has a constant value during the in-situ self-weight consolidation process.
5. The void ratio was estimated using shear wave techniques without causing any disturbance. As the void ratio is related to the density and undrained shear strength, the shear wave technique is recommended for in-situ density and undrained shear strength measurements.
6. In-situ soil properties such as effective stress state, consolidation state, degree of consolidation, void ratio, expected additional settlement, and permeability were estimated by comparing laboratory test results with the field shear wave velocity values.

CHAPTER V
UNDRAINED SHEAR STRENGH AND SHEAR WAVE VELOCITY

5.1 Introduction

From the results shown in section 4.5.6, the void ratio – vertical effective stress relationship of a normally-consolidated soft clay is linear in a semi-logarithmic scale. Meanwhile, the undrained shear strength of clay is an important parameter in the estimation of the ground resistance for foundation engineering. The undrained shear strength of clay is affected by its void ratio and therefore is very sensitive to specimen disturbance. Generally, the undrained shear strength is measured by vane shear tests in the field and undrained triaxial tests in the laboratory. However, the soil can be disturbed during those tests. Furthermore, the correlation between laboratory and field values is insufficient. Therefore, an accurate method involving minimum soil disturbance is required for in-situ undrained shear strength evaluation.

The empirical equations for in-situ undrained shear strength shown in section 2.3.4 are related to the in-situ effective stress. Therefore, it is possible to evaluate the undrained shear strength – shear wave velocity relationship, as the effective stress – shear wave velocity relationship has already been evaluated in previous chapters.

The shear wave velocity of soil is related to the effective stress and void ratio (Eq. 2.43). The void ratio homogenization factor F_e presents the density and soil fabric effect on the shear wave velocity when the confining pressure is constant. In chapter 4, only the normally-consolidated state was considered. Thus, the void ratio and effective stress have a one-to-one relationship, making it impossible to determine different void ratio values under the same effective stress state. Therefore, an unloading process after normal consolidation is introduced in order to produce different void ratio conditions for a unique effective stress value. This is possible because the swelling index differs from the compression index.

In this chapter, laboratory loading – unloading tests are performed in order to compose different void ratio conditions under the same effective stress states. After unloading is completed, laboratory vane tests are performed to measure the vane resistance of each different density specimen. The α and β parameters for the effective stress – shear wave velocity during the loading and unloading process are different, because loading is a normally consolidation process whereas unloading represents over-consolidation behavior. Finally, the void ratio – undrained shear strength – shear wave velocity relationship is evaluated.

5.2 Experimental Program

5.2.1 Site of Interest

The soil sample used in this study corresponds with that used in chapter 4 (disturbed reclaimed soil from Kwang-Yang, Korea). Therefore, the disturbed samples were remolded following the same experimental procedure outlined in section 4.3.

5.2.2 Experimental Devices

The sedimentation tube and sensor devices for specimen reproduction are identical to those described in section 4.2.2. The electronic peripheral devices, i.e., wave form generator, multi channel filter, and digital oscilloscope, are shown in Fig. 3.10.

5.2.3 Specimen Remolding

The disturbed soil samples from the reclaimed site were reconstituted using the laboratory sedimentation tube devices. The experimental properties correspond with those outlined in section 4.3: 300g of dried kaolinite clay from Kwang-Yang reclaimed site, 300% initial water content, 0.3% slurry salt concentration.

5.3 Consolidation Test

5.3.1 Basic Concept

Compression and swelling were performed in order to represent different void ratio conditions under the same vertical effective stress state. The vertical effective stress – shear wave velocity relationship during normal compression becomes unique when the specimens' initial states are equal. However, in this study, the specimens are unloaded to the same vertical effective stress state with different over consolidation ratios. This means that the initial states of unloading differ, and thus the vertical effective stress – shear wave velocity relationship for unloading should be evaluated for each specimen.

The undrained shear strengths of each specimen are measured after unloading using a laboratory vane shear tester. The relationship between the undrained shear strength and over consolidation ratio can be estimated from the test results.

5.3.2 Testing Sequence

Four initially homogenized specimens were slightly confined with 8.4kPa load, which is also the final unloaded condition after the unloading process. Different loads were applied to normally compress each specimen. After compression, the additional loads were removed to accommodate swelling. The shear wave velocities were measured during loading and unloading. Finally, the undrained shear strength was measured upon completion of unloading.

Upon convergence of the shear wave velocity and volumetric expansion, the load cap was removed from the oedometric cell and a laboratory vane shear test was performed immediately. Fig. 5.1 shows a photograph taken after the laboratory vane shear test.

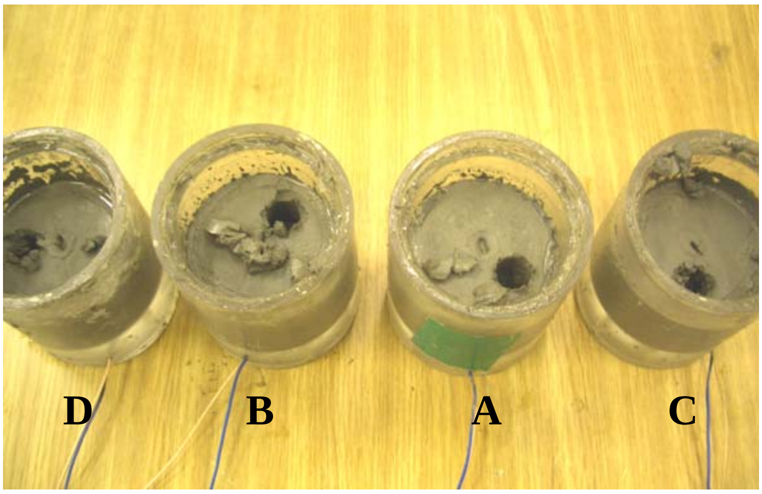

Figure 5.1 Photographic image taken after laboratory vane shear test.

5.4 Experimental Results and Analysis

5.4.1 Shear Wave Velocity Variation

The vertical effective stress – shear wave velocity relationship for normal compression of each specimen does not vary, because the α and β parameters are assumed to be unique. However, the unloading curve of each specimen is different because the specimens' maximum pre-consolidation stresses are different, and thus the over consolidation behaviors are different.

The loading and unloading test results are summarized in Table 5.1. Fig. 5.2 shows the vertical effective stress – shear wave velocity relationship during loading and unloading.

Table 5.1 Summary of experimental results.

Specimen	Stress [kPa]		*OCR*	Shear Wave Velocity [m/s]			Void Ratio			Undrained Shear Strength [kPa]
	Initial	After Load		Before Load	After Load	After Unload	Before Load	After Load	After Unload	
A	8.4	25.2	3	54.9	91.0	80.0	2.50	2.30	2.32	2.5
B	8.4	42.0	5	55.9	113.3	94.2	2.43	1.98	2.01	6.5
C	8.4	58.8	7	55.0	127.0	106.7	2.43	1.88	1.92	8.0
D	8.4	75.6	9	55.4	156.0	113.9	2.44	1.79	1.83	11.0

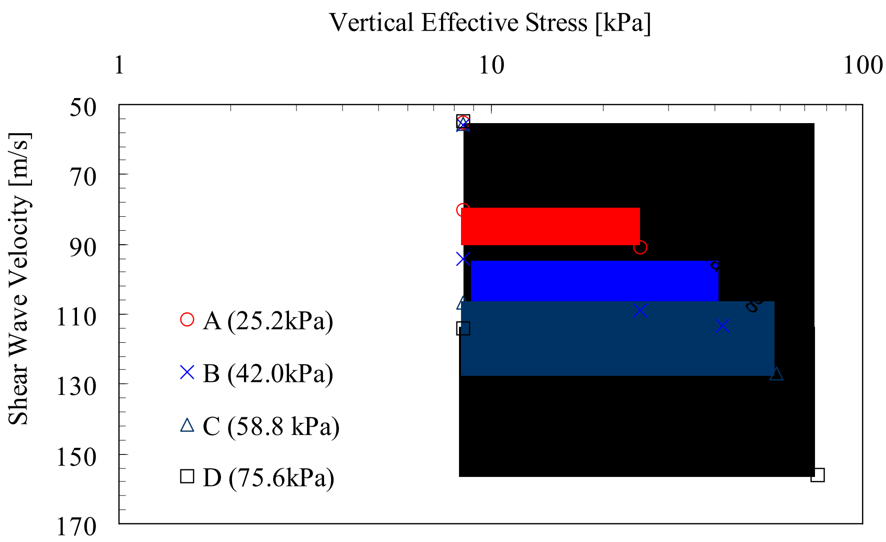

Figure 5.2 Vertical effective stress – shear wave velocity relationship during loading and unloading.

5.4.2 Vertical Effective Stress – Shear Wave Velocity Relation

The vertical effective stress – shear wave velocity relationship of the loading process can be derived by curve fitting the final shear wave velocity values of each specimen after loading. Following the same method outlined in section 4.5.2, the parameters α and β can be determined with the least square solution, rendering:

$$\alpha = 22.86\,\text{m/sec} \quad , \quad \beta = 0.46 \tag{5.1}$$

Therefore, the vertical effective stress – shear wave velocity relationship of loading is evaluated as follows:

$$V_{s-v}^{\;load} = 22.86\left(\frac{\sigma'_v}{1\text{kPa}}\right)^{0.46} \tag{5.2}$$

Fig. 5.2 shows that the vertical effective stress – shear wave velocity trends of unloading do not follow the normal compression curve. Further, the swelling behaviors of each specimen are different because of the variance in their pre-consolidated stresses. Therefore, the vertical effective stress – shear wave velocity relationship of unloading should be evaluated separately for each specimen.

The derivation of the unloading stress – shear wave velocity equation of specimen A is impossible because only two stress – shear wave points were measured. At least three stress – shear wave points are required to derive stress – shear wave velocity equations. Therefore, the relations are evaluated for specimen B, C, and D.

Specimen B was unloaded from 42kPa to 8.4kPa. The vertical effective stress –

shear wave velocity relationship during unloading is evaluated as follows:

$$V_{s-v}^{\;unload-B} = 79.08\left(\frac{\sigma_v'}{1\text{kPa}}\right)^{0.10} \tag{5.3}$$

Specimen C was unloaded from 58.8kPa to 8.4kPa. The vertical effective stress – shear wave velocity relationship during unloading is evaluated as follows:

$$V_{s-v}^{\;unload-C} = 89.83\left(\frac{\sigma_v'}{1\text{kPa}}\right)^{0.09} \tag{5.4}$$

Specimen D was unloaded from 75.6kPa to 8.4kPa. The vertical effective stress – shear wave velocity relationship during unloading is evaluated as follows:

$$V_{s-v}^{\;unload-D} = 86.61\left(\frac{\sigma_v'}{1\text{kPa}}\right)^{0.15} \tag{5.5}$$

The vertical effective stress variations of each specimen are estimated by substituting measured shear wave velocity data into Eqs. 5.2, 5.3, 5.4, and 5.5. Eq. 5.2 evaluates the vertical effective stress during loading while the other equations derive the stress change during unloading. The vertical shear wave velocity and void ratio variation of each specimen are plotted together with the vertical effective stress, as shown in the following figures (Figs. 5.3, 5.4, and 5.5):

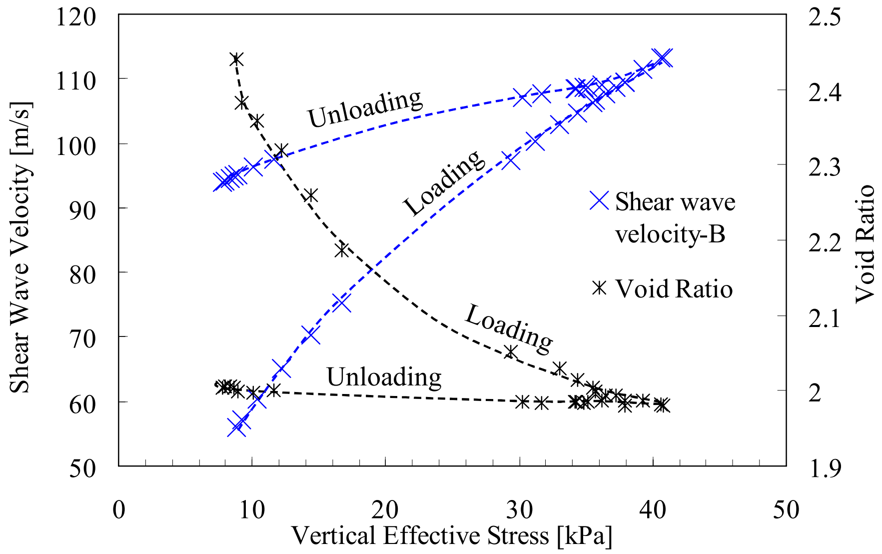

Figure 5.3 Shear wave velocity and void ratio variation. (B specimen: 42kPa load).

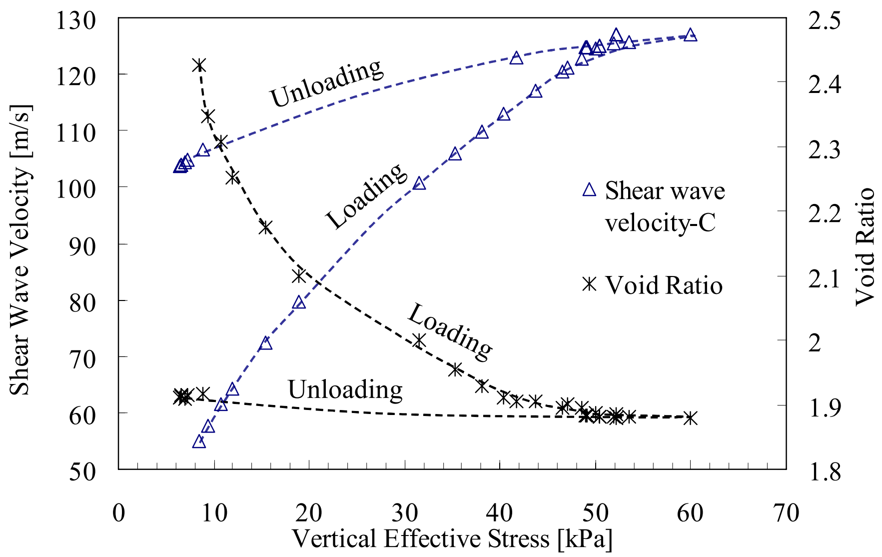

Figure 5.4 Shear wave velocity and void ratio variation (C specimen: 58.8kPa load).

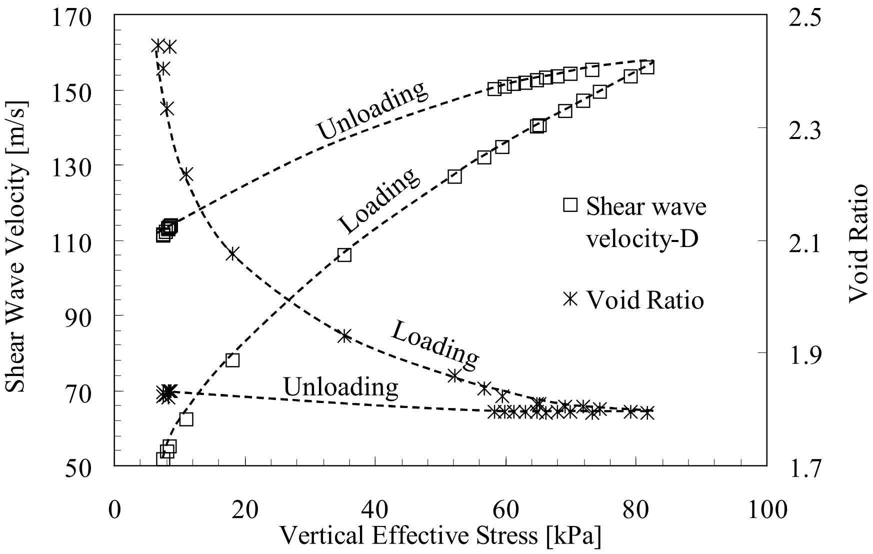

Figure 5.5 Shear wave velocity and void ratio variation (D specimen: 75.6kPa load).

5.4.3 Void Ratio – Shear Wave Velocity Relation

Normal Consolidated – Loading

The void ratio – shear wave velocity relations of normal compression loading are plotted in Fig. 5.6. The result shows that the void ratio – shear wave velocity of normally compressed specimens follows a single equation. The void ratio – vertical shear wave velocity equation is derived as follows:

$$e = 4.77 - 1.37 \log V_{s-v} \tag{5.6}$$

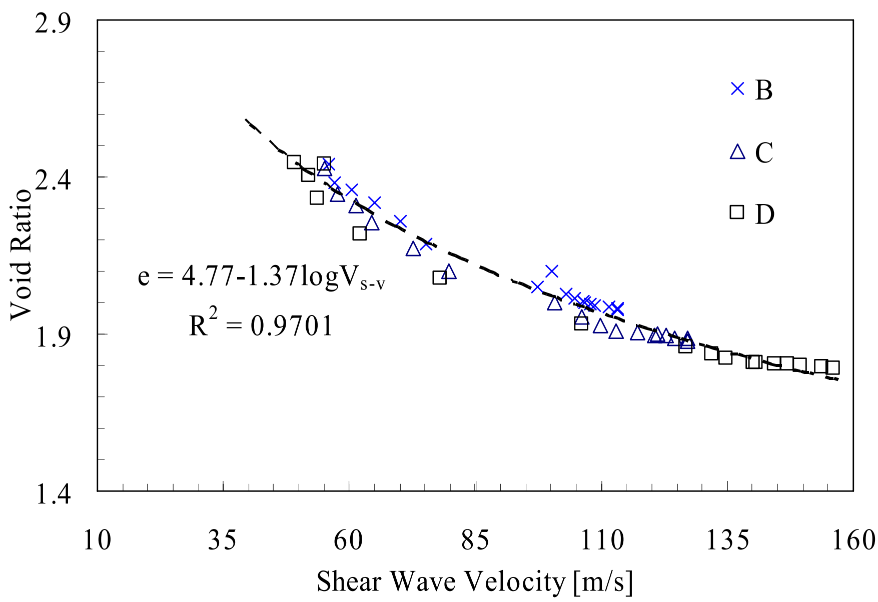

Figure 5.6 Vertical shear wave velocity – void ratio relationship during loading.

<u>Over-consolidated – Unloading</u>

The void ratio – shear wave velocity variations of unloading are shown in Fig. 5.7. As the initiations of each specimen are different, the vertical shear wave velocity – void ratio equations are derived for each specimen:

$$e_B = 2.62 - 0.31 \log V_{s-v} \qquad \text{for specimen B (42kPa} \rightarrow \text{8.4kPa)} \tag{5.7}$$

$$e_C = 2.66 - 0.37 \log V_{s-v} \qquad \text{for specimen C (58.8kPa} \rightarrow \text{8.4kPa)} \tag{5.8}$$

$$e_D = 2.34 - 0.25 \log V_{s-v} \qquad \text{for specimen D (75.6kPa} \rightarrow \text{8.4kPa)} \tag{5.9}$$

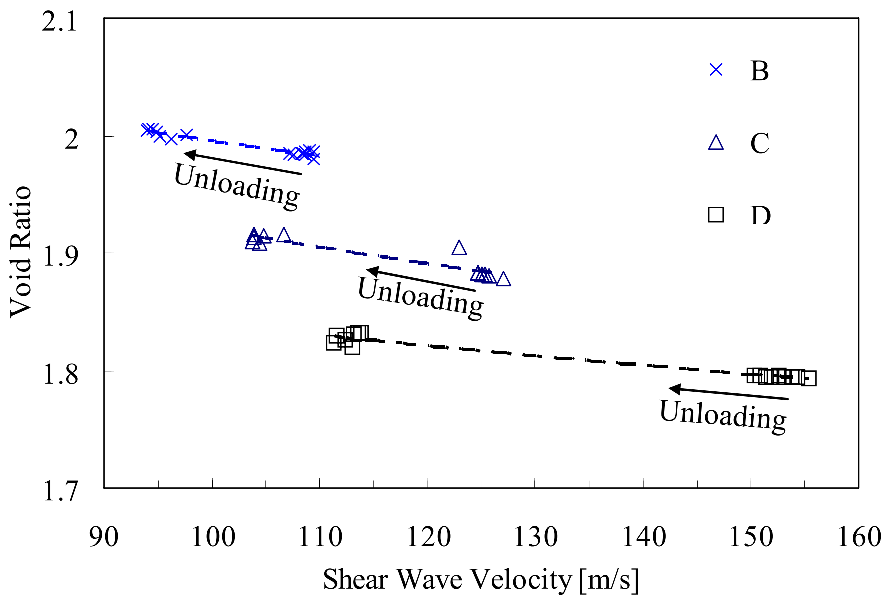

Figure 5.7 Vertical shear wave velocity – void ratio relationship during unloading.

5.4.4 Undrained Shear Strength – Void Ratio Relation

The final void ratio and undrained shear strength measured after unloading represent the over-consolidated condition of a clay sediment. However, Figs. 5.3, 5.4, and 5.5 show that the degree of void ratio increase after unloading is not significantly high. Thus, it can be assumed that the void ratio remains constant after unloading from an engineering perspective. Therefore, the measured undrained shear strength – void ratio relationship shown in Fig. 5.8 represents the undrained shear strength – void ratio relationship of a normally-consolidated state. The undrained shear strength – void ratio equation from Fig. 5.8 is written as follows:

$$S_u = 35.8 - 14.5\,e \quad \text{[kPa]} \tag{5.10}$$

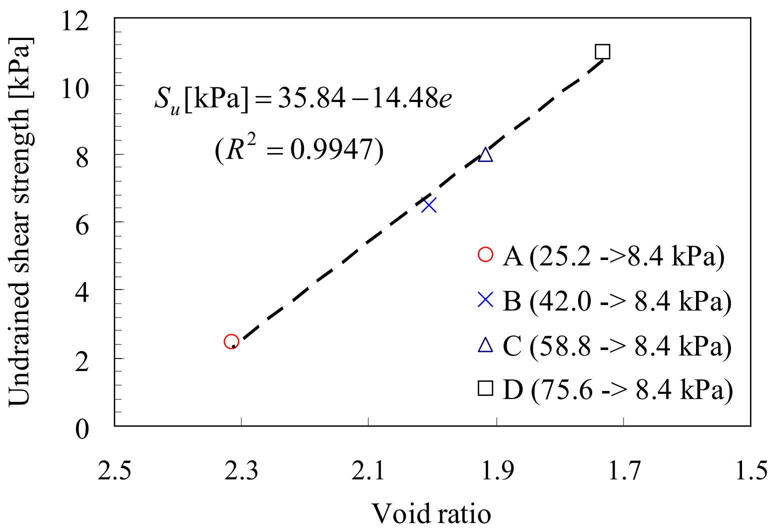

Figure 5.8 Undrained shear strength – void ratio relationship.

5.4.5 Undrained Shear Strength – Shear Wave Velocity Relation

For the evaluation of the undrained shear strength – shear wave velocity relationship of normally-consolidated clay, the undrained shear strength can be estimated only using the in-situ shear wave velocity information, without an incidental vane shear test. Therefore, the correlation between undrained shear strength and shear wave velocity is meaningful in this study.

Fig. 5.9 shows the undrained shear strength – shear wave velocity relationship. The shear wave velocity values are measured data and the undrained shear strength values are estimated from Eq. 5.10 using the measured void ratio data.

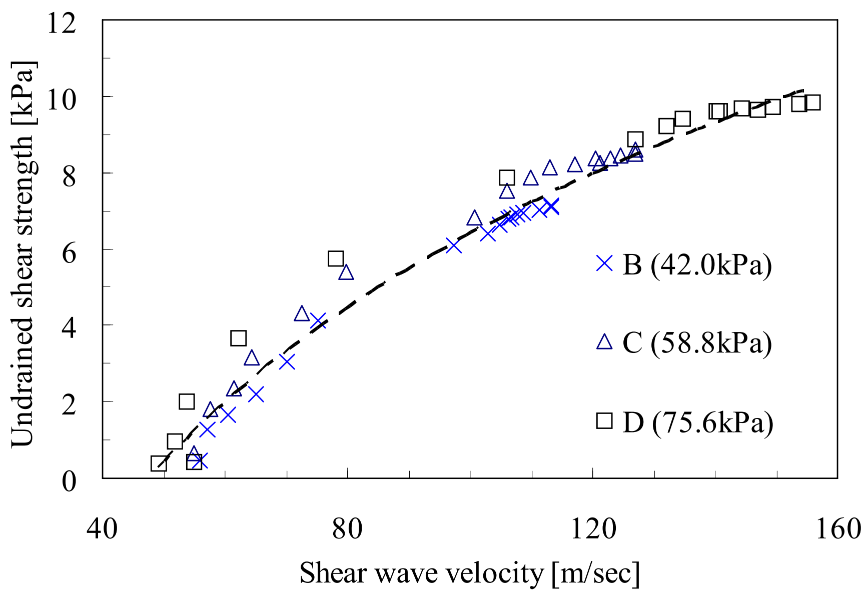

Figure 5.9 Estimated undrained shear strength – shear wave velocity relationship.

The undrained shear strength – shear wave velocity relationship of normally-consolidated reclaimed clay can be approximated from the shear wave velocity – void ratio relationship (Eq. 5.6) and the undrained shear strength – void ratio relationship (Eq. 5.10). The undrained shear strength – shear wave velocity relationship is derived as follows:

$$S_u = 35.8 - 14.5e = 35.8 - 14.5(4.77 - 1.37\log V_{s-v}) \tag{5.11}$$

$$S_u = 19.9\log V_{s-v} - 33.4 \tag{5.12}$$

Another Approach – Considering Over Consolidation

The measured undrained shear strength and vertical shear wave velocity data after unloading is plotted in Fig. 5.10. Under the same vertical effective stress state (8.4kPa), the undrained shear strength varies according to the different density conditions. The undrained shear strength – shear wave velocity relationship is approximated as:

$$S_u = 51.4 \log V_{s-v} - 95.3 \tag{5.13}$$

where S_u is the undrained shear strength.

The empirical equations shown in section 2.3.4 correlate the undrained shear strength with the pre-consolidation stress. As the final unloaded stresses (8.4kPa) are identical, the pre-consolidated stress value represents the over consolidation ratio. Therefore, Fig. 5.11 shows the relationship between the undrained shear strength and the over consolidation ratio (pre-consolidation stress).

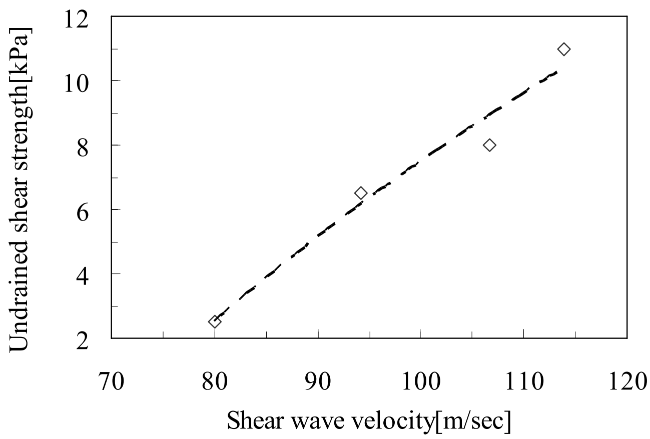

Figure 5.10 Vertical shear wave velocity – undrained shear strength relationship.

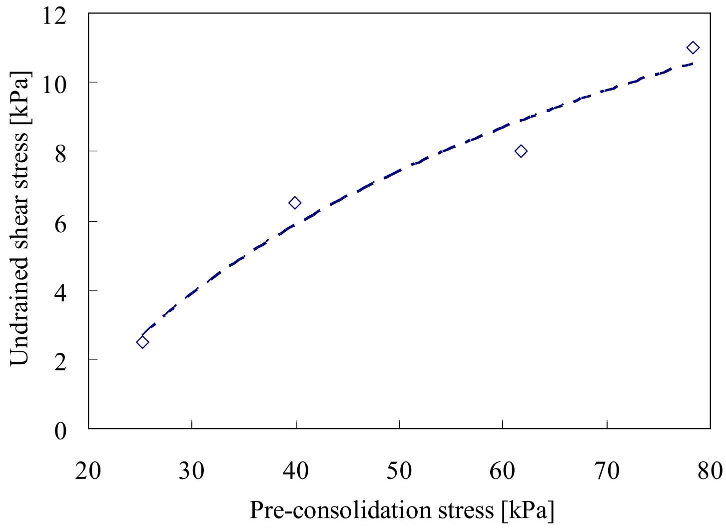

Figure 5.11 Pre-consolidation stress – undrained shear strength relationship.

The undrained shear strength – pre-consolidation stress relationship is approximated as follows:

$$S_u = 16.0 \log \sigma_c' - 19.7 \tag{5.14}$$

where σ_c' is the pre-consolidation stress.

Even though undrained vane shear tests were performed for over-consolidated specimens, Eq. 5.114 gives an important idea to evaluate the undrained shear strength and shear wave velocity relationship during self-weight consolidation process.

The pre-consolidation stress, σ_c' for over-consolidated clay also corresponds with the current overburden effective stress state during self-weight consolidation. In other words, the vertical effective stress values σ_v' from Eq. 5.2 can represent σ_c' in Eq. 5.14.

From Eq. 5.2 the vertical effective stress is expressed as:

$$\sigma'_v = \left(\frac{V_{s-v}}{22.86}\right)^{\frac{1}{0.46}} = \left(\frac{V_{s-v}}{22.86}\right)^{2.17} \tag{5.15}$$

Eq. 5.15 is then substituted into Eq. 5.14.

$$S_u = 16.0 \log \sigma'_c - 19.7 = 16.0 \log \left\{ \left(\frac{V_{s-v}}{22.86}\right)^{2.17} \right\} - 19.7 \tag{5.16}$$

$$S_u = 34.7 \log V_{s-v} - 66.9 \tag{5.17}$$

Therefore, Eq. 5.14 represents the vertical effective stress – shear wave velocity relationship for the normally compressed condition.

5.5 Summary and Conclusions

The undrained shear strength – shear wave velocity relationship for self weight consolidated clay was evaluated from laboratory loading-unloading tests and vane shear test results. The main findings are summarized as follows.

1. The vertical effective stress – shear wave velocity relationship for a normally compressed load can be evaluated using the final shear wave velocity value for each applied load. However, the vertical effective stress – shear wave velocity relationship of unloaded clays should be evaluated separately because the initiation and stress history of each specimen are different.
2. The void ratio – shear wave velocity relationship for loading has a single equation, while unloading has different void ratio – shear wave velocity relationships.
3. The undrained shear strength values were measured by a laboratory vane shear test after unloading. The undrained shear strength shows a linear relationship with the void ratio.
4. The undrained shear strength – shear wave velocity relationship could be evaluated by integrating the void ratio – shear wave velocity relationship and the void ratio – undrained shear strength relationship. The approximated undrained shear strength – shear wave velocity relationship can be used to accurately predict the in-situ undrained shear strength of reclaimed deposits without disturbance.
5. The approximated undrained shear strength – shear wave velocity relationship

for normally-consolidated clay has an upper bound for application. This limitation should be addressed in further studies.

6. Finally, the test results show that the shear wave velocity can be employed to evaluate the effective stress, void ratio, and undrained shear strength for normally-consolidated clay deposits.

CHAPTER VI
CONCLUSIONS AND RECOMMENDATIONS

6.1 Conclusion

This thesis focuses on the evaluation of the consolidation state and strength of soft soil through the use of shear waves. The main objectives were to evaluate the consolidation state and other design parameters using the evaluated effective stress value from the shear wave velocity in clays. A series of shear wave-based laboratory tests were performed to characterize several different clay deposit types. The main conclusions from this study are as follows:

6.1.1 Consolidation State of Soft Soils

The consolidation state and properties of clay deposits in nature were characterized by performing shear wave-based tests on an undisturbed Shelby tube oedometric specimen. Several different loads were applied. The final shear wave velocity and void ratio values were measured for each loading. The effective stress – shear wave velocity relationship was evaluated by a least square approximation of the experimental results.

The in-situ consolidation state was evaluated by comparing the in-situ shear wave velocity with the estimated effective stress – shear wave velocity trend. The site is evaluated as over-consolidated if the in-situ shear wave velocity is higher than the value estimated in the laboratory. Otherwise it is categorized as under-consolidated.

The site is normally-consolidated when the in-situ shear wave velocity is close to the laboratory result.

The degree of consolidation of under-consolidated specimens and the over consolidation ratio of over-consolidated samples are calculable by comparing the in-situ present stress state with the expected amount of effective stress of the normally-consolidated condition.

The compressibility parameters C_s and C_c of each sample were evaluated from the effective stress – void ratio curve. The inflection point accurately corresponds with the estimated pre-consolidated stress value. Using the compressibility parameters, the in-situ settlement can be predicted in accordance with additional loads.

Three case studies were discussed for field application. The foreshore site was evaluated to be under-consolidated. The submarine deposit and thick clay deposit have a similar distribution; the top layer shows an over-consolidated state while the deep layers become normally- or under-consolidated. The *OCR* of the surface layer in the thick clay deposit is larger than that of the submarine deposit. The accuracy of the in-situ consolidation state evaluation method suggested in this study depends on the in-situ shear wave velocity data. Inaccurate data may yield widely variant results. Therefore, reliable in-situ shear wave velocity testing is one of the most important prerequisites for a reliable in-situ consolidation state evaluation via the approach suggested in this study.

6.1.2 Consolidation State of Dredged and Reclaimed Clay

The sedimentation and self-weight consolidation behavior of dredged and reclaimed kaolinite deposits were characterized through a series of shear wave based laboratory tests. Sedimentation tests were performed in order to represent the in-situ soil structure and fabric, while laboratory consolidation tests were carried out to simulate the self-weight consolidation test in situ. Bender element sensors were used to measure the shear wave velocity of the experimental specimens during laboratory consolidation tests wherein the in-situ self-weight consolidation process was simulated.

The vertical effective stress – shear wave velocity relationship was obtained using the converged shear wave velocity corresponding to each applied load. As the soil compositions and particle arrangement of a reclaimed deposit are treated as being unique, the derived vertical effective stress – shear wave velocity equation is applicable for any depth of that single site.

The design parameters, that is, effective stress, consolidation state, degree of consolidation, coefficient of consolidation, void ratio, coefficient of earth pressure at rest, and permeability, were estimated from the shear wave velocity measurements. The effective stress, the degree of consolidation, and the coefficient of earth pressure increase with increased shear wave velocity while the coefficient of consolidation and void ratio decrease as the shear wave velocity increases.

For field applications, the in-situ design parameters were estimated from the soil property – shear wave velocity relationships and the in-situ shear wave velocity data. Therefore, further settlement and consolidation time were predictable.

6.1.3 Undrained Shear Strength and Shear Waves.

The undrained shear strength – shear wave velocity relationship for self weight consolidated clay was evaluated from laboratory loading-unloading tests and vane shear test results.

The void ratio – shear wave velocity relationship for normally-consolidated loading has a single equation, while unloading has different void ratio – shear wave velocity relationships depending on the over consolidation behavior.

The undrained shear strength was measured by a laboratory vane shear test after unloading. The undrained shear strength shows a linear relationship with the void ratio. From the void ratio – shear wave velocity relationship, the undrained shear strength – shear wave velocity relationship could be evaluated. The approximated undrained shear strength – shear wave velocity relationship can be employed to predict the in-situ undrained shear strength of reclaimed deposits, without disturbance.

Ultimately, the test results presented in this thesis demonstrate that the shear wave velocity can be employed to evaluate the effective stress, void ratio, and undrained shear strength for normally-consolidated clay deposits.

6.2 Recommendations for Future Studies

Further study is recommended as follows:

- Characterization of different types of clay such as bentonite, illite, and montmorillonite;
- Development of a combined tool for in-situ design parameter evaluation using shear waves;
- Extension of the proposed characterization method to different drainage conditions;
- Consideration of the size effect between laboratory and in-situ scales;
- Suggestion of a in-situ guideline for in-situ shear wave velocity monitoring and application.

APPENDIX

A.1 Shear Wave Signals for a Single Load Step (Submarine deposit. 15m. 3rd Step)

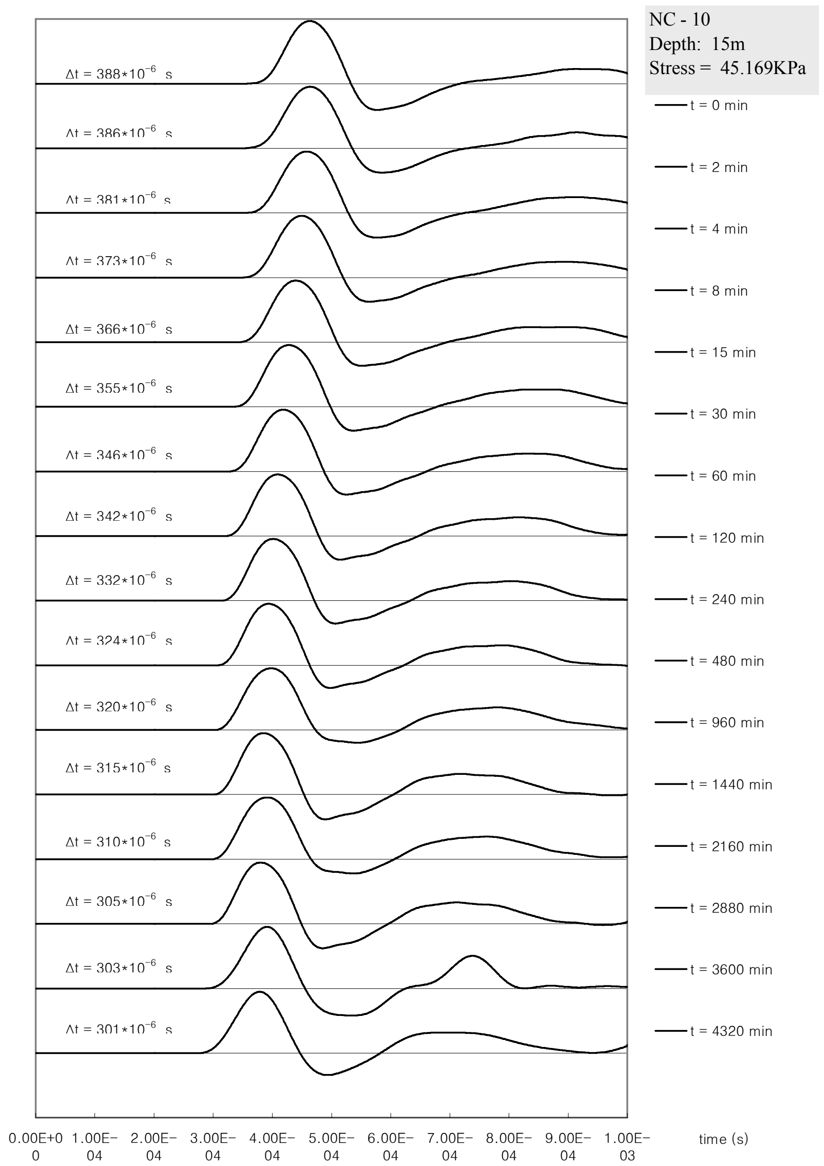

A.2 Final Shear Wave Arrivals for each Load Step (Submarine deposit. 15m)

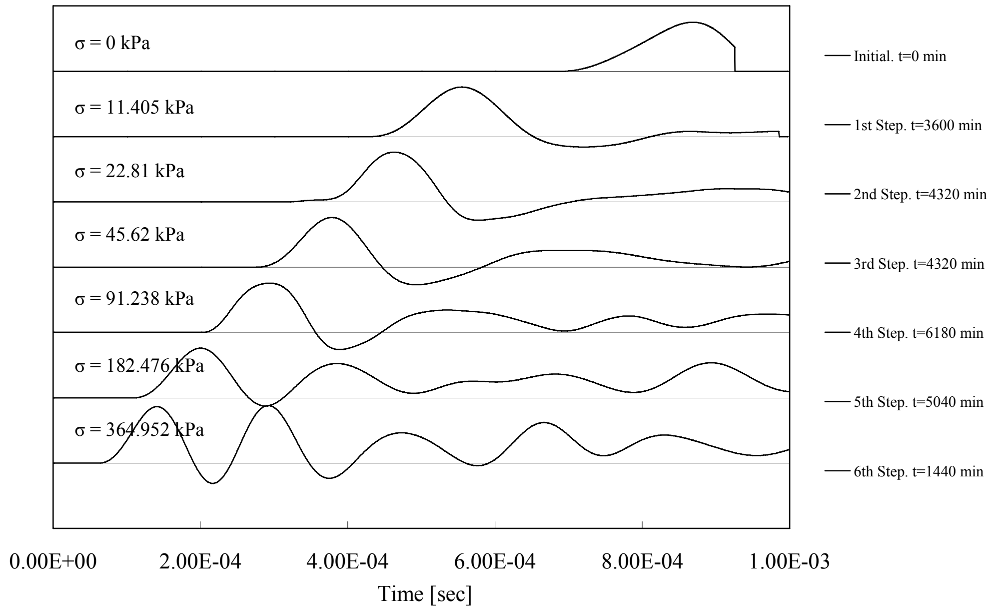

B.1 Mathgram of the vertical effective stress – shear wave velocity relationship evaluation (Submarine deposit. 15m. Ch.3).

IB-SHELBY TUBE TEST: 15m

Estimation of parameter (α, β)

$$Vs = \alpha \cdot \left[\frac{(1 + Ko)\cdot\sigma_v}{2\cdot p_a}\right]^{\beta}$$

α is the empirical parameter [m/sec], β is the empirical parameter, Ko is the coefficient of lateral earth pressure (assumed as 0.5), p_a is the atmospheric pressure (1kPa).

lateral earth pressure coefficient: $Ko := 1 - \sin(20\cdot deg)$ $\quad p_a := 1$

Vertical stress: $Stress := \begin{pmatrix} 11.40475 \\ 22.8095 \\ 45.61899 \\ 91.23798 \\ 182.47597 \\ 364.95193 \end{pmatrix}$ kPa $\quad$ S-Velocity: $Vel := \begin{pmatrix} 69.406 \\ 81.24 \\ 99.52 \\ 123.018 \\ 173.285 \\ 230.19 \end{pmatrix}$

$N := rows(Stress)$ $\quad N = 6$ $\quad YVs(\alpha, \beta, Stress) := \alpha \cdot \left[\frac{(1 + Ko)\cdot Stress}{2\cdot p_a}\right]^{\beta}$

$$sse(\alpha, \beta) := \sum_{k=0}^{N-1} \left(Vel_k - YVs(\alpha, \beta, Stress_k)\right)^2 \qquad k := 0 .. N-1$$

Initial guess: $\alpha := 25.576$ $\quad \beta := 0.381$

Given $\quad sse(\alpha, \beta) = 0 \quad \alpha > 0 \quad \beta > 0$

$\begin{pmatrix} \alpha \\ \beta \end{pmatrix} := Minerr(\alpha, \beta)$ $\quad sse(\alpha, \beta) = 219.717$ $\quad \alpha = 25.576$ $\quad \beta = 0.382$

$\sigma := 1, 2 .. 500$

Plot:

$c := 0 .. 50$

$Str_c := 10 + \frac{c}{50}\cdot 530$

$PVs_c := \alpha \cdot \left[\frac{(1 + Ko)\cdot Str_c}{2\cdot p_a}\right]^{\beta} \cdot \frac{m}{sec}$

$\alpha = 25.576$ $\quad \beta = 0.382$

$i := 0 .. \frac{N}{2} - 1$

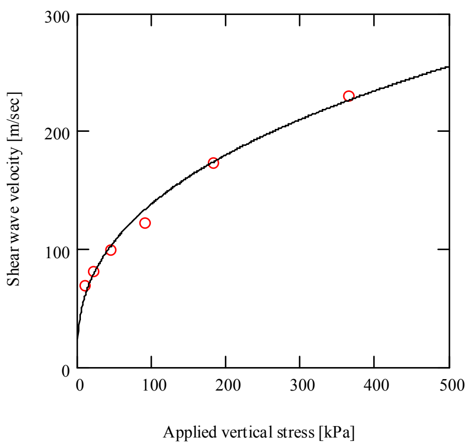

B.2 Mathgram of vertical effective stress – shear wave velocity relationship evaluation (Dredged and Reclaimed deposit. Ch.4).

IN-SHELBY TUBE TEST: SB-17

Estimation of parameter (α, β)

$$Vs = \alpha \cdot \left[\frac{(1+Ko)\cdot\sigma_v}{2\cdot p_a}\right]^\beta$$

α is the empirical parameter [m/sec], β is the empirical parameter, Ko is the coefficient of lateral earth pressure (assumed as 0.5), p_a is the atmospheric pressure (1kPa).

lateral earth pressure coefficient: $Ko := 1 - \sin(18\cdot deg)$ $p_a := 1$

Vertical stress: $Stress := \begin{pmatrix} 15.4 \\ 30.8 \\ 46.2 \\ 61.7 \end{pmatrix}$ kPa S-Velocity: $Vel := \begin{pmatrix} 67.979 \\ 106.3 \\ 123.9693 \\ 153.024 \end{pmatrix}$

$N := rows(Stress)$ $N = 4$ $YVs(\alpha,\beta,Stress) := \alpha\cdot\left[\frac{(1+Ko)\cdot Stress}{2\cdot p_a}\right]^\beta$

$$sse(\alpha,\beta) := \sum_{k=0}^{N-1}\left(Vel_k - YVs(\alpha,\beta,Stress_k)\right)^2$$ $k := 0..\,N-1$

Initial guess: $\alpha := 37.02$ $\beta := 0.288$

Given $sse(\alpha,\beta) = 0$ $\alpha > 0$ $\beta > 0$

$\begin{pmatrix}\alpha \\ \beta\end{pmatrix} := Minerr(\alpha,\beta)$ $sse(\alpha,\beta) = 41.506$ $\alpha = 16.285$ $\beta = 0.564$

$\sigma := 1, 2..\,700$

Plot:

$c := 0..\,50$

$Str_c := 10 + \frac{c}{50}\cdot 530$

$PVs_c := \alpha\cdot\left[\frac{(1+Ko)\cdot Str_c}{2\cdot p_a}\right]^\beta\cdot\frac{m}{sec}$

$\alpha = 16.285$ $\beta = 0.564$

$i := 0..\,\frac{N}{2} - 1$

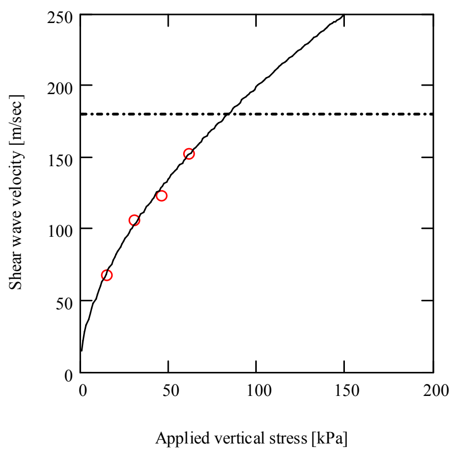

B.3 Mathgram of Degree of Consolidation, Coefficient of Consolidation, Permeability evaluation (Dredged and Reclaimed deposit. 10m. Ch.4).

Coefficient of Consolidation and Degree of Consolidation 10.0m

$$t := \begin{pmatrix} 0.1 \\ 1 \\ 2 \\ 4 \\ 8 \\ 15 \\ 30 \\ 60 \\ 120 \\ 240 \\ 464 \\ 720 \\ 1440 \\ 1680 \\ 2160 \\ 2880 \\ 4890 \\ 5760 \\ 6300 \\ 7860 \\ 10080 \\ 11520 \\ 15000 \\ 19320 \\ 21900 \end{pmatrix} \quad H := \begin{pmatrix} 65.5 \\ 53.51 \\ 50.16 \\ 47.55 \\ 46.31 \\ 45.93 \\ 45.682 \\ 45.495 \\ 45.347 \\ 45.202 \\ 45.09 \\ 45 \\ 44.915 \\ 44.89 \\ 44.865 \\ 44.83 \\ 44.76 \\ 44.74 \\ 44.735 \\ 44.69 \\ 44.667 \\ 44.64 \\ 44.6 \\ 44.565 \\ 44.53 \end{pmatrix} \quad Vs := \begin{pmatrix} 18.09392265 \\ 40.84732824 \\ 61.24542125 \\ 90.05681818 \\ 111.3221154 \\ 115.112782 \\ 119.9002625 \\ 124.3032787 \\ 124.5796703 \\ 124.523416 \\ 127.733711 \\ 132.3529412 \\ 133.2789318 \\ 133.2047478 \\ 138.9009288 \\ 138.7925697 \\ 139.875 \\ 139.8125 \\ 139.796875 \\ 140.977918 \\ 140.4622642 \\ 141.2658228 \\ 143.8709677 \\ 152.0989761 \\ 153.024055 \end{pmatrix} \quad ee := \begin{pmatrix} 2.612857143 \\ 1.927714286 \\ 1.736285714 \\ 1.587142857 \\ 1.516285714 \\ 1.494571429 \\ 1.4804 \\ 1.469714286 \\ 1.461257143 \\ 1.452971429 \\ 1.446571429 \\ 1.441428571 \\ 1.436571429 \\ 1.435142857 \\ 1.433714286 \\ 1.431714286 \\ 1.427714286 \\ 1.426571429 \\ 1.426285714 \\ 1.423714286 \\ 1.4224 \\ 1.420857143 \\ 1.418571429 \\ 1.416571429 \\ 1.414571429 \end{pmatrix} \qquad Hdr := H\cdot\frac{1}{2}$$

$N := \text{rows}(H) \qquad N = 25$

$i := 0..\ N - 1$

lateral earth pressure coefficient: $Ko := 1 - \sin(18\cdot\deg)$

$p_a := 1$

$\alpha := 16.285 \ \beta := 0.564$

$$\sigma_i := 2\cdot e^{\frac{\ln\left(\frac{Vs_i}{\alpha}\right)}{\beta}}\cdot\frac{p_a}{1+Ko} \qquad uo := \sigma_{N-1} \qquad u_i := uo - \sigma_i \qquad uo = 62.808$$

$$U_i := 1 - \frac{u_i}{uo}$$

$\sigma =$

	0
0	1.426
1	6.04
2	12.385
3	24.535
4	35.729
5	37.914
6	40.755
7	43.446
8	43.618
9	43.583
10	45.595
11	48.559
12	49.163
13	49.115
14	52.9
15	52.827

$U =$

	0
0	0.023
1	0.096
2	0.197
3	0.391
4	0.569
5	0.604
6	0.649
7	0.692
8	0.694
9	0.694
10	0.726
11	0.773
12	0.783
13	0.782
14	0.842
15	0.841

$$Tv := \begin{pmatrix} 0.0005 \\ 0.0072 \\ 0.0305 \\ 0.12 \\ 0.256 \\ 0.291 \\ 0.304 \\ 0.393 \\ 0.396 \\ 0.396 \\ 0.44 \\ 0.517 \\ 0.534 \\ 0.534 \\ 0.665 \\ 0.665 \\ 0.69 \\ 0.69 \\ 0.69 \\ 0.727 \\ 0.712 \\ 0.742 \\ 0.828 \\ 1.78 \\ 10 \end{pmatrix}$$

$$Cv := \frac{Tv \cdot Hdr^2}{t} \cdot 10^{-6}$$

$$k := \frac{9.81 \cdot 1000 Cv \cdot (1 + ee) \cdot \frac{1}{60}}{\frac{\sigma \cdot 1000}{0.25}}$$

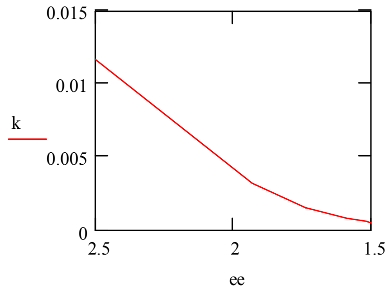

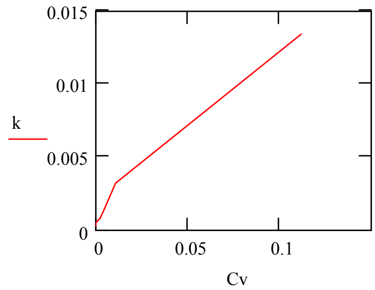

REFERENCES

주재우, 정규향, 조진구 (2003), “Mikasa 압밀이론에 의한 준설토지반의 압밀기간 산정에 관한 연구”, *한국지반공학회논문집*, 제 19권, 6호, pp. 299 – 306.

한국지반공학회, *준설매립과 지반환경*, 2004.3.

현대건설주식회사 기술연구소, *매립지반의 표층고화공법 연구 보고서*, 2000. 7.

Been, K. and Sills, G.C. (1981), “Self-weight consolidation of soft soils: an experimental and theoretical study, *Géotechnique*, Vol. 31, No. 4, pp. 519 – 535.

Buchan, S., and Smith, D.T. (1999), “Deep-sea sediment compression curves: some controlling factors, spurious overconsolidation, predictions, and geophysical reproduction”, *Marine Georesources and Geotechnology*, Vol. 17, pp. 65 – 81.

Cargill, K.W. (1985), *Mathematical model of the consolidation / dessication processes in dredged material*, Technical Report No. D-85-4, U.S. Army Corps of Engineers, Waterways Experiment Station, Vicksburg, MS.

Casagrande, A. (1936), “Determination of the preconsolidation load and its practical significance”, *Proceedings, 1st International Conference on Soil Mechanics and Foundation Engineering*, Cambridge, Mass., Vol. 3, pp. 60 – 64.

Chandler, R.J. (1988), "The in situ measurement of the undrained shear strength of clays using the field vane", STP104, *Vane Shear Strength Testing in Soils: Field and Laboratory Studies*, ASTM, pp. 13 – 44.

Das, B.M. (1997), *Advanced Soil Mechanics*, 2nd ed., Taylor & Francis, Washington, DC.

Das, B.M. (1998), *Principles of Geotechnical Engineering*, 4th ed., International Thomson Publishing, Boston.

Das, B.M. (1999), *Principles of Foundation Engineering*, 4th ed. PWS Publishing, Pacific Grove.

Dyvik, R., and Madshus, C. (1985), "Lab measurements of G_{max} using bender element", *Proc. ASCE Convention on Advances in the Art of Testing Soils under Cyclic Conditions*, pp. 186 – 196.

Gibson, R.E., England, G.L., and Hussey, M.J.L. (1967), "The theory of one-dimensional consolidation of saturated clays, I. Finite non-linear consolidation of thin homogeneous layers", *Géotechnique*, Vol. 17, pp. 261 – 273.

Gibson, R.E.. Schiffman, R.L.m and Cargill, K.W. (1981), "The theory of one-dimensional consolidation of saturated clays, II. Finite non-linear consolidation of thick homogeneous layers", *Canadian Geotechnical Journal*, Vol. 18, pp. 280 – 293.

Gjerapic, G., and Znidarcic, D. (2000a), *Consolidation and dessication analysis for Poplar island site development plan, Baltimore harbor*, Technical Report to Gahagan

& Bryant Associates, Inc., by University of Colorado, Boulder, CO.

Hardin, B.O. and Richart, F.E. (1963), "Elastic wave velocities in granular soils", *Journal of Soil Mechanics and Foundations*, ASCE, Vol. 89, SM1, pp. 33 – 65.
Hardin, B.O. and Drnevich, V.P. (1972), "Shear modulus and damping in soils: measurement and parameter effects", *ASCE J. Soil Mechanics Foundation Division*, 98, pp. 603 – 624.

Hardin, B.O. (1978), "Nature of stress-strain behavior for soils", *Proc. Specialty Conference on Earthquake Engineering and Soil Dynamics*, ASCE, New York, 1, pp. 3 – 90.

Imai, G., Tsuruya, K., and Yano, K. (1979), "A treatment of salinity in water content determination of very soft cays", *Soil & Foundations*, Vol. 19, No. 3, pp. 84 – 89.

Imai, G. (1980), "Settling behavior of clay suspension", *Soils & Foundations*, Vol. 20, No. 2, pp.61 – 77.

Imai, G. (1981), "Experimental studies on sedimentation mechanism and sediment formation of clay materials", *Soil & Foundations*, Vol. 21, No. 1, pp.7 -20.

Jamiolkowski, M., Ladd, C.C., Germaine, J.T., and Lancellotta, R. (1985), "New developments in field and laboratory testing of soils", *Proc. XI. Intl. Conf. Soil Mech. Found. Eng*., Vol. 1, pp. 57 – 153.

Kynch, G.J. (1952), "A theory of sedimentation", *Trans. Faraday Soc*. Vol. 48, pp. 168 – 176.

Ladd, C.C., Foote, R., Ishihara, F., Schlosser, F., and Poulos, H.G. (1977), "Stress-deformation and strength characteristics", *Proc. IX. Intl. Conf. Soil Mech. Found. Eng*., Vol. 2, pp. 421 – 494.

Lambe, T.W., and Whitman, R.V. (1969), *Soil Mechanics*, John Wiley and Sons, New York.

Lee, J.S. and Santamarina, J.C. (2005), "Bender elements: performance and signal interpretation", *Journal of Geotechnical and Geoenvironmental Engineering*, ASCE, Vol. 131, No. 9, pp. 1063 – 1070.

Lee, K. and Sills, G.C. (1981), "The consolidation of a soil stratum, including self-weight effects and large strains". *Numerical & Analyt. Meth. Geomech*. Vol. 5, No. 4, pp. 405 – 428.

Lee, S.R., Kim, Y.S., and Kim, Y.S. (2000), "Analysis of Sedimentation / Consolidation by Finite Element Method", *Computers and Geotechnics*, Vol. 27, pp. 141 – 160.

Mikasa, M. (1963), *The Consolidation of Soft Clay*, Kajima Institution Publishing Co., Ltd.

Mikasa, M. (1965), *The Consoliation of Soft Clay: a New Consolidation Theory and its application*, Japanese Soc. Civil Eng.

Pane, V. and Schiffman, R.L. (1985), "A note on sedimentation and consolidation", *Géotechnique*, Vol. 35, No. 1, pp. 69 – 72.

Pane, V. and Schiffman, R.L. (1987), "The permeability of clay suspensions", *Géotechnique*, Vol. 37, No. 2, pp. 273 – 288.

Pradhan, T.B.S., Imai, G., Ueno, Y., and Dam, L.T.K. (1995), "Subsequent consolidation of clay subjected to undrained cyclic loading", *Recent advances in geotechnical earthquake engineering and soil dynamics*. pp. 61 – 64.

Santamarina, J.C., Klein, K.A., and Fam, M.A. (2001), *Soils and Waves*, John Wiley & Sons, New York.

Schiffman, R.L., Pane, V., and Gibson, R.E. (1984), "The theory of one-dimensional consolidation of saturated clays: IV. an overview of nonlinear finite strain sedimentation and consolidation", *Sedimentation / Consolidation Models*, ASCE, New York, pp. 1 – 29.

Shirley, D.J., and Hampton, L.D. (1978), "Shear wave measurements in laboratory sediments", *J. Acoust. Soc. Am.*, 64(2), pp. 607 – 613.

Sivaram, B., and Swamee, P. (1977), "A computational method for consolidation coefficient", *Soils & Foundations*, Vol. 17, No. 2, pp. 48 – 52.

Skempton, A.W. (1957), "Discussion: The planning and design of new Hong Kong airport", *Proc. Inst. Civil Eng.*, Vol. 7, pp. 305 – 307

Terzaghi, K. (1943), *Theoretical Soil Mechanics*, John Wiley and Sons, New York.

Terzaghi, K., and Peck, R.B. (1996), *Soil Mechanics in Engineering Practice*, 3rd ed., John Wiley and Sons, New York.

Viggiani, G. and Atkinson, J.H. (1995), "Stiffness of fine-grained soils at very small strains", *Géotechnique*, Vol. 45, pp. 249 – 265.

Znidarcic, D., and Liu, J.C. (1989), "Consolidation characteristics determination for dredged materials", *Proceedings of the 22nd Annual Texas A&M Dredging Seminar*, Tacoma, WA, pp. 45 – 65.

요약문

연약 점토 지반에 대한 압밀 상태 및 강도 평가는 향후 토목 구조물 시공으로 인해 유발되는 지반 변위 및 지지력 산정을 위해 매우 중요하다. 특히 유효응력과 간극비는 여러 압밀 이론들에 의해 제시되는 압밀 상태 및 강도 평가를 위한 주요 변수들이다. 하지만 실제 현장에서 지반의 압밀 진행 과정에 따른 신뢰성 있는 유효응력 및 간극비 산정에 어려움이 따르고 있는 실정이다. 본 논문에서는 흙의 전단파 속도가 유효응력과 간극비의 함수라는 점에 착안하여 실내 실험을 통한 유효응력 – 전단파 속도, 간극비 – 전단파 속도 상관 관계를 도출하여 이를 현장 전단파 실측 데이터와 비교함으로써 현장의 유효응력 및 간극비 상태를 도출함으로써 현장의 압밀 상태 및 강도를 평가하는 실험적 모델을 제시하는 것을 목표로 한다.

Shelby tube로 채취 가능한 자연 상태의 연약 점토 지반의 경우, 시료 교란을 최소화하여 밴더엘리먼트 센서를 장착하여 단계별 하중을 재하하는 압밀 실험을 수행하였다. 실내 실험을 통해 도출된 유효응력 – 전단파 속도 상관 관계를 현장의 전단파 속도와 비교하여 현장의 압밀 상태를 평가한다. 현장 전단파 속도가 실내 실험값 보다 큰 경우에는 과압밀, 그 반대의 경우에는 미압밀, 그리고 현장 전단파 속도와 실내 실험값이 오차 범위 내에 근사하면 정규압밀 상태로 평가한다.

비교란 시료 채취가 불가능한 준설 매립 점토 지반의 경우, 침강 실험을 통해 시료를 재성형 하였으며, 실내 압밀 실험을 수행하여 준설 매립 점토 지반의 자중 압밀 과정을 재현하였다. 실내 실험을 통해 도출된 유효응력 – 전단파 속도, 간극비 – 전단파 속도 상관 관계를 이용하여, 해당 지반의 전단파 속도에 따른 압밀도, 압밀계수, 횡토압계수, 투수계수 변화를 도출할 수 있었다. 일반적으로, 흙의 전단파 속도가 증가할수록 유효응력, 압밀도, 횡토압계수 등이 증가하며, 간극비, 압밀계수, 투수계수 등은 감소한다.

연약 점토 지반의 비배수 전단 강도는 간극비의 영향을 크게 받는다. 실내 침강 실험으로 재성형 된 시료에 대해 압밀 실험을 수행한 후 재하 하중을 제거하여 동일한 하중에 대해 과압밀비 • 간극비가 상이한 상태를 재현하였다. 서로 다른 간극비를 지닌 흙에 대해 실내 Vane 전단 실험을 수행하여 해당 흙에 대한 간극비 – 비배수 전단 강도 상관 관계를 획득하였다. 이를 기존 압밀 실험에서 유도된 간극비 – 전단파 속도 상관 관계와 비교하면 최종적으로 해당 흙의 비배수 전단 강도 – 전단파 속도 상관 관계를 도출할 수 있다.

본 연구를 통해서 전단파 속도를 이용하여 연약 점토 지반의 유효응력, 간극비, 비배수 전단 강도, 압밀상태, 압밀도, 압밀계수, 횡토압계수, 투수계수 등을 평가 할 수 있는 기법이 제시되었다. 제시된 전단파 속도 기법은 앞으로 준설 매립 지반 등의 연약 지반 시공 현장에서 폭 넓게 활용될 수 있을 것으로 기대된다.

감사의 글

지반공학의 매력에 빠져 KAIST 건설 및 환경공학과에서 학부, 석사 과정을 거쳐 오늘에 이르기까지 은총 베풀어주신 주님과 변함 없는 사랑과 은혜를 베풀어주신 모든 분들께 깊이 감사를 드립니다.

학부 과정에서부터 지금까지 늘 부족한 저에게 꿈과 이상을 심어주시고, 학문적 열정과 자부심을 키워주신 조계춘 교수님께 충심으로 감사를 드립니다. 또한 항상 자상한 가르침과 학문적 조언을 아끼지 않아주신 이승래 교수님과 김동수 교수님께 감사를 드립니다. 아울러 6년이라는 짧지 않은 시간 동안 토목공학자로써의 길을 밝혀주신 KAIST 건설 및 환경공학과의 모든 교수님들께 진심으로 감사의 마음을 전합니다.

지반시스템 연구실과 함께 한 지난 2년의 대학원 생활은 제 인생에 있어서 너무도 값진 시간들이었습니다. 학문적 고민을 함께해준 태혁이형, 늘 나 자신을 돌아보게 해준 승형이형, 물심양면으로 도와준 준수형, 항상 힘이 되어준 기일이형, 성실함의 표본 민수형, 똑똑한 유학생 Thanh, 늘 내 편이 되어준 나윤이, 그리고 만사가 든든한 희환이에게 고개 숙여 감사를 드립니다. 또한 연구에 많은 도움을 주신 홍은수 박사님, 박현일 박사님, 심영종 박사님, 그리고 정순용 박사님께 감사를 드립니다.

지반 공학 분야는 한 식구라는 유대감을 바탕으로 아낌없는 조언과 도움을 주신 지반공학연구실과 지반동역학연구실 선배님들께 감사드립니다. 특히 항상 찾아가면 반겨주시던 추연욱 박사님, 서원석 박사님, 윤종구 박사님, 정현이형, 은석이형, 위용이형, 준웅이형, 윤기형, 호영이형, 남룡이형, 종태형, 승진이형, 세현이형, 현구형에게 고마움을 전합니다. 또한 같은 동료로써 늘 힘이 되어준 정찬이형, 헌준이형, 지용이형에게 고맙고, 사나이의 진한 의리로 뭉친 학부 00학번 - 경환, 석우, 동규, 진욱, 석범, 준경, 스칸, 태양 모두의 건승을 기원합니다. 대학원 생활의 활력소이자 매주 수요일을 기다리게 만들어준 F.C. Civil 축구 동호회 여러분 모두에게 감사드립니다. 또한 토목구조물 모형 제작 동아리 산마루 회원 모두에게 고마움을 전합니다.

지금은 서로 다른 꿈과 목표를 향해 열심히 살고 있지만, 고등학교 때부터 변함없는 우정으로 소중한 시간들을 함께해준 계룡산 친구들 - 인생의 동반자 철빈, 대사를 함께 도모할 준영, 늘 한결 같은 동현, 세심한 민수, 홍일점 주리, 그리고 도미 유학생 승화와 언제나 나를 응원해주는 윤희, 창현, 동준, 원규, 승연, 상연, 정아를 비롯한 충북과학고 10기 동기들, 그리고 충북막강 916 과 재응공동 충북과학고 모임을 통해 소중한 추억을 함께한 충북과학고 후배 모두에게 감사드립니다. 아울러 못난 제자를 연구의 길로 이끌어주신 이민호 선생님을 비롯한 충북과학고등학교 은사님 모두의 은혜에 깊이 감사를 드립니다.

마지막으로 제 인생의 가장 큰 보물인 사랑하는 가족에게 감사의 마음을 전합니다. 저를 비롯한 삼남매를 행복과 사랑으로 키워주시고, 모자란 맏아들을 언제나 믿어주고 꿈을 키워주신 아버지, 어머니의 은혜에 깊이 감사드리고, 더불어 사랑한다는 말을 전합니다. 그리고 어느덧 의젓하게 자라서 각자의 꿈과 목표를 향해 열심히 살아가고 있는 동생 민정이와 자성이에게도 고마움을 표 합니다. 아울러 석사 생활 내내 고락을 함께해준 주현이에게 깊은 고마움을 전합니다.

이밖에 지면상으로 일일이 언급을 못했지만, 도움을 주신 다른 모든 분들께 다시 한번 깊이 감사드리며, 열정과 성실 그리고 겸양의 미덕으로 오늘보다 더 나은 내일을 열어갈 수 있도록 더욱 열심히 할 것을 약속 드리며 이만 감사의 글을 줄이고자 합니다.

VITA

Name : Il-Han Chang

Date of Birth : February 16th , 1982

Place of Birth : New York City, USA

EDUCATION

March 1998 ~ February 2000

Chung Buk Science High School, Korea

March 2000 ~ February 2004

Korea Advanced Institute of Science and Technology (KAIST), Korea

B.S. Civil and Environmental Engineering

June 2001 ~ August 2001

University of California, Berkeley (UCB), USA

Summer Session

March 2004 ~ February 2006

Korea Advanced Institute of Science and Technology (KAIST), Korea

M.S. Civil and Environmental Engineering

EXPERIENCE

June 2002 ~ January 2003

Samsung Engineering and Construction, Korea

Samsung Group Internship

LIST OF PUBLICATIONS

Dissertation

1. "Evaluation of the Consolidation State and Strength of Soft Clay using Shear Waves", M.S. Dissertation, Department of Civil and Environmental Engineering, KAIST, Korea, January, 2006.

Journal Papers – International

1. Chang, I.H., Cho, G.C., Lee, J.G., and Kim, L.H., "Characterization of clay sedimentation using piezoelectric bender elements", *Key Engineering Materials*, submitted for publication (2005.11).

Conference Papers – International

1. Chang, I.H., Cho, G.C., Lee, J.G., and Kim, L.H. (2005), "Characterization of clay sedimentation using piezoelectric bender elements", The 1st International Conference on Advanced Nondestructive Evaluation, ICC Jeju, Jeju Island, Korea, Novermeber 7~9, 2005, p. 14.
2. Chang, I.H., and Cho, G.C. (2005), "Characterization of clay sedimentation using bender element sensors", Proceedings of Eighteenth KKCNN Symposium on Civil Engineering, Ambassador Hotel Kaohsiung, Taiwan, December 18~20, 2005, pp. 501 – 508.

Conference Papers – Domestic, Korea

1. 장일한, 송기일, 조계춘, 이주공 (2005). "전단파속도를 이용한 연약지반 압밀상태 평가", Current Geotechnical Issues of Thick Clay Deposits, Joint Symposium of ISSMGE ATC 7 & KGSTC, 2005. 9. 21-22, Busan, Korea, pp. 57-64.

2. 장일한, 고영희, 이정학, 조계춘 (2005). “전단파를 이용한 준설매립 점토 지반의 압밀 상태 평가”, 2005년도 대한토목학회 정기 학술대회, 제주국제컨벤션센터 (ICC Jeju), 2005. 10. 20-21, pp. 3421-3424.

Research Reports

1. “A study on the evaluation of in-situ effective stress and consolidation state using shear waves”, KAIST, Hyundai development company & Now Eng. Co. Ltd., in Korean, March 2005.

2. “A study on the estimation of in-situ consolidation characteristic for the branch line railroad construction at the west side of Kwang-Yang harbor using shear wave”, KAIST, Daelim industrial company & Saekwang Eng. Co. Ltd., in Korean, June 2005.

HONORS AND AWARDS

1. 2000. 3 Excellent Freshmen Scholarship (U.C. Berkeley summer session visit. 2001. June-August), KAIST.

2. 2004. 9 Kim, Bo-Jung Fundamental Science Scholarship, KAIST.

3. 2005. 12 KKCNN Adachi Award for Outstanding Young Researcher, Eightennth KKCNN Symposium on Civil Engineering.